DISSERTATION

BIOLOGIC AND BIOCHEMICAL FEATURES OF PRION PATHOGENESIS

Submitted by

Clare Elizabeth Hoover

Department of Microbiology, Immunology, and Pathology

In partial fulfillment of the requirements

For the Degree of Doctor of Philosophy

Colorado State University

Fort Collins, Colorado

Fall 2016

Doctoral Committee:

Advisor: Edward A. Hoover
Co-Advisor: Mark D. Zabel

Anne Avery
Ronald Tjalkens

ABSTRACT

BIOLOGIC AND BIOCHEMICAL FEATURES OF PRION PATHOGENESIS

Prions are the causative agents of a group of fatal neurodegenerative diseases known as transmissible spongiform encephalopathies. Prions are unique in that disease is initiated when the normal prion protein (PrP^{C}) undergoes a conformational change and propagates through a process of templated conversion to an infectious, misfolded, isoform (PrP^{RES}, PrP^{CWD}, or PrP^{Sc}) which can assemble into oligomers and amyloid fibrils. Disease is associated with prion accumulation in the central nervous system, causing the pathologic lesions of neurodegeneration, white matter spongiosis, and a reactive astrogliosis. Previous work has demonstrated the process of prion propagation and disease pathogenesis can be influenced by conversion cofactors, inhibitors, and biologic systems.

Heat shock proteins have been shown to protect against the toxic disease effects of denatured and aggregated proteins in several models of neurodegenerative diseases including Alzheimer's disease, Parkinson's disease, and spinocerebellar ataxia. In this dissertation, I investigated if heat shock protein 72 (HSP72) expression in neurons could protect against prion disease-associated pathology through a cell culture and mouse model of murine-adapted scrapie strain RML. In contrast to the role in other neurodegenerative diseases, HSP72 did not alter the prion disease course or amount of prion conversion in either disease model.

Chronic wasting disease (CWD) is a naturally occurring, horizontally transmitted prion disease affecting wild and captive cervid populations that is rapidly expanding into new states and countries. Studies investigating the distribution of PrP^{CWD} during early subclinical CWD

infection have detected prions in the oropharyngeal lymphoid tissues as early as 1.5 months; however, the complete tissue distribution of PrP^{CWD} immediately following prion exposure and the chronological progression of prion tissue accumulation remains unknown. Here, I show prions initially accumulate in the oropharyngeal lymphoid tissues following mucosal exposure and rapidly disseminate to all systemic lymphoid tissues prior to neuroinvasion. These findings will help better understand the early pathogenesis of CWD prior to clinical disease and potentially identify therapeutic targets.

Prion disease diagnosis relies on demonstration of the misfolded isoform by immunodetection, amyloid seeding assays, or animal bioassays, all assays which may require separate sample preparations precluding examination by multiple tests. To address this limitation, I developed a new technique to detect PrP^{CWD} amyloid seeding in fixed paraffin-embedded (FPE) tissues by real-time quaking induced conversion (RT-QuIC). FPE RT-QuIC proved to be more sensitive than IHC for prion detection and the use of RT-QuIC amyloid formation kinetics yielded a semi-quantitative estimate of the prion burden in samples without the cost and time of animal bioassays.

The normal cellular prion protein resides in cell membrane lipid rafts, which has been shown to be a site of pathogenic conversion. Previous *in vitro* assays have highlighted the ability of lipids to promote prion formation but knowledge is limited regarding the capacity of lipids to inhibit prion formation. Here, I show endogenous polar brain lipids directly inhibit prion amyloid formation in RT-QuIC in a dose-dependent manner. This work is the first to identify an inhibitory role of lipids and suggests the prion conversion process is influenced by a balance of pro-conversion and inhibitory molecules.

ACKNOWLEDGEMENTS

There are many individuals who have generously contributed time and effort to the studies presented in this dissertation. I'd like to start out by acknowledging my co-advisors, Drs. Edward Hoover and Mark Zabel. Their vision, guidance, and encouragement to explore new ideas were vital to my success in this endeavor. To Ed, thank you for adopting a fellow buckeye and giving me a place to grow and develop as a research scientist. His scientific insights and love of mentoring is inspiring and I am proud to count myself among his many graduate students. To Mark, thank you for your advice and continual optimism throughout my graduate studies.

Thank you as well to all members of the Hoover, Mathiason, and Zabel labs, past and present, including Dr. Candace Mathiason, Dr. Nicholas Haley, Dr. Anca Selariu, Amy Nalls, Sherry WeMott-Colton, Laura Pulscher, Sarah Accardi, and Kassi Willingham. In particular, thanks to Dr. Davis Seelig for sharing his histology knowledge with me, Dr. Nathaniel Denkers and Erin McNulty for their deer handling expertise, Dr. Davin Henderson for his RT-QuIC and biochemistry expertise, and thanks to Kristen Davenport for being a sounding board, comma editor, and fellow student on this journey. Special thanks to Nikki Buhrdorf for teaching me how to be a mentor and having a hand, literally, in the majority of the experiments I present in this dissertation. Thank you to members of the Prion Research Center and my graduate committee for their suggestions and critiques.

Thank you to Dr. Michael Oglesbee of the Department of Veterinary Biosciences at The Ohio State University for his pathology mentorship and generous contributions that included cells, mice, and input on heat shock protein study design.

I've also completed a rigorous residency program and would like to thank all of the faculty and staff of the Colorado State University Diagnostic Laboratory. These thanks extend to the histology section for their assistance in quickly preparing blocks and developing my histology skills. Thank you to my fellow residents including Dr. Alana Pavuk, Dr. Kelly Walton, Dr. Shannon McLeland, Dr. Paula Schaffer, Dr. Deanna Dailey, Dr. Craig Miller, and Dr. Jenn Malmberg for their comradery and friendship.

For my family, the constant in my life, I could not have achieved any of this without you. Words cannot express how grateful I am to my mother, father, brother, grandmother, mother-in-law and sister-in-law, for their many years of support.

To Viola, who joined me on the final leg of this adventure. I hope you always get excited about your new discoveries.

And finally, to Matt. Thank you for all the dishes, meals, smiles, hugs, faith, encouragement and love behind the scenes that keep me going every day. I love you more than any other.

The research presented in this dissertation was supported by funds from NIH 1-R01-NS0610902, NIH 1-R01-NS-078745, and 9-T32 OD0-10437.

DEDICATION

For Oscar, who started me on this journey.

TABLE OF CONTENTS

INTRODUCTION

Prion diseases

Prion diseases, or transmissible spongiform encephalopathies (TSEs), are a collection of unique, uniformly fatal, neurodegenerative diseases that affect humans and animals. Originally classified as "slow viruses", these diseases are caused by an unconventional pathogen, a misfolded protein, and result in central nervous system neuropathology characterized by neuropil vacuolation (spongiosis), neuronal degeneration, and a reactive gliosis (1,2). The first identified TSE was scrapie in sheep, initially described in the 18th century (3,4). Currently, animal TSEs have expanded to include bovine spongiform encephalopathy (BSE), transmissible mink encephalopathy (TME), feline spongiform encephalopathy (FSE), and chronic wasting disease (CWD) (2). TSEs have been clinically recognized in humans since the early 20th century when Hans Gerhard Creutzfeldt and Alfons Maria Jakob described a progressive neurological disorder, later named Creutzfeldt-Jakob disease (CJD) (5). Additional human TSEs that have emerged through transmissibility observations include Kuru in the Fore tribe of New Guinea and variant Creutzfeldt-Jakob disease (2). Genetic-origin prion diseases also include fatal familial insomnia and Gerstmann-Straussler-Sheinker syndrome (2).

The studies described in this proposal are framed within the context of the protein-only hypothesis. Unlike the dogma of DNA to RNA to protein established by Watson and Crick, the infectious agent causing prion diseases is widely accepted to be a protein devoid of genetic material (6,7). Studies characterizing the unique properties of prions were performed on the prototypic TSE, scrapie. Initial studies established the infectious nature of scrapie by successfully transmitting the disease to naïve sheep following a long incubation time, greater

than 14 months, leading to the classification of a slow virus (1,8). Studies performed by Alper and Gordon to characterize the scrapie infectious agent established it was resistant to formalin, heat, and UV inactivation, treatments known to inactivate viruses and bacteria (9-11). Due to these unique properties, multiple theories were proposed regarding the nature of the scrapie agent including a protein, polysaccharide, or membrane fragment absent of nucleic acid (12). In 1982, Stanley Prusiner isolated and purified the scrapie agent, characterized it as a partially protease-resistant protein, and proposed the term "small proteinaceous infectious protein", or prion, for this unique pathogen (13-15).

The protein-only hypothesis proposes the infectious prion is a misfolded isoform of the normal cellular prion protein, PrP^{C}, and propagates by post-translational templated conversion of the α-helical host protein to an abnormal conformation characterized by increased β-sheet content (7,16-18). Once the abnormal conformation is adopted, the protein becomes resistant to detergents and protease digestion, and can assemble into oligomers, amyloid fibrils, and aggregates (19,20). Of these different protein formations, prion oligomers have been identified as containing the greatest toxic activity and amyloid aggregates may potentially serve a protective function by sequestering oligomers (21). The exact mechanism of prion cytotoxicity remains unknown, however it has been proposed that oligomers can interact with and disrupt cell membranes (19). In this dissertation, the term PrP^{RES} is used to describe the infectious misfolded prion protein in general while PrP^{Sc} is used to refer to scrapie prions and PrP^{CWD} used to refer to CWD prions.

The protein-only hypothesis has been investigated in the pathogenesis of other protein misfolding neurodegenerative diseases including Alzheimer's disease (AD), Parkinson's disease (PD), Amyotrophic lateral sclerosis (ALS), and polyglutamine (polyQ) repeat diseases (22,23).

These diseases also feature host protein misfolding, aggregation, and associated neurodegeneration (23). Despite recent studies demonstrating the respective disease-associated alternative protein conformations, like tau in AD and α-synuclein in PD, can initiate disease in transgenic mouse models, the likelihood of disease transmission remains low (24-26). Nevertheless, the similarities in protein-misfolding propagation between these diseases can provide insights into toxic mechanisms and pathogenesis.

The cellular prion protein, PrP^C

The normal cellular prion protein, PrP^C, is encoded by the single-copy *PRNP* gene and the protein sequence is highly conserved with greater than 90% homology among species (27,28). In humans, it is transcribed as a 253 amino acid polypeptide and post-translational modifications include removal of the N-terminal and C-terminal signal sequences that in vivo traffic the protein from the endoplasmic reticulum to lipid rafts in the outer cell membrane (2,19). The protein structure is characterized by a disordered N-terminal domain (NTD) that contains a proline and glycine rich "pseudorepeat" and four octapeptide repeats, which is separated from the structured C-terminal domain (CTD) by a short hydrophobic region (2,28). The structured C-terminal domain contains a two β-sheets and three α-helices and is the region that takes on the characteristic conformation change by acquiring an increase in β-sheets during prion disease (28). The function of PrP^C has been associated with signal transduction, cationic metal binding, synapse transmission, and apoptosis, however its exact role is unknown as PrP^C knockout mice display minimal pathology or functional deficits (29-31).

The functional PrP^C protein is located in the outer lipid bilayer of the cell membrane by a GPI anchor where it resides in detergent insoluble lipid rafts, a location that has been shown to

influence PrP^{RES} formation and propagation (32-34). Cell culture and transgenic mouse studies established the CTD GPI anchor is not required for PrP^{RES} formation but is necessary for disease propagation between cells and pathology (35). Without the GPI anchor, anchorless PrP^{RES} favored large amyloid accumulations in mice without the formation of smaller, oligomer and fibril forms and mice did not display clinical disease (36). Additionally, alterations in the lipid bilayer composition or disruption of lipid rafts decreased PrP^{C} concentration at the cell surface which resulted in decreased PrP^{RES} (37,38). These studies highlight the importance of the lipid bilayer and lipid raft location as determined by the GPI anchor in the pathogenesis of prion disease.

Perspectives on prion propagation adopted in this dissertation:

This thesis seeks to address several unanswered questions on prion propagation and pathogenesis at the cellular and whole-organism level. First, I examine how a natural cellular system, the heat shock response, which functions to prevent protein denaturation and aggregation, influences prion propagation. Second, the propagation and tissue distribution of prions during early CWD pathogenesis is investigated in the natural host. In the process of this study, a new technique was developed that allows detection and semi-quantitative estimation of tissue prion burdens by real-time quaking induced conversion (RT-QuIC) in fixed paraffin-embedded tissues. Lastly, the influence of brain-derived lipids on RT-QuIC prion propagation is investigated.

Chaperone proteins and prion propagation:

The maintenance of correct protein structure is a complex process. Bacteria and eukaryotic cells have evolved protein quality-control systems of molecular chaperones, including the heat shock proteins, that protect against protein unfolding or misfolding as a result of stress or ageing (39,40). In eukaryotes one of the major heat-shock protein families is a group of 70 kDa mass proteins, known as HSP70s, with the main stress-inducible member being HSP72 along with its co-chaperone HSP40 (41,42). In prokaryotes the main stress inducible heat shock protein is HSP104 while the HSP70 family plays a more accessory role (42). During periods of cellular stress brought on by environmental conditions such as elevated temperatures or hypoxia, these proteins function to maintain proteostasis in an ATP-dependent manner by refolding misfolded proteins and targeting damaged and unfolded proteins to the ubiquitin-proteosome pathway or lysosomes for degradation (39,40).

The common features of protein misfolding and aggregation in neurodegenerative diseases have led to investigations of heat shock proteins as potential therapeutic targets (43). Heat shock proteins have been found to co-localize with aggregates and inclusion bodies found in protein-misfolding diseases including Alzheimer's disease, Parkinson's disease, and polyQ protein diseases, suggesting they are able to interact with these proteins (39). Cell culture and transgenic mouse studies have established a correlation between increasing HSP72 expression and decreased respective protein accumulations (44-47). Proposed mechanisms for HSP72 neuroprotection include stabilizing the native protein structure to prevent the initial misfolding or stabilizing misfolded intermediates to promote the on-pathway formation of fibrils and aggregates over toxic oligomeric forms (39). Extracellular HSP72 may also activate microglia promoting degradation of extracellular aggregates (48,49).

The interaction between heat shock proteins and prion propagation has been best studied in yeast. HSP104, the major inducible chaperone, has a paradoxical relationship with regards to prion propagation in yeast: it has been shown to be both a crucial cofactor for prion formation and "cure" prion disease by breaking up prion amyloid deposits (50,51). In fact, these functions are not mutually exclusive and are part of a spectrum of HSP104 prion-disaggregase activity where wild-type expression levels of HSP104 breaks down prion amyloid aggregates into smaller fragments that nucleate additional prion formation and HSP104 over-expression can disaggregate enough amyloid to "cure" cells (52,53). In contrast to yeast, the role of heat shock proteins in mammalian prion diseases remains largely unknown. A single study suggested HSP72 protects against prion cellular degeneration *in vitro*, however, additional research is needed to characterize the role of heat shock proteins *in vivo* (54).

Chronic wasting disease

Chronic wasting disease (CWD) is a naturally occurring TSE that affects both nondomestic and domestic cervid species, including white-tailed deer, mule deer, wapiti, moose, and reindeer (55). CWD was first identified in a captive herd of mule deer in Fort Collins, CO in 1967 and classified as a spongiform encephalopathy in the 1980s (56,57). Since its identification, CWD has expanded to 24 states, two Canadian provinces, The Republic of Korea, and most recently a wild reindeer in Norway (58-60). Disease prevalence in affected regions has been reported as high as 30% in wild populations and up to 80% in captive populations (61). Clinical signs of CWD include primarily progressive weight loss and variable difficulty swallowing, ataxia and head tremors, polydipsia, and polyphagia (55,56,62). Histologic lesions

of neuronal degeneration, astrocytosis, and amyloid plaques of PrP^{CWD} are similar to those observed in other TSEs (63).

CWD presents a particular challenge due to its uniquely efficient horizontal transmission (30,55). Natural CWD transmission is presumed to occur through direct or indirect environmental exposure via the oral and/or aerosol routes to contaminated excreta such as saliva, feces, and urine (64-68). Once established in the environment, CWD has been demonstrated to persist for multiple years, potentially through complexing with soil (67,69,70). Although not considered a major route of spread, vertical transmission of CWD has been described in offspring from infected dams (71).

Similar to other prion diseases, like scrapie and vCJD, CWD disease progression is influenced by the primary sequence of the *PRNP* gene of the host animal. Lower disease incidence and a prolonged disease course are reported with the following polymorphisms in cervids: white-tailed deer are G96S and Q95H, elk M132L; and mule deer S225F (72-74). The alternate alleles are reported to occur with less frequency in cervids, comprising less than 25% of populations (58). The *PRNP* genotype not only impacts prion disease progression but has also been reported to influence the development of CWD prion strains (75).

Prion disease progression in the host

Insights into the sequence of disease progression in TSEs following oral exposure are derived from investigations of the prototypic TSE, scrapie. Following oral prion exposure there are three proposed phases of disease: first, mucosal uptake and drainage to gastrointestinal-associated lymphoid tissue (GALT); second, systemic lymphoid spread; and last, neuro-invasion (76). In scrapie, the earliest prions were detected in GALT including oropharyngeal lymphoid

tissues (tonsil, retropharyngeal lymph nodes), jejunum, and ileum, with subsequent spread to systemic lymphoid tissues as disease progressed (76). This early lymphoid accumulation of prions has proven essential for neuroinvasion as blockade of lymphoid drainage to regional lymph nodes or disruption of Peyer's patches delayed PrP^{Sc} deposition in nervous tissues following oral inoculation (77,78). Neuroinvasion is proposed to occur at peripheral nerves enervating lymphoid tissues or the enteric nervous system and. In scrapie, was detected in the enteric nervous system prior to trafficking to brainstem (79). Following neuroinvasion at peripheral lymphoid tissues, prions undergo retrograde transport through the sympathetic and parasympathetic nerves to the central nervous system (80,81).

Although investigations of sequential disease progression are not possible in human TSEs, variant-CJD also displays accumulation in lymphoid tissues in addition to nervous tissues (82-84). Investigations of disease progression in CWD have identified PrP^{CWD} accumulation in lymphoid tissues during the pre-clinical period, suggesting a disease pathogenesis similar to scrapie (85,86). However, studies of the earliest time period post-CWD exposure and chronological tissue propagation of PrP^{CWD} in the cervid host are lacking and vital to identification of pre-clinical therapeutic targets.

Detection of prion disease

To accurately evaluate TSE disease progression, sensitive diagnostic techniques are required to identify PrP^{CWD} during the pre-clinical period when there potentially is a low prion burden in tissues. The diagnosis of prion disease relies on identification of the disease-associated misfolded prion conformational state, either through immunodetection, or amyloid

detection assays. Traditionally, immunohistochemistry and/or western blot and animal bioassays have been considered the gold standards of prion detection (87).

Immunodetection assays

Conventional diagnosis of prion disease via antibody immunodetection in western blotting and immunohistochemistry relies on demonstration of a proteinase-resistant fragment, measuring 27-30 kDa in western blotting, which is associated with disease (2). Immunohistochemistry protocols rely on formic acid or proteinase-K digestion to remove PrP^{C} from tissues leaving PrP^{RES} and sensitivities approach 100% (88,89). Western blotting also provides information regarding the distribution of prion glycosylation patterns in samples (90). Limitations of immunodetection methods include false negative results due to harsh proteolytic treatments that remove protease-sensitive prion forms or prion burdens below detection thresholds (90-92).

Amyloid seeding assays

I*n vitro* assays have been developed to amplify small prion amounts in samples from early disease time points and in excreta when the prion burden could potentially be below the threshold of detection by traditional assays. These assays, including serial protein-misfolding cyclic amplification (sPMCA), amyloid seeding assay (ASA), and real-time quaking induced conversion (RT-QuIC), rely on the conversion of PrP^{C} substrate to the disease-specific conformation (93-95). In sPMCA, the PrP^{C} substrate is in the form of brain homogenate derived from transgenic mice and prion seeds are amplified by alternating cycles of templated fibril elongation and sonication (95). Prion-induced amplified products are detected through western blotting. In comparison, RT-QuIC employs prion templated conversion of bacterially-produced recombinant PrP^{C} substrate into amyloid structures (Figure I.1) (94). Repeated cycles of

shaking, or quaking, accelerates the amyloid formation reaction by breaking formed amyloid fibrils into smaller seeds that propagate the seeded conversion. Prion amyloid formation is monitored in real-time with thioflavin T dye binding and fluorescence emission spectral shift that is recorded by a fluorometer (96).

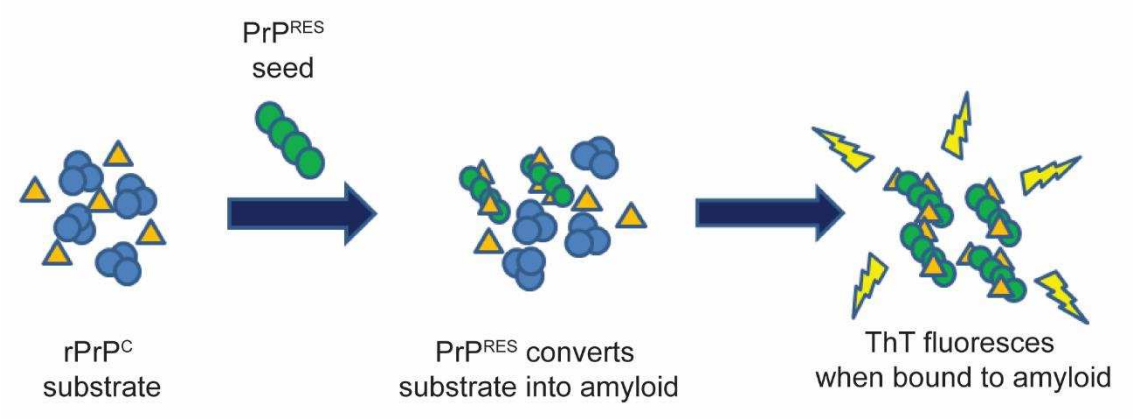

Figure I.1 Diagram of the RT-QuIC reaction
Bacterially-produced recombinant PrP^{C} substrate is converted into amyloid fibrils by prion-seeded templated conversion. Amyloid formation is measured in real-time by thioflavin T (ThT) binding to amyloid fibrils causing a shift in fluorescence spectral emission.

RT-QuIC has successfully been applied to the detection of prions in complex body fluids and tissues, including brain, lymph nodes, saliva, urine, cerebrospinal fluid, and nasal brushings with sensitivities of 70-100% and specificities of 96-98% when evaluated in a diagnostic setting (97-104). In addition to the sensitive detection of PrP^{RES} in samples, the real-time analysis of amyloid formation kinetics in RT-QuIC has been applied to semi-quantitatively estimate the prion burden in a sample (105). This is achieved through comparison of prion amyloid formation rates or end-point dilutions with those of known animal bioassayed materials (105,106).

One limitation of prion diagnostics is the requirement of separate sample types for individual assays: formaldehyde-fixed tissue for immunohistochemistry and frozen tissue homogenates for western blotting and RT-QuIC. The use of separate samples creates potential

disparate assay results due to variable PrP^{RES} deposition and assay sensitivities. In this dissertation, a new technique for detection and quantification of prions in fixed paraffin-embedded tissues is described.

Prion conversion cofactors

In the context of the protein-only hypothesis, research has focused on identifying cofactors that facilitate conversion from PrP^{C} to infectious PrP^{RES}. To date, RNA and lipids, in particular the anionic lipid phosphatidylethanolamine, have been identified as cofactors capable of promoting PrP^{RES} formation from bacterially produced recombinant PrP^{C} *in vitro* (107-109). In contrast to amyloidogenic cofactors, screening assays to identify prion therapeutics have detected molecules, both endogenous and pharmacologic origin, that inhibit amyloid formation in cell culture systems (110). The RT-QuIC amyloid seeding reaction is variably inhibited at high sample concentrations, such as 10^{-1} to 10^{-3}, but takes place following dilution, presumably due to dilution of inhibitors (84,105,111). The identity of these endogenous amyloid formation inhibitors in RT-QuIC remains unknown.

Questions on prion disease addressed in this dissertation:

This dissertation seeks to answer several questions regarding prion disease progression, including: (1) can a natural protein quality-control system, the heat shock response, be used to mitigate prion pathogenicity and disease progression; (2) what is the tissue distribution and chronological progression of prion accumulation during early CWD infection in the natural cervid host; (3) can endogenous molecules in brain homogenates inhibit or regulate prion

amyloid formation in RT-QuIC? As part of these studies, a new technique for identification and quantification of prions in fixed paraffin-embedded tissues was developed and described.

Dissertation research:

The above background on prion disease pathogenesis and propagation provide the foundation on which the research in this dissertation is based. The first objective investigated the ability of the heat shock system, specifically HSP72, to ameliorate prion-associated neurodegeneration. I hypothesized the expression of HSP72 in neurons could prevent PrP^{Sc} conversion, aggregation, and protect against prion-associated cytotoxicity. These studies were carried out in a neuroblastoma (N2a) cell line and transgenic C57Bl/6 mice engineered to constitutively express HSP72. HSP72-expressing cells and mice were inoculated with mouse-adapted scrapie (RML) and evaluated for disease progression as compared to wild-type controls. I found that unlike literature demonstrating HSP72 protected against cytotoxicity in animal models of protein misfolding diseases, HSP72 neuronal expression did not alter disease pathogenesis *in vitro* or *in vivo*.

There is limited knowledge regarding the site of entry of CWD prions and early pathways of PrP^{CWD} tissue dissemination prior to neuroinvasion. Knowledge of such disease progression is vital to understanding how CWD is transmitted so efficiently and developing preclinical therapeutic strategies. Therefore, the second objective of this dissertation was to evaluate the distribution of PrP^{CWD} in a natural host, white-tailed deer, during the early stages of disease. I hypothesized PrP^{CWD} tissue distribution would be influenced by exposure route and would have a lymphoid replication phase prior to neuroinvasion. White-tailed deer were exposed to CWD by either a mucosal (oral and oro-nasal) or intravenous (IV) route. IV-exposed deer were

evaluated for PrP^{CWD} distribution at 15 minutes or 3 days post-exposure while mucosal-exposed deer were evaluated at 15 minutes, 3 days, and monthly from 1 to 4 months. PrP^{CWD} tissue distribution was evaluated by RT-QuIC and tyramide-signal amplification.

The requirement of separate tissue sample types, formaldehyde-fixed and frozen homogenates, for prion detection can create disparate PrP^{RES} detection results due to variable prion deposition or limit retrospective studies when only paraffin-embedded samples are available. In addition, the estimation of tissue prion burdens are restricted to costly and time-consuming animal bioassays or cell-culture assays which can be precluded by sample type or lack of PrP^{C} and sample compatibility. To overcome these limitations, I developed a new technique that combined traditional histologic methodologies and RT-QuIC to detect PrP^{CWD} in fixed paraffin-embedded (FPE) tissues. FPE RT-QuIC amyloid amplification kinetics were used to provide semi-quantitative estimations of the prion titer in tissues.

During development of FPE RT-QuIC methodology, I observed detection of prion-seeded amyloid seeding at high concentrations, in direct contrast to previous observations. Therefore, the fourth objective of this dissertation was to identify the amyloid formation inhibitors present in brain homogenates using RT-QuIC. I hypothesized endogenous lipids present in brain homogenates inhibited the amyloid formation reaction and investigated this activity with biochemical lipid extraction protocols and RT-QuIC experiments. The results of this objective will provide a basis for future investigations into the biologic relevance of the identified inhibitors.

The results of this work contribute to the knowledge of prion pathogenesis in multiple areas including heat shock proteins, CWD pathogenesis in the natural host, and novel identification of prion amyloid formation inhibitors, as well as development of an enhanced

PrP^{RES} detection method with experimental and diagnostic applications. In these ways, this work advances the understanding of prion propagation and prion disease diagnosis.

INTRODUCTION REFERENCES

1. Sigurdsson, B. (1954) Rida, a chronic encephalitis of sheep. . *The British veterinary journal*, 341-354
2. Prusiner, S. B. (1998) Prions. *Proc Natl Acad Sci U S A* **95**, 13363-13383
3. Besnoit, C. a. M. C. (1898) Note sur les lesions nerveuses de la tremblante du mouton. *Rev Vet*, 397-400
4. Wang, F., and Ma, J. (2013) Role of lipid in forming an infectious prion? *Acta Biochim Biophys Sin (Shanghai)* **45**, 485-493
5. Zabel, M. D., and Reid, C. (2015) A brief history of prions. *Pathog Dis* **73**, ftv087
6. Watson, J. D., and Crick, F. H. (1953) Molecular structure of nucleic acids; a structure for deoxyribose nucleic acid. *Nature* **171**, 737-738
7. Soto, C., and Castilla, J. (2004) The controversial protein-only hypothesis of prion propagation. *Nature medicine* **10 Suppl**, S63-67
8. Cuille J.; Chelle PL. (1938) Investigations of scrapie in sheep. *Vet Med* **34**, 417-418
9. Latarjet, R., Muel, B., Haig, D. A., Clarke, M. C., and Alper, T. (1970) Inactivation of the scrapie agent by near monochromatic ultraviolet light. *Nature* **227**, 1341-1343
10. Gordon, W. S. (1946) Advances in veterinary research. *The Veterinary record* **58**, 516-525
11. Alper, T., Haig, D. A., and Clarke, M. C. (1966) The exceptionally small size of the scrapie agent. *Biochemical and biophysical research communications* **22**, 278-284
12. Alper, T., Cramp, W. A., Haig, D. A., and Clarke, M. C. (1967) Does the agent of scrapie replicate without nucleic acid? *Nature* **214**, 764-766
13. Prusiner, S. B. (1982) Novel proteinaceous infectious particles cause scrapie. *Science* **216**, 136-144
14. Prusiner, S. B., Bolton, D. C., Groth, D. F., Bowman, K. A., Cochran, S. P., and McKinley, M. P. (1982) Further purification and characterization of scrapie prions. *Biochemistry* **21**, 6942-6950
15. Bolton, D. C., McKinley, M. P., and Prusiner, S. B. (1982) Identification of a protein that purifies with the scrapie prion. *Science* **218**, 1309-1311
16. Pan, K. M., Baldwin, M., Nguyen, J., Gasset, M., Serban, A., Groth, D., Mehlhorn, I., Huang, Z., Fletterick, R. J., Cohen, F. E., and et al. (1993) Conversion of alpha-helices into beta-sheets features in the formation of the scrapie prion proteins. *Proc Natl Acad Sci U S A* **90**, 10962-10966
17. Weissmann, C. (1991) A 'unified theory' of prion propagation. *Nature* **352**, 679-683
18. Caughey, B. W., Dong, A., Bhat, K. S., Ernst, D., Hayes, S. F., and Caughey, W. S. (1991) Secondary structure analysis of the scrapie-associated protein PrP 27-30 in water by infrared spectroscopy. *Biochemistry* **30**, 7672-7680
19. Caughey, B., Baron, G. S., Chesebro, B., and Jeffrey, M. (2009) Getting a grip on prions: oligomers, amyloids, and pathological membrane interactions. *Annual review of biochemistry* **78**, 177-204
20. McKinley, M. P., Bolton, D. C., and Prusiner, S. B. (1983) A protease-resistant protein is a structural component of the scrapie prion. *Cell* **35**, 57-62
21. Silveira, J. R., Raymond, G. J., Hughson, A. G., Race, R. E., Sim, V. L., Hayes, S. F., and Caughey, B. (2005) The most infectious prion protein particles. *Nature* **437**, 257-261

22. Olanow, C. W., and Prusiner, S. B. (2009) Is Parkinson's disease a prion disorder? *Proc Natl Acad Sci U S A* **106**, 12571-12572
23. Soto, C. (2003) Unfolding the role of protein misfolding in neurodegenerative diseases. *Nature reviews. Neuroscience* **4**, 49-60
24. Peeraer, E., Bottelbergs, A., Van Kolen, K., Stancu, I. C., Vasconcelos, B., Mahieu, M., Duytschaever, H., Ver Donck, L., Torremans, A., Sluydts, E., Van Acker, N., Kemp, J. A., Mercken, M., Brunden, K. R., Trojanowski, J. Q., Dewachter, I., Lee, V. M., and Moechars, D. (2015) Intracerebral injection of preformed synthetic tau fibrils initiates widespread tauopathy and neuronal loss in the brains of tau transgenic mice. *Neurobiol Dis* **73**, 83-95
25. Luk, K. C., Kehm, V. M., Zhang, B., O'Brien, P., Trojanowski, J. Q., and Lee, V. M. (2012) Intracerebral inoculation of pathological alpha-synuclein initiates a rapidly progressive neurodegenerative alpha-synucleinopathy in mice. *J Exp Med* **209**, 975-986
26. Luk, K. C., Kehm, V., Carroll, J., Zhang, B., O'Brien, P., Trojanowski, J. Q., and Lee, V. M. (2012) Pathological alpha-synuclein transmission initiates Parkinson-like neurodegeneration in nontransgenic mice. *Science* **338**, 949-953
27. Wopfner, F., Weidenhofer, G., Schneider, R., von Brunn, A., Gilch, S., Schwarz, T. F., Werner, T., and Schatzl, H. M. (1999) Analysis of 27 mammalian and 9 avian PrPs reveals high conservation of flexible regions of the prion protein. *Journal of molecular biology* **289**, 1163-1178
28. Surewicz, W. K., and Apostol, M. I. (2011) Prion protein and its conformational conversion: a structural perspective. *Topics in current chemistry* **305**, 135-167
29. Westergard, L., Christensen, H. M., and Harris, D. A. (2007) The cellular prion protein (PrP(C)): its physiological function and role in disease. *Biochimica et biophysica acta* **1772**, 629-644
30. Aguzzi, A., Sigurdson, C., and Heikenwaelder, M. (2008) Molecular mechanisms of prion pathogenesis. *Annual review of pathology* **3**, 11-40
31. Steele, A. D., Lindquist, S., and Aguzzi, A. (2007) The prion protein knockout mouse: a phenotype under challenge. *Prion* **1**, 83-93
32. Naslavsky, N., Stein, R., Yanai, A., Friedlander, G., and Taraboulos, A. (1997) Characterization of detergent-insoluble complexes containing the cellular prion protein and its scrapie isoform. *The Journal of biological chemistry* **272**, 6324-6331
33. Caughey, B., Race, R. E., Ernst, D., Buchmeier, M. J., and Chesebro, B. (1989) Prion protein biosynthesis in scrapie-infected and uninfected neuroblastoma cells. *Journal of virology* **63**, 175-181
34. Mange, A., Nishida, N., Milhavet, O., McMahon, H. E., Casanova, D., and Lehmann, S. (2000) Amphotericin B inhibits the generation of the scrapie isoform of the prion protein in infected cultures. *Journal of virology* **74**, 3135-3140
35. Priola, S. A., and McNally, K. L. (2009) The role of the prion protein membrane anchor in prion infection. *Prion* **3**, 134-138
36. Chesebro, B., Trifilo, M., Race, R., Meade-White, K., Teng, C., LaCasse, R., Raymond, L., Favara, C., Baron, G., Priola, S., Caughey, B., Masliah, E., and Oldstone, M. (2005) Anchorless prion protein results in infectious amyloid disease without clinical scrapie. *Science* **308**, 1435-1439
37. Gilch, S., Kehler, C., and Schatzl, H. M. (2006) The prion protein requires cholesterol for cell surface localization. *Molecular and cellular neurosciences* **31**, 346-353

38. Gilch, S., Bach, C., Lutzny, G., Vorberg, I., and Schatzl, H. M. (2009) Inhibition of cholesterol recycling impairs cellular PrP(Sc) propagation. *Cell Mol Life Sci* **66**, 3979-3991
39. Muchowski, P. J., and Wacker, J. L. (2005) Modulation of neurodegeneration by molecular chaperones. *Nature reviews. Neuroscience* **6**, 11-22
40. Lindquist, S. (1986) The heat-shock response. *Annual review of biochemistry* **55**, 1151-1191
41. Kiang, J. G., and Tsokos, G. C. (1998) Heat shock protein 70 kDa: molecular biology, biochemistry, and physiology. *Pharmacol Ther* **80**, 183-201
42. Lindquist, S., and Craig, E. A. (1988) The heat-shock proteins. *Annu Rev Genet* **22**, 631-677
43. Morimoto, R. I., and Santoro, M. G. (1998) Stress-inducible responses and heat shock proteins: new pharmacologic targets for cytoprotection. *Nature biotechnology* **16**, 833-838
44. Auluck, P. K., Chan, H. Y., Trojanowski, J. Q., Lee, V. M., and Bonini, N. M. (2002) Chaperone suppression of alpha-synuclein toxicity in a Drosophila model for Parkinson's disease. *Science* **295**, 865-868
45. Klucken, J., Shin, Y., Masliah, E., Hyman, B. T., and McLean, P. J. (2004) Hsp70 Reduces alpha-Synuclein Aggregation and Toxicity. *The Journal of biological chemistry* **279**, 25497-25502
46. Cummings, C. J., Sun, Y., Opal, P., Antalffy, B., Mestril, R., Orr, H. T., Dillmann, W. H., and Zoghbi, H. Y. (2001) Over-expression of inducible HSP70 chaperone suppresses neuropathology and improves motor function in SCA1 mice. *Hum Mol Genet* **10**, 1511-1518
47. Shinder, G. A., Lacourse, M. C., Minotti, S., and Durham, H. D. (2001) Mutant Cu/Zn-superoxide dismutase proteins have altered solubility and interact with heat shock/stress proteins in models of amyotrophic lateral sclerosis. *The Journal of biological chemistry* **276**, 12791-12796
48. Kakimura, J., Kitamura, Y., Takata, K., Umeki, M., Suzuki, S., Shibagaki, K., Taniguchi, T., Nomura, Y., Gebicke-Haerter, P. J., Smith, M. A., Perry, G., and Shimohama, S. (2002) Microglial activation and amyloid-beta clearance induced by exogenous heat-shock proteins. *FASEB journal : official publication of the Federation of American Societies for Experimental Biology* **16**, 601-603
49. Broquet, A. H., Thomas, G., Masliah, J., Trugnan, G., and Bachelet, M. (2003) Expression of the molecular chaperone Hsp70 in detergent-resistant microdomains correlates with its membrane delivery and release. *The Journal of biological chemistry* **278**, 21601-21606
50. Kryndushkin, D. S., Engel, A., Edskes, H., and Wickner, R. B. (2011) Molecular chaperone Hsp104 can promote yeast prion generation. *Genetics* **188**, 339-348
51. Sweeny, E. A., and Shorter, J. (2015) Mechanistic and Structural Insights into the Prion-Disaggregase Activity of Hsp104. *Journal of molecular biology*
52. Wegrzyn, R. D., Bapat, K., Newnam, G. P., Zink, A. D., and Chernoff, Y. O. (2001) Mechanism of prion loss after Hsp104 inactivation in yeast. *Mol Cell Biol* **21**, 4656-4669
53. Chernoff, Y. O., Lindquist, S. L., Ono, B., Inge-Vechtomov, S. G., and Liebman, S. W. (1995) Role of the chaperone protein Hsp104 in propagation of the yeast prion-like factor [psi+]. *Science* **268**, 880-884

54. Resenberger, U. K., Muller, V., Munter, L. M., Baier, M., Multhaup, G., Wilson, M. R., Winklhofer, K. F., and Tatzelt, J. (2012) The heat shock response is modulated by and interferes with toxic effects of scrapie prion protein and amyloid beta. *The Journal of biological chemistry* **287**, 43765-43776
55. Williams, E. S. (2005) Chronic wasting disease. *Veterinary pathology* **42**, 530-549
56. Williams, E. S., and Young, S. (1980) Chronic wasting disease of captive mule deer: a spongiform encephalopathy. *Journal of wildlife diseases* **16**, 89-98
57. Williams, E. S., and Young, S. (1982) Spongiform encephalopathy of Rocky Mountain elk. *Journal of wildlife diseases* **18**, 465-471
58. Haley, N. J., and Hoover, E. A. (2015) Chronic wasting disease of cervids: current knowledge and future perspectives. *Annu Rev Anim Biosci* **3**, 305-325
59. ProMED-mail. (2016) Chronic Wasting Disease, Cervid - Europe: (Norway). *ProMed-mail* **20160410.4149651**
60. USGS. (2016) Map of Chronic Wasting disease in North America. http://www.nwhc.usgs.gov/images/cwd/cwd_map.jpg
61. Keane, D. P., Barr, D. J., Bochsler, P. N., Hall, S. M., Gidlewski, T., O'Rourke, K. I., Spraker, T. R., and Samuel, M. D. (2008) Chronic wasting disease in a Wisconsin white-tailed deer farm. *Journal of veterinary diagnostic investigation : official publication of the American Association of Veterinary Laboratory Diagnosticians, Inc* **20**, 698-703
62. Sigurdson, C. J., and Miller, M. W. (2003) Other animal prion diseases. *British medical bulletin* **66**, 199-212
63. Williams, E. S., and Young, S. (1993) Neuropathology of chronic wasting disease of mule deer (Odocoileus hemionus) and elk (Cervus elaphus nelsoni). *Veterinary pathology* **30**, 36-45
64. Denkers, N. D., Hayes-Klug, J., Anderson, K. R., Seelig, D. M., Haley, N. J., Dahmes, S. J., Osborn, D. A., Miller, K. V., Warren, R. J., Mathiason, C. K., and Hoover, E. A. (2013) Aerosol transmission of chronic wasting disease in white-tailed deer. *Journal of virology* **87**, 1890-1892
65. Mathiason, C. K., Powers, J. G., Dahmes, S. J., Osborn, D. A., Miller, K. V., Warren, R. J., Mason, G. L., Hays, S. A., Hayes-Klug, J., Seelig, D. M., Wild, M. A., Wolfe, L. L., Spraker, T. R., Miller, M. W., Sigurdson, C. J., Telling, G. C., and Hoover, E. A. (2006) Infectious prions in the saliva and blood of deer with chronic wasting disease. *Science* **314**, 133-136
66. Haley, N. J., Seelig, D. M., Zabel, M. D., Telling, G. C., and Hoover, E. A. (2009) Detection of CWD prions in urine and saliva of deer by transgenic mouse bioassay. *PloS one* **4**, e4848
67. Miller, M. W., Williams, E. S., Hobbs, N. T., and Wolfe, L. L. (2004) Environmental sources of prion transmission in mule deer. *Emerg Infect Dis* **10**, 1003-1006
68. Tamguney, G., Miller, M. W., Wolfe, L. L., Sirochman, T. M., Glidden, D. V., Palmer, C., Lemus, A., DeArmond, S. J., and Prusiner, S. B. (2009) Asymptomatic deer excrete infectious prions in faeces. *Nature* **461**, 529-532
69. Johnson, C. J., Phillips, K. E., Schramm, P. T., McKenzie, D., Aiken, J. M., and Pedersen, J. A. (2006) Prions adhere to soil minerals and remain infectious. *PLoS pathogens* **2**, e32
70. Smith, C. B., Booth, C. J., and Pedersen, J. A. (2011) Fate of prions in soil: a review. *J Environ Qual* **40**, 449-461

71. Nalls, A. V., McNulty, E., Powers, J., Seelig, D. M., Hoover, C., Haley, N. J., Hayes-Klug, J., Anderson, K., Stewart, P., Goldmann, W., Hoover, E. A., and Mathiason, C. K. (2013) Mother to offspring transmission of chronic wasting disease in reeves' muntjac deer. *PloS one* **8**, e71844
72. Johnson, C. J., Herbst, A., Duque-Velasquez, C., Vanderloo, J. P., Bochsler, P., Chappell, R., and McKenzie, D. (2011) Prion protein polymorphisms affect chronic wasting disease progression. *PloS one* **6**, e17450
73. Johnson, C., Johnson, J., Clayton, M., McKenzie, D., and Aiken, J. (2003) Prion protein gene heterogeneity in free-ranging white-tailed deer within the chronic wasting disease affected region of Wisconsin. *Journal of wildlife diseases* **39**, 576-581
74. O'Rourke, K. I., Spraker, T. R., Hamburg, L. K., Besser, T. E., Brayton, K. A., and Knowles, D. P. (2004) Polymorphisms in the prion precursor functional gene but not the pseudogene are associated with susceptibility to chronic wasting disease in white-tailed deer. *The Journal of general virology* **85**, 1339-1346
75. Duque Velasquez, C., Kim, C., Herbst, A., Daude, N., Garza, M. C., Wille, H., Aiken, J., and McKenzie, D. (2015) Deer Prion Proteins Modulate the Emergence and Adaptation of Chronic Wasting Disease Strains. *Journal of virology* **89**, 12362-12373
76. van Keulen, L. J., Vromans, M. E., and van Zijderveld, F. G. (2002) Early and late pathogenesis of natural scrapie infection in sheep. *APMIS : acta pathologica, microbiologica, et immunologica Scandinavica* **110**, 23-32
77. Prinz, M., Huber, G., Macpherson, A. J., Heppner, F. L., Glatzel, M., Eugster, H. P., Wagner, N., and Aguzzi, A. (2003) Oral prion infection requires normal numbers of Peyer's patches but not of enteric lymphocytes. *The American journal of pathology* **162**, 1103-1111
78. Mabbott, N. A., Young, J., McConnell, I., and Bruce, M. E. (2003) Follicular dendritic cell dedifferentiation by treatment with an inhibitor of the lymphotoxin pathway dramatically reduces scrapie susceptibility. *Journal of virology* **77**, 6845-6854
79. van Keulen, L. J., Schreuder, B. E., Vromans, M. E., Langeveld, J. P., and Smits, M. A. (2000) Pathogenesis of natural scrapie in sheep. *Archives of virology. Supplementum*, 57-71
80. Glatzel, M., Heppner, F. L., Albers, K. M., and Aguzzi, A. (2001) Sympathetic innervation of lymphoreticular organs is rate limiting for prion neuroinvasion. *Neuron* **31**, 25-34
81. Haik, S., Faucheux, B. A., Sazdovitch, V., Privat, N., Kemeny, J. L., Perret-Liaudet, A., and Hauw, J. J. (2003) The sympathetic nervous system is involved in variant Creutzfeldt-Jakob disease. *Nature medicine* **9**, 1121-1123
82. Ironside, J. W., McCardle, L., Horsburgh, A., Lim, Z., and Head, M. W. (2002) Pathological diagnosis of variant Creutzfeldt-Jakob disease. *APMIS : acta pathologica, microbiologica, et immunologica Scandinavica* **110**, 79-87
83. Hill, A. F., Butterworth, R. J., Joiner, S., Jackson, G., Rossor, M. N., Thomas, D. J., Frosh, A., Tolley, N., Bell, J. E., Spencer, M., King, A., Al-Sarraj, S., Ironside, J. W., Lantos, P. L., and Collinge, J. (1999) Investigation of variant Creutzfeldt-Jakob disease and other human prion diseases with tonsil biopsy samples. *Lancet* **353**, 183-189
84. Wadsworth, J. D., Joiner, S., Hill, A. F., Campbell, T. A., Desbruslais, M., Luthert, P. J., and Collinge, J. (2001) Tissue distribution of protease resistant prion protein in variant

Creutzfeldt-Jakob disease using a highly sensitive immunoblotting assay. *Lancet* **358**, 171-180
85. Fox, K. A., Jewell, J. E., Williams, E. S., and Miller, M. W. (2006) Patterns of PrPCWD accumulation during the course of chronic wasting disease infection in orally inoculated mule deer (Odocoileus hemionus). *The Journal of general virology* **87**, 3451-3461
86. Sigurdson, C. J., Williams, E. S., Miller, M. W., Spraker, T. R., O'Rourke, K. I., and Hoover, E. A. (1999) Oral transmission and early lymphoid tropism of chronic wasting disease PrPres in mule deer fawns (Odocoileus hemionus). *The Journal of general virology* **80 (Pt 10)**, 2757-2764
87. Bolea, R., Monleon, E., Schiller, I., Raeber, A. J., Acin, C., Monzon, M., Martin-Burriel, I., Struckmeyer, T., Oesch, B., and Badiola, J. J. (2005) Comparison of immunohistochemistry and two rapid tests for detection of abnormal prion protein in different brain regions of sheep with typical scrapie. *Journal of veterinary diagnostic investigation : official publication of the American Association of Veterinary Laboratory Diagnosticians, Inc* **17**, 467-469
88. Spraker, T. R., O'Rourke, K. I., Balachandran, A., Zink, R. R., Cummings, B. A., Miller, M. W., and Powers, B. E. (2002) Validation of monoclonal antibody F99/97.6.1 for immunohistochemical staining of brain and tonsil in mule deer (Odocoileus hemionus) with chronic wasting disease. *Journal of veterinary diagnostic investigation : official publication of the American Association of Veterinary Laboratory Diagnosticians, Inc* **14**, 3-7
89. Spraker, T. R., Zink, R. R., Cummings, B. A., Wild, M. A., Miller, M. W., and O'Rourke, K. I. (2002) Comparison of histological lesions and immunohistochemical staining of proteinase-resistant prion protein in a naturally occurring spongiform encephalopathy of free-ranging mule deer (Odocoileus hemionus) with those of chronic wasting disease of captive mule deer. *Veterinary pathology* **39**, 110-119
90. Safar, J. G., Geschwind, M. D., Deering, C., Didorenko, S., Sattavat, M., Sanchez, H., Serban, A., Vey, M., Baron, H., Giles, K., Miller, B. L., Dearmond, S. J., and Prusiner, S. B. (2005) Diagnosis of human prion disease. *Proc Natl Acad Sci U S A* **102**, 3501-3506
91. Tzaban, S., Friedlander, G., Schonberger, O., Horonchik, L., Yedidia, Y., Shaked, G., Gabizon, R., and Taraboulos, A. (2002) Protease-sensitive scrapie prion protein in aggregates of heterogeneous sizes. *Biochemistry* **41**, 12868-12875
92. Haley, N. J., Mathiason, C. K., Carver, S., Telling, G. C., Zabel, M. D., and Hoover, E. A. (2012) Sensitivity of protein misfolding cyclic amplification versus immunohistochemistry in ante-mortem detection of chronic wasting disease. *The Journal of general virology* **93**, 1141-1150
93. Colby, D. W., Zhang, Q., Wang, S., Groth, D., Legname, G., Riesner, D., and Prusiner, S. B. (2007) Prion detection by an amyloid seeding assay. *Proc Natl Acad Sci U S A* **104**, 20914-20919
94. Atarashi, R., Moore, R. A., Sim, V. L., Hughson, A. G., Dorward, D. W., Onwubiko, H. A., Priola, S. A., and Caughey, B. (2007) Ultrasensitive detection of scrapie prion protein using seeded conversion of recombinant prion protein. *Nature methods* **4**, 645-650
95. Saborio, G. P., Permanne, B., and Soto, C. (2001) Sensitive detection of pathological prion protein by cyclic amplification of protein misfolding. *Nature* **411**, 810-813
96. LeVine, H., 3rd. (1999) Quantification of beta-sheet amyloid fibril structures with thioflavin T. *Methods in enzymology* **309**, 274-284

97. Haley, N. J., Carver, S., Hoon-Hanks, L. L., Henderson, D. M., Davenport, K. A., Bunting, E., Gray, S., Trindle, B., Galeota, J., LeVan, I., Dubovos, T., Shelton, P., and Hoover, E. A. (2014) Detection of chronic wasting disease in the lymph nodes of free-ranging cervids by real-time quaking-induced conversion. *Journal of clinical microbiology* **52**, 3237-3243
98. McGuire, L. I., Peden, A. H., Orru, C. D., Wilham, J. M., Appleford, N. E., Mallinson, G., Andrews, M., Head, M. W., Caughey, B., Will, R. G., Knight, R. S., and Green, A. J. (2012) Real time quaking-induced conversion analysis of cerebrospinal fluid in sporadic Creutzfeldt-Jakob disease. *Annals of neurology* **72**, 278-285
99. Peden, A. H., McGuire, L. I., Appleford, N. E., Mallinson, G., Wilham, J. M., Orru, C. D., Caughey, B., Ironside, J. W., Knight, R. S., Will, R. G., Green, A. J., and Head, M. W. (2012) Sensitive and specific detection of sporadic Creutzfeldt-Jakob disease brain prion protein using real-time quaking-induced conversion. *The Journal of general virology* **93**, 438-449
100. Henderson, D. M., Denkers, N. D., Hoover, C. E., Garbino, N., Mathiason, C. K., and Hoover, E. A. (2015) Longitudinal Detection of Prion Shedding in Saliva and Urine by Chronic Wasting Disease-Infected Deer by Real-Time Quaking-Induced Conversion. *Journal of virology* **89**, 9338-9347
101. Zanusso, G., Bongianni, M., and Caughey, B. (2014) A test for Creutzfeldt-Jakob disease using nasal brushings. *The New England journal of medicine* **371**, 1842-1843
102. Haley, N. J., Siepker, C., Walter, W. D., Thomsen, B. V., Greenlee, J. J., Lehmkuhl, A. D., and Richt, J. A. (2016) Antemortem Detection of Chronic Wasting Disease Prions in Nasal Brush Collections and Rectal Biopsy Specimens from White-Tailed Deer by Real-Time Quaking-Induced Conversion. *Journal of clinical microbiology* **54**, 1108-1116
103. Zanusso, G., Monaco, S., Pocchiari, M., and Caughey, B. (2016) Advanced tests for early and accurate diagnosis of Creutzfeldt-Jakob disease. *Nat Rev Neurol*
104. Henderson, D. M., Manca, M., Haley, N. J., Denkers, N. D., Nalls, A. V., Mathiason, C. K., Caughey, B., and Hoover, E. A. (2013) Rapid antemortem detection of CWD prions in deer saliva. *PloS one* **8**, e74377
105. Henderson, D. M., Davenport, K. A., Haley, N. J., Denkers, N. D., Mathiason, C. K., and Hoover, E. A. (2015) Quantitative assessment of prion infectivity in tissues and body fluids by real-time quaking-induced conversion. *The Journal of general virology* **96**, 210-219
106. Wilham, J. M., Orru, C. D., Bessen, R. A., Atarashi, R., Sano, K., Race, B., Meade-White, K. D., Taubner, L. M., Timmes, A., and Caughey, B. (2010) Rapid end-point quantitation of prion seeding activity with sensitivity comparable to bioassays. *PLoS pathogens* **6**, e1001217
107. Deleault, N. R., Piro, J. R., Walsh, D. J., Wang, F., Ma, J., Geoghegan, J. C., and Supattapone, S. (2012) Isolation of phosphatidylethanolamine as a solitary cofactor for prion formation in the absence of nucleic acids. *Proc Natl Acad Sci U S A* **109**, 8546-8551
108. Deleault, N. R., Lucassen, R. W., and Supattapone, S. (2003) RNA molecules stimulate prion protein conversion. *Nature* **425**, 717-720
109. Wang, F., Wang, X., Yuan, C. G., and Ma, J. (2010) Generating a prion with bacterially expressed recombinant prion protein. *Science* **327**, 1132-1135

110. Trevitt, C. R., and Collinge, J. (2006) A systematic review of prion therapeutics in experimental models. *Brain : a journal of neurology* **129**, 2241-2265
111. Mori, T., Atarashi, R., Furukawa, K., Takatsuki, H., Satoh, K., Sano, K., Nakagaki, T., Ishibashi, D., Ichimiya, K., Hamada, M., Nakayama, T., and Nishida, N. (2016) A direct assessment of human prion adhered to steel wire using real-time quaking-induced conversion. *Sci Rep* **6**, 24993

CHAPTER 1:
Heat shock protein 72 expression in neurons does not alter prion pathogenesis

Summary

Heat shock proteins are molecular chaperones that function during periods of stress to maintain cellular proteostasis by rescuing denatured proteins and preventing aberrant aggregation. Expression of the major inducible member of the 70 kDa heat shock protein family (HSP72), has been shown to protect against the pathologic effects in models of neurodegenerative diseases, including Alzheimer's disease, Parkinson's disease, and spinocerebellar ataxia, by decreasing protein aggregation and preventing cytotoxicity. Prion investigations in yeast have illustrated heat shock proteins have disaggregase activity which can both propagate prions and "cure" cells, however, the role of heat shock proteins in mammalian prion diseases remains unknown. We investigated this role *in vitro* by exposing murine neuroblastoma cells stably transfected to constitutively express HSP72 (N2a-HSP72) and their vector transfected controls to mouse-adapted scrapie (RML) brain homogenate or normal FVB mouse brain controls. Following RML prion exposure, the N2a-V cells exhibited a reduced growth rate compared with RML-exposed N2a-HSP72 cells. However, examination of the prion burden by real-time quaking induced conversion revealed no differences between the groups. We extended our HSP72 study to *in vivo* studies by inoculating transgenic C57Bl/6 mice engineered to constitutively express HSP72 in neurons or C57Bl/6 control mice with RML prions by intracranial or intraperitoneal routes. We observed no differences in the course of prion disease, brain prion accumulation, or pathology between the two mouse strains. Overall, we demonstrate the expression of HSP72 in neurons does not alter prion pathogenicity.

Background

Organisms have cellular protein quality controls mechanisms to maintain proteostasis and counteract protein denaturation and aggregation that can occur during periods of stress (1). One of the best characterized systems is a group of molecular chaperones, the heat shock proteins, with a member of the 70 kDa protein family (HSP72) being the major stress-inducible protein in mammals (1,2). These proteins are upregulated under control of the HSF1 promotor following stress triggers including hypoxia, ischemia, and hyperthermia, and act to refold proteins back to functional conformations or target damaged proteins for degradation via the ubiquitin-proteosome system (1,3).

Several neurodegenerative diseases share the feature of aberrant protein folding and aggregation with prion diseases, including Alzheimer's disease (AD), Parkinson's disease, and the polyglutamine-repeat disease Huntington's disease (3,4). In several of these diseases, the expression of molecular chaperones, particularly HSP72, improved disease-related pathogenesis. Cell culture studies of AD demonstrated expression of HSP72 decreased tau aggregation and rescued neurons from amyloid-β associated toxicity (5,6). HSP72 expression also decreased toxicity in drosophila model of α-synuclein-mediated neurodegeneration demonstrated by increased cell viability but did not alter protein aggregation levels (7,8). *In vivo* models of AD and spinocerebellar ataxia have shown that overexpression of HSP72 suppresses clinical disease and decreases the levels of pathogenic protein aggregation in the brain (9,10). These studies highlight the protective role HSP72 can play in neurodegenerative diseases and has generated discussion regarding its potential as a therapeutic target (11).

The majority of studies investigating the interactions of heat shock proteins and prions are limited to yeast or mammalian cell culture. In yeast, the major inducible stress protein is

HSP104 and research has illustrated its important disaggregase function in prion pathogenesis (12). HSP104 is required for propagation of prion pathogenesis as it operates to break apart prion aggregates and create more seeds to nucleate prion conversion (13,14). In contrast, overexpression of HSP104 can "cure" yeast of prion infection by disaggregating enough prion to remove infection (13,15).

Investigations of HSP72 function in mammalian *in vitro* models of TSEs have identified similarities with other protein misfolding diseases. Scrapie infection in murine neuroblastoma cells disrupts the ability of cells to mount the heat shock response due to increased degradation of HSF1, suggesting heat shock proteins are involved in prion pathogenesis (16). Moreover, a follow up investigation found that pharmacologic induction of the heat shock response or elevated levels of HSP72 due to co-culture conditions prolonged cell survival of prion-infected cells (17).

Based on literature demonstrating the protective role of HSP72 in protein-misfolding diseases, we hypothesized expression of HSP72 could prevent prion-associated pathology. We investigated the protective role of HSP72 *in vitro* and *in vivo* using cell culture and mouse-adapted models of scrapie, by comparing survival and pathology following prion challenge in the face of constitutive HSP72 expression in neurons. In contrast to the function of HSP104 in yeast and HSP72 neurodegenerative disease models, we did not observe a positive influence on HSP72 pathogenesis or survival in cell culture or mice. Instead, HSP72 expression did not alter the prion disease course, levels of prion accumulation, or prion-induced pathology.

Methods

Murine neuroblastoma cell culture and infection

Murine neuroblastoma cells (N2a) engineered to constitutively express heat shock protein 72 were kindly provided by Dr. Michael Oglesbee at The Ohio State University. Briefly, cells were stably transfected with a plasmid vector containing the human HSP72 construct driven by the β-actin promotor (N2a-HSP72) or the empty plasmid vector alone (designated N2a-V) (18,19). Selection of transfected cells was ensured with a neomycin resistance gene. Cells were maintained in Advanced Minimal Essential Media (MEM) (Gibco) supplemented with 10% fetal bovine serum (Gibco), 1% penicillin-streptomycin (Gibco), 1% GlutaMax (Thermo Fisher Scientific), and 0.8% geneticin (G418) (Thermo Fischer Scientific) selection antibiotic. Media was changed every 4 days and cells were passaged weekly using 0.25% trypsin-EDTA (Gibco) to release the cells.

N2a cells were exposed to Rocky Mountain Laboratory strain of mouse-adapted scrapie (RML) prion brain homogenate or prion-negative FVB normal mouse brain homogenate. Brain homogenate inoculum was diluted to 0.1% in sterile 1xPBS. One x 10^5 cells were incubated with 100 µL of 0.1% brain inoculum for 30 minutes at room temperature and then plated in one well of a 12-well plate at 37°C with 1 mL of prepared media. Cell culture media was changed 24 hours after plating. Cells were observed daily for cell density and cytopathic effect and cell Cohorts were harvested at 72 hours post-exposure and counted. The cell infection experiment was repeated three times and the data averaged.

Real-time quaking induced conversion (RT-QuIC) of cell lysates

Cell lysis

At the time of collection, brain-homogenate exposed cells and control cells were passaged as previously described. One x 10^5 cells were pelleted by centrifugation at 1,000 x rpm and lysed with 100 µL of lysis buffer (5mM EDTA, 150 mM NaCl, 1.0% Triton™ X-100 [Sigma-Aldrich]). Cell lysates were subjected to 2 freeze/thaw cycles prior to centrifugation at 15,000 x rpm to pellet debris. Supernatants were removed and stored at -80°C until RT-QuIC analysis.

RT-QuIC substrate purification:

Recombinant truncated Syrian hamster prion protein (SHrPrP), containing residues 90-231, was purified as previously described (20,21). BL21 Rosetta (Novagen) Escherichia coli containing the truncated protein construct were cultured from a glycerol stock at 37°C in lysogeny broth (LB) media with the selection antibiotics kanamycin and chloramphenicol to express SHrPrP until the culture optical density at 600 nm (OD^{600}) reached at least 2.5. E. coli cell lysis was carried out using Bugbuster™ reagent supplemented with Lysonase™ (EMD Biosciences) according to the manufacturer recommended protocol. Inclusion bodies were harvested by centrifugation at 15,000 x g and dissolved in solubilization buffer (8M guanidine hydrochloride, 100 mM Na_2HPO_4) prior to application to NiNTA flow resin (Qiagen) that had been previously equilibrated with denaturation buffer (6M guanidine hydrochloride, 100 mM Na_2HPO_4, 10mM Tris, pH 8.0). The NiNTA resin-SHrPrP was loaded onto a XK16-60 column (GE Healthcare) and purified using a Bio-Rad Duoflow™ FPLC. To induce protein refolding, a gradient from denaturation buffer to refolding buffer (100 mM Na_2HPO_4, 10mM Tris pH 5.5) was applied. Refolding was followed by a gradient from refolding to elution buffer (100mM

Na_2HPO_4, 10 mM Tris, 0.5 M imidazole) and fractions from the elution peak were pooled and dialyzed in two changes of buffer (20mM NaH_2PO_4, pH 5.5) overnight. Final protein concentration was calculated by measuring the A_{280} and using a coefficient of extinction of 25,900 in Beer's Law. Purified SHrPrP was stored at 4°C until use.

RT-QuIC conditions

RT-QuIC was performed as previously described (20,22). Cell lysates were diluted 1,000-fold and brain homogenates were diluted to the desired concentration in 0.1% sodium dodecyl sulfate (SDS)/1xPBS prior to seeding RT-QuIC. The RT-QuIC reaction was carried out by adding 2 μL of diluted sample to a buffer containing 20mM NaH_2PO_4, 430mM NaCl, 1.0 EDTA, 1mM Thioflavin T (ThT) and 0.1 mg/mL SHrPrP in one well of a black, optical-bottom 96-well plate (Nunc). RT-QuIC experiments were carried out in a BMG Labtech Polarstar™ fluorometer with cycles of 1 minute shaking (700 rpm, double orbital) followed by 1 minute rest, repeated for 15 minutes. ThT fluorescence was read (excitation 450 nm, emission 480 nm, gain of 1700) at the conclusion of each 15 minute shake/rest cycle and each well was measured with 20 flashes per well with an orbital average of 4. Each RT-QuIC experiment was performed for a minimum of 200 cycles or 48 hours. RT-QuIC amyloid formation was determined to be positive if the fluorescence exceeded a threshold determined to be 5 standard deviations above the average baseline fluorescence. RT-QuIC amyloid formation rates in RT-QuIC were analyzed by calculating the inverse of the time to threshold.

Animals

Transgenic C57BL/6 mice engineered to constitutively express HSP72 in neurons under control of the neuron-specific enolase promoter (TgNSE-HSP72) were generated as previously described and kindly provided by Dr. Michael Oglesbee, the Ohio State University of Columbus,

OH (23). Mice were bred and maintained at Colorado State University according to protocols approved by the Institutional Animal Care and Use committee. Age-matched C57Bl/6 mice used as controls were purchased from Jackson Laboratories (Bar Harbor, ME).

Prion inoculation protocol

The prion positive inoculum used was the Rocky Mountain Laboratory strain of mouse-adapted scrapie (RML), as characterized previously (24). RML was passaged 5 times through FVB mice and a 10% weight/volume brain homogenate was prepared in sterile 1xPBS. The negative control inoculum was a 10% weight/volume normal brain homogenate of FVB mouse origin prepared similarly. Both positive and negative inocula were diluted to a final concentration of 0.1% (wt/vol) in sterile PBS containing 100 U/mL penicillin-streptomycin.

To study the effect of HSP72 expression on prion trafficking to nervous tissues, we used an intraperitoneal (IP) route to mimic peripheral prion exposure. Six to eight week old, mixed sex, mice of TgNSE-HSP72 or C57Bl/6 were restrained and inoculated with 100 μL of 0.1% RML or FVB brain homogenate with a minimum of 5 mice per inoculum group. To study the effect of HSP72 expression following direct exposure, mice were inoculated by intracranial route. First, six to eight week old mice of mixed sex were anesthetized through inhalational isoflurane. Mice were then inoculated with 30 μL of either 0.1% RML or FVB inocula via a 29-guage needle through the calvarium into the left parietal lobe of the cerebral cortex. Throughout the course of study, mice were evaluated for clinical signs of prion disease as has been previously published (25) (severe ataxia, weight loss, tail rigidity, general tremors) and euthanized at the onset of terminal neurologic disease or at 400 days when the study was completed. The distribution of mice by strain and inoculation group are summarized in Figure

1.1. Following euthanasia, mice were necropsied and brains collected with clean prion-free instruments. The brain was divided in half sagittally, with half being frozen at -80ºC until processing and the other half fixed in 10% neutral buffered formalin until sectioning and routine histology processing.

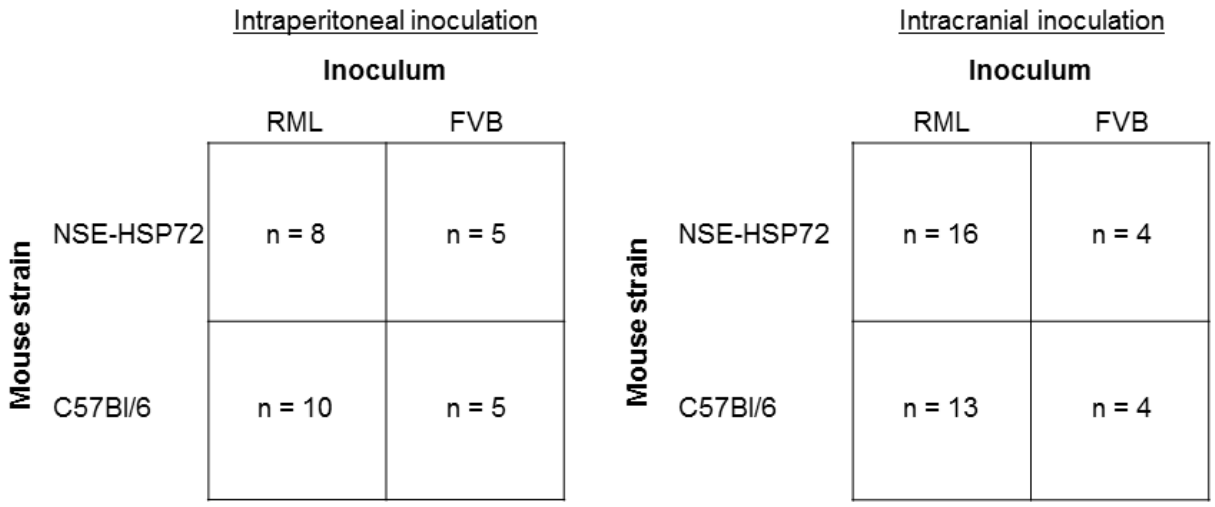

Figure 1.1 Summary of inoculation groups and mouse strain distribution.
The tables summarize the number of mice in each inoculation group by mouse strain and inoculum.

Mouse tissue processing

Formalin fixed mouse brain halves were sectioned coronally into 2-3 mm slices to represent the following anatomic locations: cerebral cortex, hippocampus and thalamus, midbrain, cerebellum, and brainstem. Brain sections were cassetted and submitted for routine histologic paraffin embedding.

Characterization of infected mice

All mouse brains were evaluated for PrP^{Sc} by western blot and immunohistochemistry.

Western blotting

Mouse brain homogenates were evaluated for PrP^{Sc} deposition by western blotting. Endogenous PrP^{C} in brain samples was digested by incubating 9 µL of 10% brain homogenate with proteinase K (PK) at a final concentration of 5 µg/mL at 37ºC for 30 minutes with shaking followed by 45ºC for 10 minutes with shaking. Samples were mixed with a final 1x concentration of reducing agent /LDS sample buffer (Invitrogen) and heated at 95ºC for 5 minutes. Samples were loaded on a NuPAGE 10% Bis-Tris gel (Invitrogen) and electrophoresed at 130 V for 2 hours. Proteins were transferred to a polyvinylidene fluoride (PVDF) membrane using a Transblot Turbo™ system (Bio-Rad) following manufacturer recommendations. The membrane was loaded into a pre-wetted SNAP i.d. blot holder (Millipore) then sequentially blocked with blocking buffer (Blocker Casein in TBS [Thermo-Scientific] and 0.1% Tween-20 [Sigma]) for 3 minutes and probed with antibody BAR224 (Cayman Chemical) conjugated to horseradish-peroxidase (HRP) diluted to 0.2µg/mL in blocking buffer for 10 minutes. Antibody was removed by vacuuming through the membrane using the SNAP i.d. system (Millipore) and the membrane was washed three times with 30 mL wash buffer (50% Blocker Casein in TBS, 50% 1X TBS, 0.1% Tween-20) with continuous vacuum. The membrane was developed with ECL-Plus Western Blotting Detection Reagents (GE) and viewed on a Luminescent Image Analyzer LAS-3000 (GE).

Histology and Immunohistochemistry

Brain sections were stained with hematoxylin and eosin (H&E) for routine histologic examination and evaluated for PrP^{Sc} deposition by immunohistochemistry (IHC). IHC was

performed as follows: tissues were paraffin-embedded following routine histologic processing. Five μm tissue sections were cut with a microtome (Leica) from paraffin embedded tissue blocks and placed on positively charged glass slides. Slides were heated in an incubator prior to routine deparaffinization by immersion in xylene and tissue rehydration by immersion in a series of graded alcohols (100%, 95%, and 70%). Slides were rinsed and then endogenous PrP^C was digested by treatment with 1.0 μg/mL PK in 1.0mM $CaCl_2$, 50mM Tris buffer (pH7.6) for 30 minutes at 37ºC. Epitopes were exposed through hydrated autoclaving heat-induced epitope retrieval (The Retriever™, Prestige Medical) in 10 mM EDTA (pH 6.0) followed by a brief 5 minute immersion in 88% formic acid. Sequentially, endogenous peroxide activity was blocked by treatment with 3.0% hydrogen peroxide in methanol and tissue sections were blocked with TNB blocker (Perkin-Elmer). Slides were incubated with anti-prion primary antibody BAR224 (Cayman Chemical) diluted to 2 μg/mL in blocker overnight at 4ºC. Immunoreactivity was detected by incubation with Envision+™ anti-mouse secondary antibody conjugated with horseradish peroxidase (Dako) and visualized by incubation with AEC substrate chromogen (Dako). Slides were washed with TNT buffer (1.0M Tris, 0.15M NaCl, 0.05% Tween-20 [pH 7.5]) between each step in the above protocol. Slides were counterstained with Mayer's hematoxylin (Dako) and bluing reagent (0.1% sodium bicarbonate, 1xPBS) prior to coverslip mounting with aqueous mounting media (Dako).

Results

HSP72 expression potentially increases cell viability in vitro following prion infection

Previous studies have demonstrated HSP72 production is decreased in neuroblastoma cells persistently infected with scrapie prions while over-expression of HSP104 in yeast can disaggregate and "cure" prion infection in yeast (16,26). Therefore, we hypothesized

constitutive expression of HSP72 would prevent prion-associated cytotoxicity as measured by increased cell survival and decreased cellular pathology. N2a cells constitutively expressing HSP72 (N2a-HSP72) or the empty vector (N2a-V) were exposed to either 0.1% RML prion mouse brain homogenate or 0.1% FVB normal mouse brain homogenate. At 24 hours post-brain inoculum exposure, cell cohorts exposed to either RML or FVB normal brain homogenate displayed decreased cell density and an increased amount of debris in the media when compared to unexposed control cells (Figure 1.2A). N2a-V cells exposed to RML often displayed decreased cell density, however, the degree of this effect often varied between experiments. By 72 hours post-exposure, unexposed N2a-HSP72 and N2a-V control cells had reached 90-100% confluency and all cell cohorts were passaged and counted. Visually, cells exposed to brain homogenate, either RML or FVB, appeared to have less cell density, with N2a-V cells exposed to RML displaying the least cell density (Figure 1.2B). Cell counts at 72 hours post-exposure confirmed the cell growth patterns observed with unexposed control cells displaying the greatest growth and N2a-V cells exposed to RML displaying the least growth (Table 1.1). No differences between N2a-HSP72 and N2a-V cell counts were observed and only minimal differences in cell density was observed between N2a-HSP72 cells exposed to FVB or RML brain homogenate. These results suggest HSP72 expression protected N2a cells against the insult of prion brain homogenate exposure.

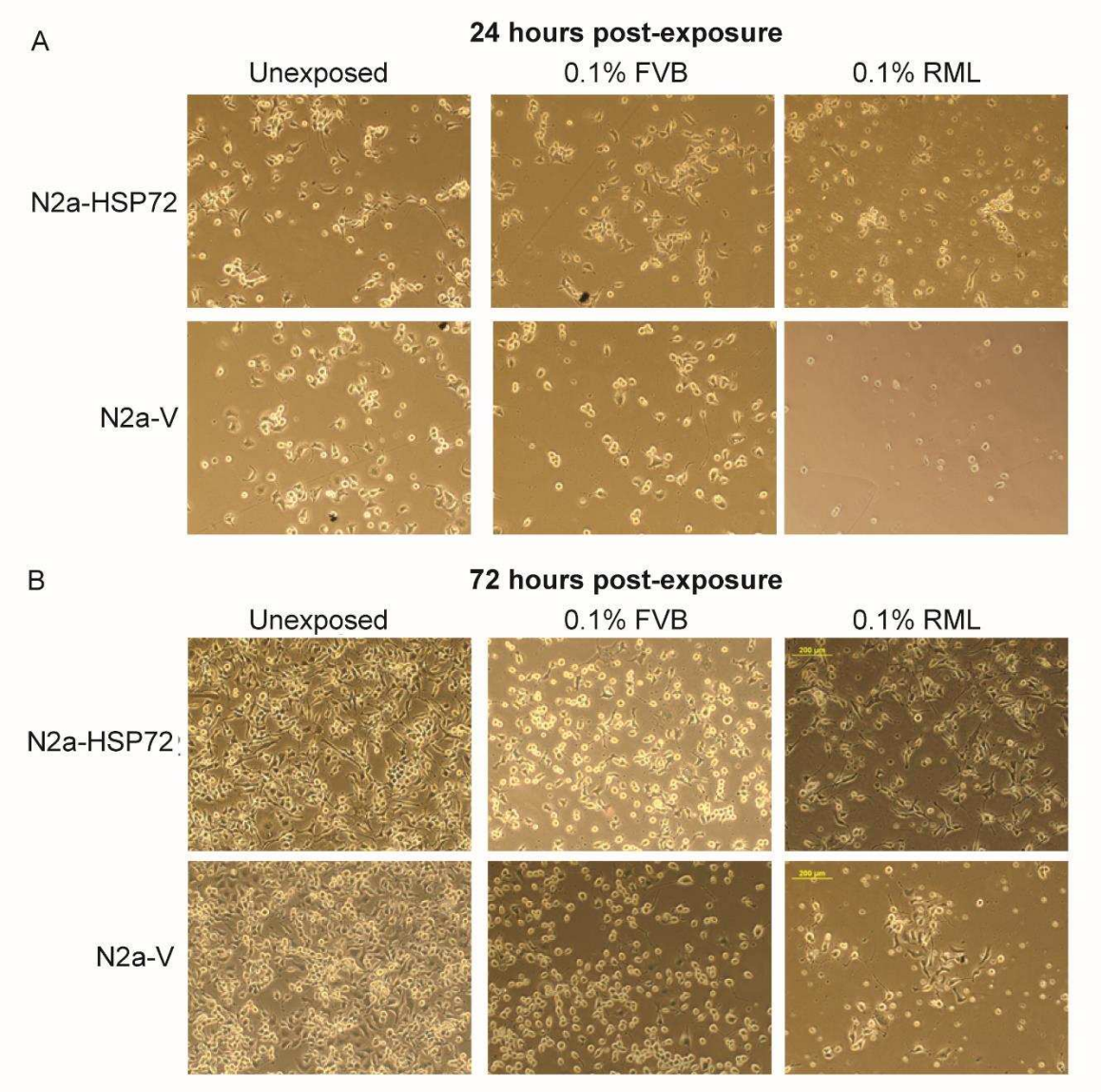

Figure 1.2 Microscopic evaluation of cells 24 and 72 hours following prion exposure.
A. Cell images 24 hours following prion exposure. Comparable cell densities are observed between unexposed cells, cells exposed to FVB brain homogenate, and N2a-HSP72 cells exposed to RML. N2a-V cells exposed to RML had the least cell density. All images 10x magnification.
B. Cell images 72 hours following prion exposure. Unexposed control cells are 90-100% confluent. Decreased cell density was observed in all cells exposed to brain homogenate inoculum. Cell density appeared equivalent between cells exposed to control FVB brain homogenate and N2a-HSP72 cells exposed to RML. N2a-V cells exposed to RML had the least cell density. All images 10x magnification.

Table 1.1 Cell counts 72 hours post-exposure.
Similar to Figure 1.2, treatment with either RML or FVB brain homogenate caused a decrease in cell viability when compared with unexposed controls. N2a-HSP72 cells exposed to RML display similar cell counts as cells exposed to FVB brain homogenate, however, N2a-V cells exposed to RML displayed the least cell viability. Data represents average cell counts from 3 experiments.

	Uninfected	0.1% FVB	0.1% RML
N2a-HSP72	1.59×10^6	0.63×10^6	0.66×10^6
N2a-V	1.64×10^6	0.50×10^6	0.31×10^6

RT-QuIC of prion-exposed cell lysates

We predicted HSP72 expression would prevent prion protein conversion; thus, we expected N2a-HSP72 cells to produce less PrP^{Sc} than N2a-V following RML infection. We compared the amount of PrP^{Sc} in cell lysates collected over 6 passages by RT-QuIC amyloid formation kinetics. First, we demonstrated mouse-origin RML prions could convert SHrPrP substrate into amyloid and be detected by RT-QuIC (Figure 1.3). We seeded the RT-QuIC reaction with a dilutional series of RML infected mouse brain homogenate from 10^{-4} to 10^{-9} and a corresponding dilutional series of FVB negative brain homogenate and were able to specifically detect RML prion-seeded amyloid formation from 10^{-4} to 10^{-6} dilutions. No spontaneous amyloid formation in FVB seeded reactions was observed.

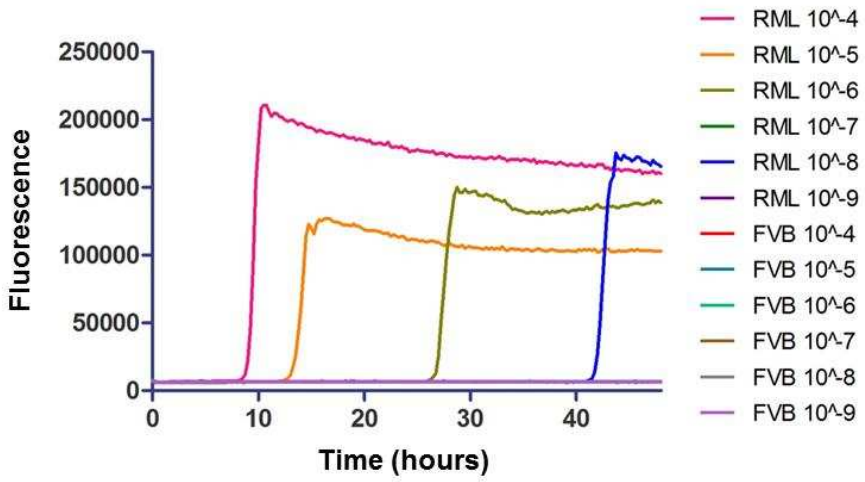

Figure 1.3 Representative RT-QuIC fluorescence curves of RML dilutional series. A dilutional series of RML brain homogenate and FVB brain homogenate demonstrate mouse-origin RML prions successfully seed the RT-QuIC reaction using SHrPrP substrate. The detection range extended from 10^{-4} to 10^{-6} dilution and intermittent detection was observed after 10^{-7}. No spontaneous amyloid formation was observed in reactions seeded with FVB brain homogenate.

Next, we analyzed cell lysates collected from the immediate post-infection time period for RT-QuIC prion-templated amyloid formation to ensure our protocol was capable of generating cell infection and our N2a clones were susceptible to infection. At 1 hour post-exposure, no prion-seeded amyloid formation was detected in cell lysates (Figure 1.4B). At 24 hours post-exposure, robust RT-QuIC amyloid formation, at levels comparable to the inoculum, was observed in cells exposed to RML indicating our N2a cells were capable of *de novo* prion conversion (Figure 1.4B). Although RT-QuIC detected prion-seeded amyloid formation in cells exposed to RML at 72 hours post-exposure, the time to detectable amyloid formation was slower, suggestive of a decreased prion burden when compared with the 24 hour collection. Overall, these findings show our N2a-HSP72 and N2a-V cells are susceptible to RML prion infection but potentially not sustaining infection.

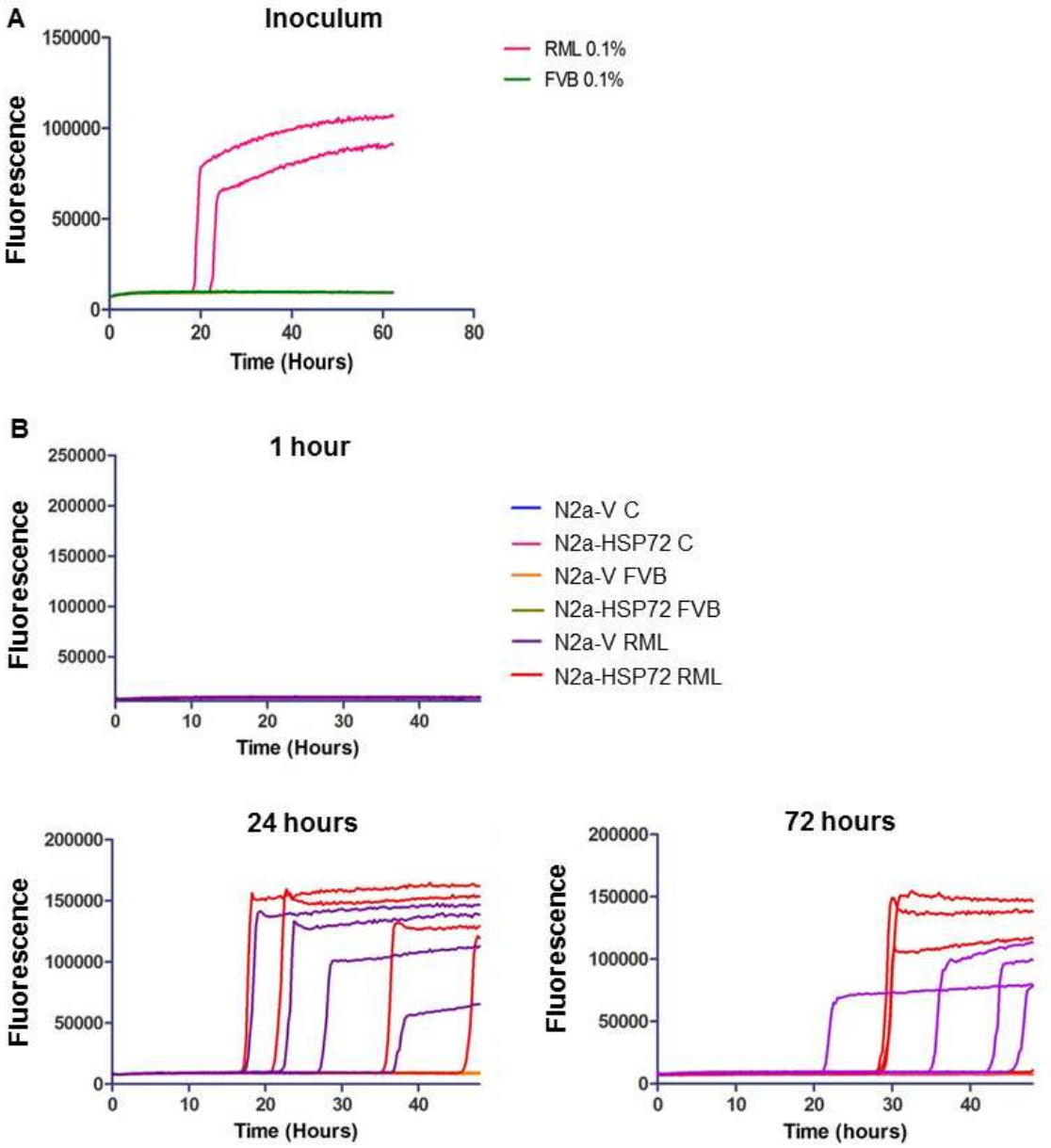

Figure 1.4 RT-QuIC of early cell culture infection.
A. RT-QuIC of cell infection inoculum. RT-QuIC detected RML at the 0.1% concentration used to inoculate N2a cells.
B. RT-QuIC of cell lysates 1 hour to 72 hours post-brain homogenate exposure. No prion-seeded RT-QuIC amplification was detected 1 hour post-exposure. Prion-seeded RT-QuIC amplification was detected in N2a-V and N2a-HSP72 cells harvested 24 hours after exposure to RML brain homogenate. No spontaneous amyloid conversion was detected in cells exposed to FVB brain homogenate or unexposed controls (N2a-V C and N2a-HSP72 C). At 72 hours post-exposure, RT-QuIC prion seeding was still restricted to cells exposed to RML inoculum, however, the time to positive was delayed by approximately 10 hours compared with the 24 hour collection. No spontaneous amyloid formation was detected in cells exposed to FVB inoculum or unexposed controls.

HSP72 functions by correcting aberrant protein folding and preventing aggregation. Therefore, we predicted cells that constitutively expressed HSP72 would produce less PrP^{Sc} and eliminate prion infection at an earlier passage when compared with control N2a-V cells. To analyze the PrP^{Sc} burden over time, we evaluated the level of prion production in cells following prion infection over 6 passages by RT-QuIC rate analysis. Previous studies have established the RT-QuIC amyloid formation rate directly correlates with the prion concentration in the sample seeding the reaction (20,21). At passage 1, RT-QuIC prion-seeded amyloid formation was limited to N2a-HSP72 and N2a-V cells exposed to RML, consistent with prion infection (Figure 1.5). Over the 6 passages, the rates of amyloid formation remained equivalent between N2a-HSP72 and N2a-V RML-infected cells ($p>0.05$, Mann-Whitney non-parametric test). We also observed that the rate of amyloid formation in these cells steadily decreased between subsequent passages indicating the amount of PrP^{Sc} was decreasing over time. We concluded HSP72 expression did not alter the formation of PrP^{Sc} in neuroblastoma cells.

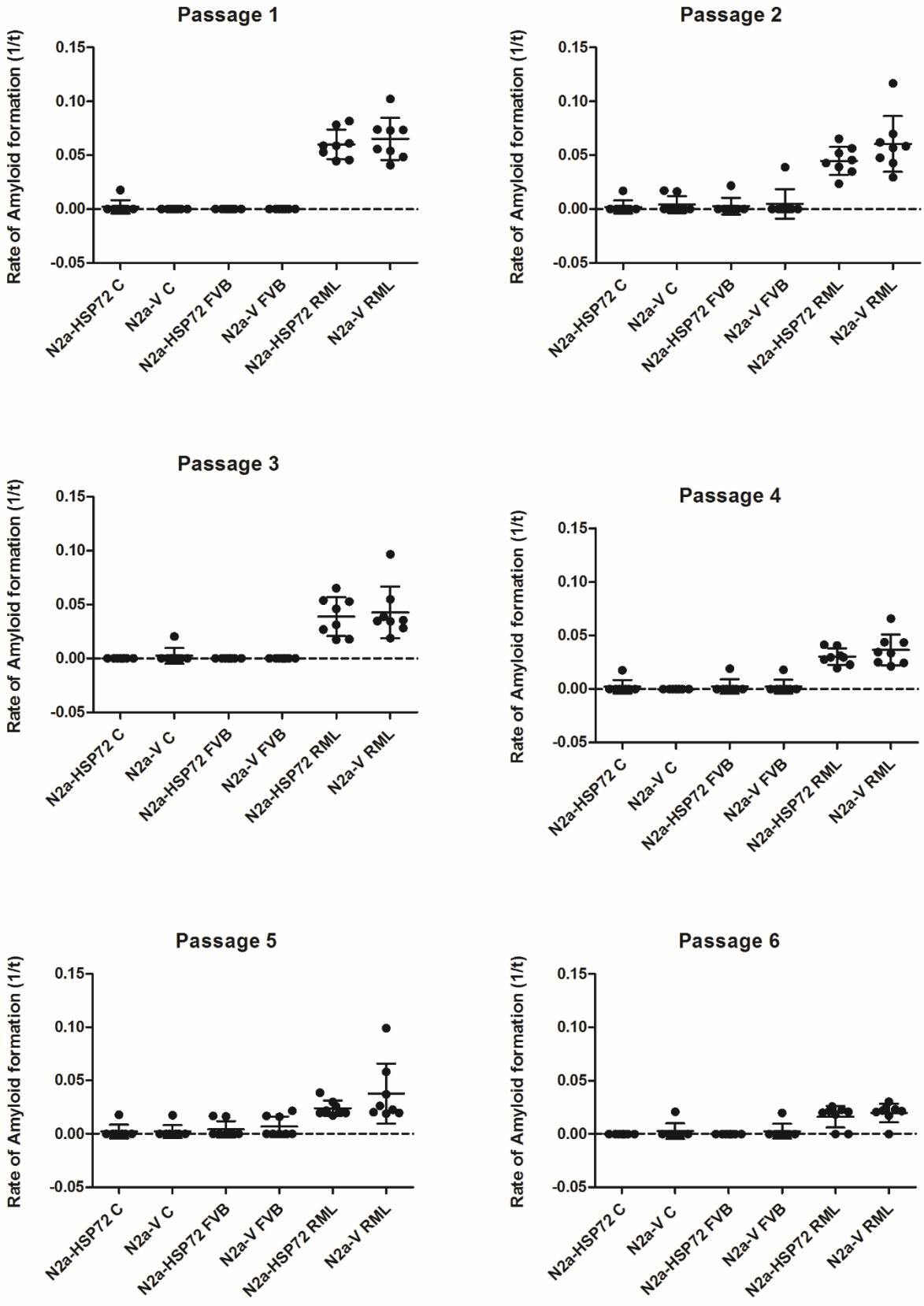
Passage 1
Passage 2
Passage 3
Passage 4
Passage 5
Passage 6
Rate of Amyloid formation (1/t)
0.15
0.10
0.05
0.00
-0.05
N2a-HSP72 C
N2a-V C
N2a-HSP72 FVB
N2a-V FVB
N2a-HSP72 RML
N2a-V RML

Figure 1.5 RT-QuIC comparison of prion levels over time
Prion-templated amyloid formation was detected in NSE-HSP72 and N2a-V cells exposed to RML in passages 1 through 6. There was no significant difference between the average rates of amyloid formation between the two cell types. The average rates of amyloid formation were observed to decrease as passages progressed consistent with a decrease in prion burden in the samples. Minimal, insignificant, amyloid formation of one to two replicates was observed in control cell samples due to spontaneous conversion of SHrPrP substrate.

HSP72 expression does not alter prion disease course

We hypothesized HSP72 would protect against prion-associated disease, therefore, we compared the survival times between NSE-HSP72 and C57Bl/6 mice inoculated with RML. Both mouse strains developed clinical signs associated with prion infection following RML intraperitoneal (IP) inoculation. No significant difference was observed in survival time between the NSE-HSP72 and C57Bl/6 mouse strains, with median survival times of 227 days and 224 days, respectively (Fig 1.6A). Negative control FVB IP inoculated mice from either genetic background did not develop clinical disease and lived for the entire study length, 400 dpi. This demonstrates HSP72 neuronal overexpression does not protect against peripheral, IP, RML exposure. Interestingly, RML intracranial (IC) inoculated NSE-HSP72 displayed a slightly shorter survival time with a median of 165 dpi when compared to RML IC inoculated C57Bl/6 mice with a median survival of 175 dpi ($p=0.0265$, log-rank test) (Fig 1.6B). In summary, these data demonstrate neuronal expression of HSP72 does not enhance survival from RML-prion disease. Although the difference between the IC NSE-HSP72 and C57Bl/6 inoculation groups is statistically significant, a larger study is necessary to evaluate if HSP72 expression biologically enhances prion disease progression.

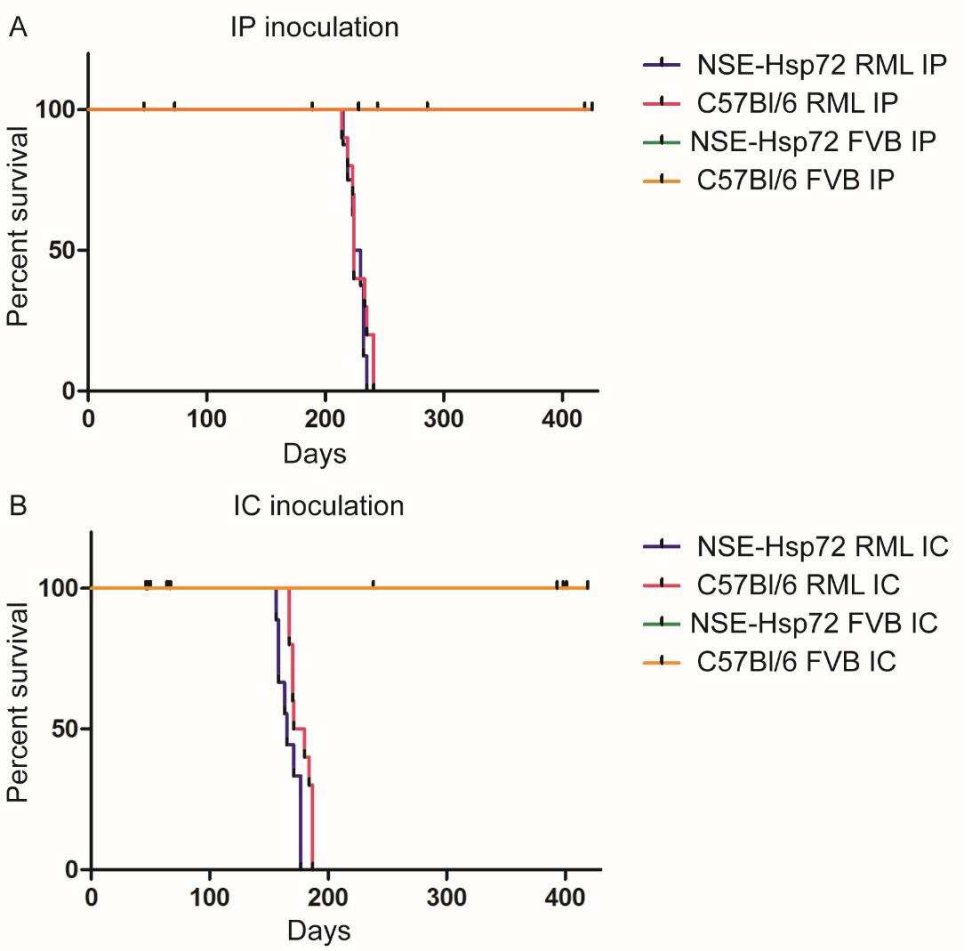

Figure 1.6 Survival curve following RML prion inoculation
A. Intraperitoneal inoculation survival curve. NSE-HSP72 mice and C57Bl/6 mice IP inoculated with RML and euthanized due to terminal disease displayed no significant differences between the disease time course. Control mice inoculated with FVB brain homogenate did not display clinical disease and survived throughout the course of the study.
B. Intracranial inoculation survival curve. NSE-HSP72 mice and C57Bl/6 mice IC inoculated with RML were euthanized due to terminal disease, however, NSE-HSP72 mice had a shorter disease course by approximately 2 weeks (*, $p<0.05$). Control mice inoculated with FVB mouse brain homogenate did not display clinical disease and survived throughout the course of the study.

HSP72 expression does not alter PrP^{Sc} production or neuropathology

The amount of PrP^{Sc} formed during disease between RML-inoculated NSE-HSP72 and C57Bl/6 mice was compared by western blotting. All animals from both IP and IC inoculation routes that displayed clinical signs and were euthanized for prion disease had demonstrable PrP^{Sc} in brain homogenates and at comparable densities (Figure 1.7). There was no apparent

difference in the level of PrP^{Sc} brain accumulation between NSE-HSP72 and C57Bl/6 mice or by inoculation routes. No animals inoculated with FVB brain homogenate displayed PrP^{Sc} in homogenates.

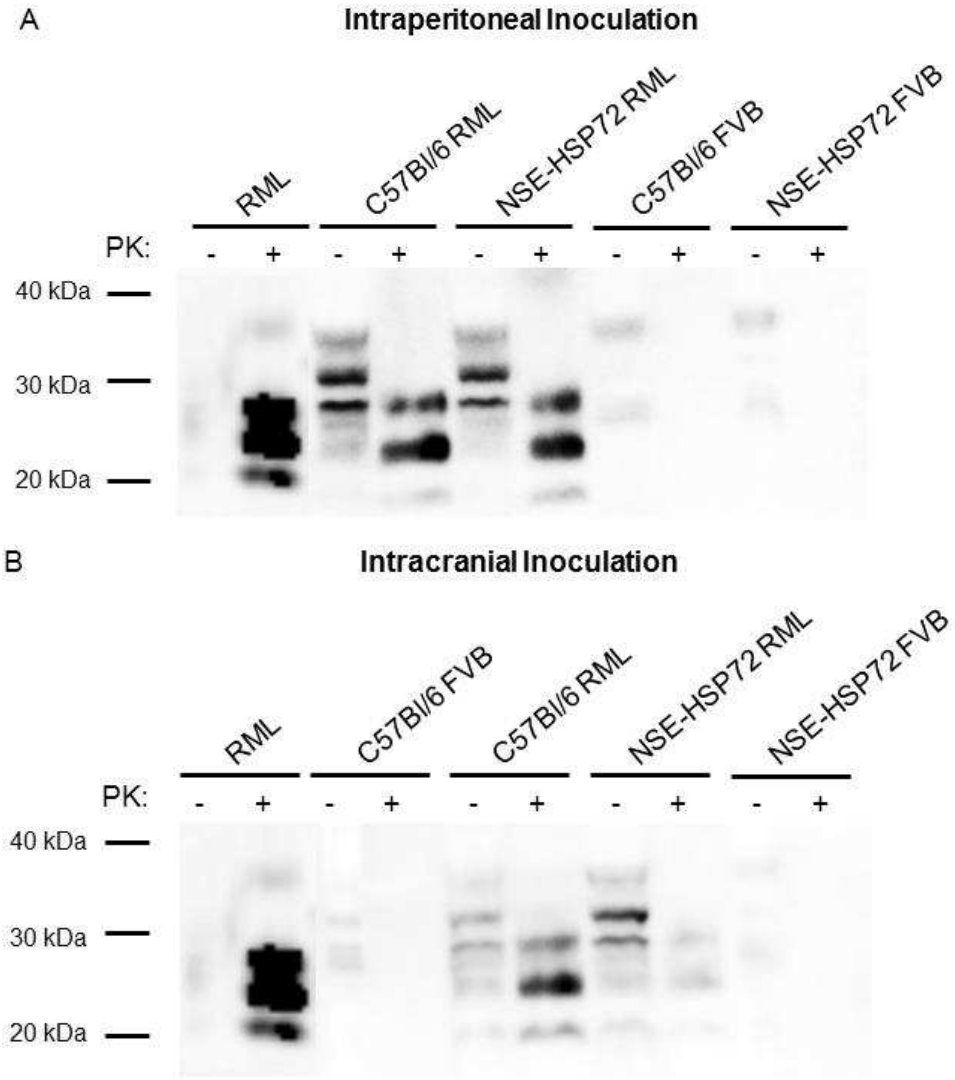

Figure 1.7 Representative western blot of PrP^{Sc} in brain homogenates from mice inoculated with RML or FVB brain homogenate.
A. Intraperitoneal inoculation. PrP^{Sc} was detected in brain homogenates from C57Bl/6 and NSE-HSP72 mice inoculated with RML following PK digestion but was not observed in FVB inoculated mice. No difference was observed in the banding pattern or relative density of PrP^{Sc} in the brain homogenates.
B. Intracranial inoculation. Similar to the IP inoculation in A, PrP^{Sc} was detected in brain homogenates from C57Bl/6 and NSE-HSP72 mice inoculated with RML following PK digestion. No difference was observed in the density or banding pattern. No PK resistant material was detected in brain homogenates from FVB inoculated mice.

To evaluate if HSP72 expression alters RML prion pathology, brain sections from RML-inoculated and FVB-control animals were examined by H&E staining and IHC. Both NSE-HSP72 and C57Bl/6 mice with inoculated with RML, either by IP or IC routes, and euthanized for terminal disease displayed similar pathology consistent with published RML lesion profiles (25). H&E evaluation of brain tissue displayed white matter vacuolation (spongiosis) of the cerebral cortex, cerebellum, and brainstem (Figure 1.8A). No difference in the degree of spongiosis was observed between animal types or inoculation routes. IHC evaluation displayed PrP^{Sc} immunoreactivity in the hippocampus, thalamus, cerebellum and brainstem, consistent with RML prion infection (Figure 1.8B). No difference in lesion distribution or severity was detected between NSE-HSP72 and C57Bl/6 mice or by inoculation route. Control mice inoculated with FVB did not display any PrP^{Sc} immunoreactivity in their brains. In summary, HSP72 expression in neurons did not alter lesion development or PrP^{Sc} accumulation in brains from mice inoculated with RML.

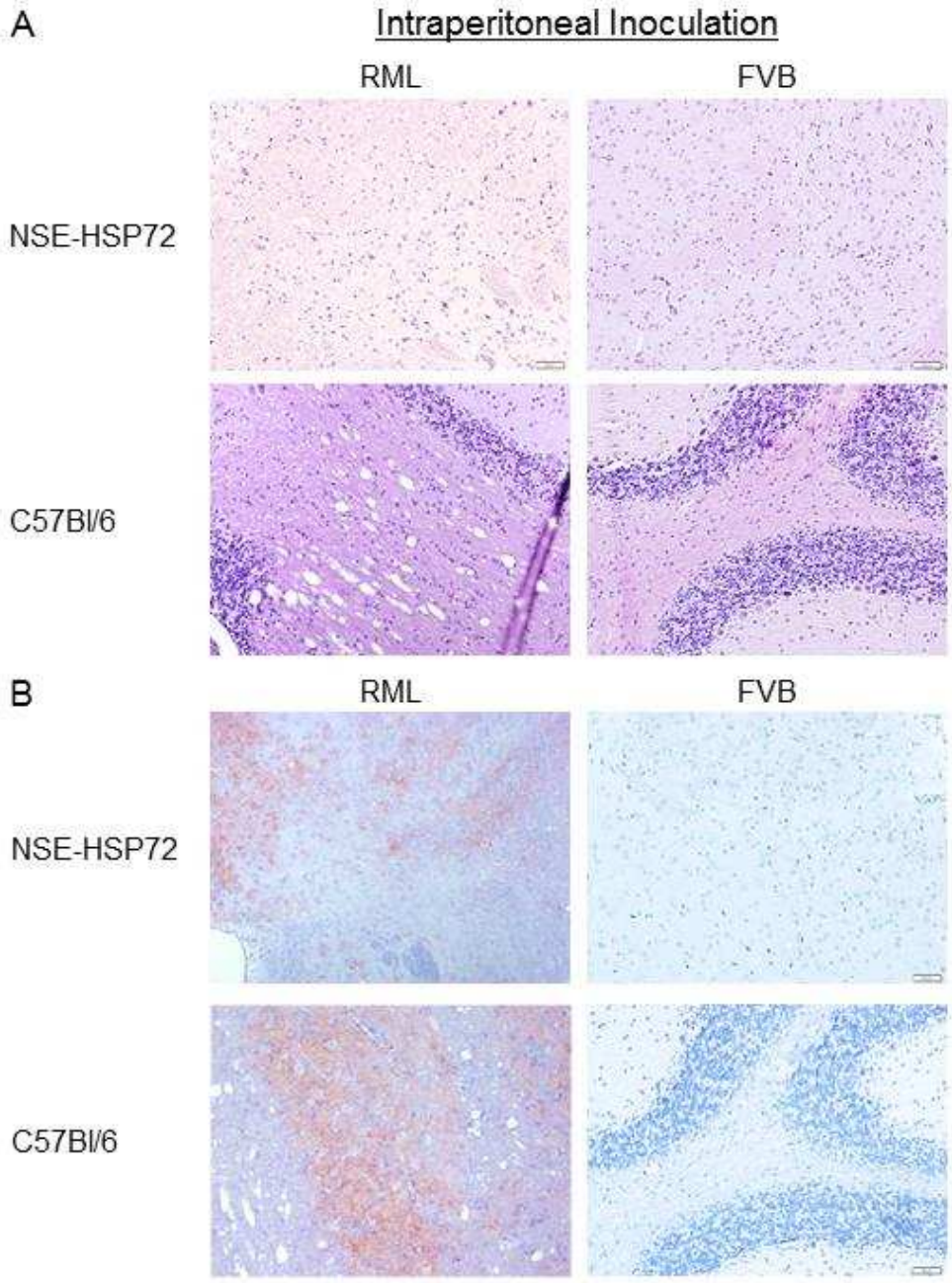

Figure 1.8 Microscopic comparison of brain lesions in NSE-HSP72 and C57Bl/6 mice inoculated with RML.

A. H&E evaluation of brain lesions. NSE-HSP72 and C57Bl/6 mice inoculated with RML displayed white matter spongiosis in the cerebral cortex and cerebellum consistent with prion infection. Mice inoculated with FVB normal brain homogenate did not display any lesions. B. IHC evaluation of PrP^{Sc} brain accumulation. PrP^{Sc} immunoreactivity, characterized by diffuse and small punctate deposits in the hippocampus, thalamus, cerebellum, and brainstem, was detected equally in NSE-HSP72 and C57Bl/6 mice inoculated with RML. Brain sections from control mice inoculated with FVB did not display any PrP^{Sc} immunoreactivity.

Discussion

Heat-shock protein 72 expression has been shown to protect against the toxic effects of protein misfolding in *in vitro* and *in vivo* models of neurodegenerative diseases (3). This protection was illustrated by a decrease in the amount of aberrant protein produced and increased cell viability (3). In contrast to these studies, we did not observe a protective effect in cell culture or mouse investigations of HSP72 expression of RML prion infection. Potential reasons for the differences between our results and other models of protein misfolding diseases include variations in HSP72 expression in the mouse models used for experiments and separate subcellular locations of HSP72 and the prion protein.

The majority of *in vivo* studies examining the influence of HSP72 on neurodegenerative diseases used a transgenic C57Bl6 mouse with HSP72 expression controlled by the β-actin promoter yielding HSP72 expression in all cell types (9,10,27). In contrast, our study focused on HSP72 expression in neurons by using transgenic mice with the gene construct under control of the neuron specific enolase promotor (23). By extending expression to other cell types, HSP72 may be initiating additional cell-mediated mechanisms of protection, such as microglial activation, that synergistically act to decrease protein aggregation (28). Additionally, as would be expected by expressing HSP72 in all cell types, the total amount of HSP72 produced is greater than when expression is restricted to neurons (23). Potentially, this increased dose of HSP72 is needed to abrogate aberrant protein aggregation and the amount of HSP72 in our mouse strain is below the therapeutic threshold. Further study is needed to investigate if HSP72 expression in additional cell types besides neurons is beneficial in prion pathogenesis.

A second potential cause of our negative mouse data is the separate cellular locations of HSP72 expression and pathogenic prions. HSP72 typically resides in the cytoplasm whereas

PrP^{C} is anchored in lipid rafts on the outer cell membrane (2,29,30). PrP^{Sc} has been shown to form on the cell surface and traffic through cells within the endosome-lysosome system (31). Despite the appearance of spatial segregation, during the stress response HSP72 has been shown to translocate to lipid rafts during the stress response and be released into the extracellular environment, both locations where it could encounter PrP^{Sc} (32). HSP72 has also been shown to be protective in mouse models of AD, another protein-misfolding disease where the nascent protein is located in the membrane and the aggregated amyloid-β is extracellular (10). This suggests HSP72 and prions should come in contact, however, it is unknown how limiting the expression of HSP72 to neurons affects the production and function of extracellular HSP72 in our transgenic mouse model.

Our *in vitro* cell culture studies provided mixed results with HSP72 expression. Observing the cell density and cell counts over 3 days post-inoculation suggested HSP72 expression protected against RML-associated prion toxicity. However, analysis of the RML burden over 6 passages following infection did not demonstrate any differences in prion production between cells expressing HSP72 or not. Analysis of the RT-QuIC amyloid formation rates immediately following prion exposure and throughout passaging demonstrated the prion concentration was gradually decreasing indicating our transfected N2a cells were able to be infected but did not efficiently propagate infection between passages. This problem has previously been recognized in prion infection cell culture, where N2a clones display variable permissiveness or resistance to scrapie prion infection and a GAG-protein construct was necessary to maintain prion propagation in RKE cells between passages (33,34). Another potential complication is the stringent passage conditions we performed, in which we potentially diluted infected cells faster than prions propagate. Some prion cell panel assays do not perform

any passage steps after infection or only do minimal cell splitting when passaging which suggests overall cellular prion replication occurs at a slow rate (unpublished data, Glenn Telling). Potential alternative experimental approaches to analyze HSP72 expression *in vitro* include identifying the most prion-susceptible N2a subclones from our vector transfected cells or terminally differentiating our N2a-cells into neurons prior to infection.

In summary, we investigated the potential for HSP72 to mitigate prion pathogenesis in cell culture and mouse models of murine-adapted scrapie. In contrast to its protective effect in models of other protein misfolding diseases, HSP72 expression in neurons did not alter the disease course or prion accumulation following infection. Further investigation is needed to know if HSP72 expression can provide protection in prion diseases when expressed in additional cell types or if HSP72 expression does not impact prion disease pathogenesis.

CHAPTER 1 REFERENCES

1. Lindquist, S. (1986) The heat-shock response. *Annual review of biochemistry* **55**, 1151-1191
2. Lindquist, S., and Craig, E. A. (1988) The heat-shock proteins. *Annu Rev Genet* **22**, 631-677
3. Muchowski, P. J., and Wacker, J. L. (2005) Modulation of neurodegeneration by molecular chaperones. *Nature reviews. Neuroscience* **6**, 11-22
4. Soto, C. (2003) Unfolding the role of protein misfolding in neurodegenerative diseases. *Nature reviews. Neuroscience* **4**, 49-60
5. Magrane, J., Smith, R. C., Walsh, K., and Querfurth, H. W. (2004) Heat shock protein 70 participates in the neuroprotective response to intracellularly expressed beta-amyloid in neurons. *The Journal of neuroscience : the official journal of the Society for Neuroscience* **24**, 1700-1706
6. Dou, F., Netzer, W. J., Tanemura, K., Li, F., Hartl, F. U., Takashima, A., Gouras, G. K., Greengard, P., and Xu, H. (2003) Chaperones increase association of tau protein with microtubules. *Proc Natl Acad Sci U S A* **100**, 721-726
7. Auluck, P. K., Meulener, M. C., and Bonini, N. M. (2005) Mechanisms of Suppression of {alpha}-Synuclein Neurotoxicity by Geldanamycin in Drosophila. *The Journal of biological chemistry* **280**, 2873-2878
8. Auluck, P. K., Chan, H. Y., Trojanowski, J. Q., Lee, V. M., and Bonini, N. M. (2002) Chaperone suppression of alpha-synuclein toxicity in a Drosophila model for Parkinson's disease. *Science* **295**, 865-868
9. Cummings, C. J., Sun, Y., Opal, P., Antalffy, B., Mestril, R., Orr, H. T., Dillmann, W. H., and Zoghbi, H. Y. (2001) Over-expression of inducible HSP70 chaperone suppresses neuropathology and improves motor function in SCA1 mice. *Hum Mol Genet* **10**, 1511-1518
10. Hoshino, T., Murao, N., Namba, T., Takehara, M., Adachi, H., Katsuno, M., Sobue, G., Matsushima, T., Suzuki, T., and Mizushima, T. (2011) Suppression of Alzheimer's disease-related phenotypes by expression of heat shock protein 70 in mice. *The Journal of neuroscience : the official journal of the Society for Neuroscience* **31**, 5225-5234
11. Morimoto, R. I., and Santoro, M. G. (1998) Stress-inducible responses and heat shock proteins: new pharmacologic targets for cytoprotection. *Nature biotechnology* **16**, 833-838
12. Sweeny, E. A., Jackrel, M. E., Go, M. S., Sochor, M. A., Razzo, B. M., DeSantis, M. E., Gupta, K., and Shorter, J. (2015) The Hsp104 N-terminal domain enables disaggregase plasticity and potentiation. *Mol Cell* **57**, 836-849
13. Chernoff, Y. O., Lindquist, S. L., Ono, B., Inge-Vechtomov, S. G., and Liebman, S. W. (1995) Role of the chaperone protein Hsp104 in propagation of the yeast prion-like factor [psi+]. *Science* **268**, 880-884
14. Kryndushkin, D. S., Engel, A., Edskes, H., and Wickner, R. B. (2011) Molecular chaperone Hsp104 can promote yeast prion generation. *Genetics* **188**, 339-348
15. Wegrzyn, R. D., Bapat, K., Newnam, G. P., Zink, A. D., and Chernoff, Y. O. (2001) Mechanism of prion loss after Hsp104 inactivation in yeast. *Mol Cell Biol* **21**, 4656-4669

16. Tatzelt, J., Zuo, J., Voellmy, R., Scott, M., Hartl, U., Prusiner, S. B., and Welch, W. J. (1995) Scrapie prions selectively modify the stress response in neuroblastoma cells. *Proc Natl Acad Sci U S A* **92**, 2944-2948
17. Resenberger, U. K., Muller, V., Munter, L. M., Baier, M., Multhaup, G., Wilson, M. R., Winklhofer, K. F., and Tatzelt, J. (2012) The heat shock response is modulated by and interferes with toxic effects of scrapie prion protein and amyloid beta. *The Journal of biological chemistry* **287**, 43765-43776
18. Buccellato, M. A., Carsillo, T., Traylor, Z., and Oglesbee, M. (2007) Heat shock protein expression in brain: a protective role spanning intrinsic thermal resistance and defense against neurotropic viruses. *Prog Brain Res* **162**, 395-415
19. Carsillo, T., Zhang, X., Vasconcelos, D., Niewiesk, S., and Oglesbee, M. (2006) A single codon in the nucleocapsid protein C terminus contributes to in vitro and in vivo fitness of Edmonston measles virus. *Journal of virology* **80**, 2904-2912
20. Henderson, D. M., Davenport, K. A., Haley, N. J., Denkers, N. D., Mathiason, C. K., and Hoover, E. A. (2015) Quantitative assessment of prion infectivity in tissues and body fluids by real-time quaking-induced conversion. *The Journal of general virology* **96**, 210-219
21. Wilham, J. M., Orru, C. D., Bessen, R. A., Atarashi, R., Sano, K., Race, B., Meade-White, K. D., Taubner, L. M., Timmes, A., and Caughey, B. (2010) Rapid end-point quantitation of prion seeding activity with sensitivity comparable to bioassays. *PLoS pathogens* **6**, e1001217
22. Henderson, D. M., Manca, M., Haley, N. J., Denkers, N. D., Nalls, A. V., Mathiason, C. K., Caughey, B., and Hoover, E. A. (2013) Rapid antemortem detection of CWD prions in deer saliva. *PloS one* **8**, e74377
23. Carsillo, T., Traylor, Z., Choi, C., Niewiesk, S., and Oglesbee, M. (2006) hsp72, a host determinant of measles virus neurovirulence. *Journal of virology* **80**, 11031-11039
24. Legname, G., Nguyen, H. O., Baskakov, I. V., Cohen, F. E., Dearmond, S. J., and Prusiner, S. B. (2005) Strain-specified characteristics of mouse synthetic prions. *Proc Natl Acad Sci U S A* **102**, 2168-2173
25. Chandler, R. L. (1961) Encephalopathy in mice produced by inoculation with scrapie brain material. *Lancet* **1**, 1378-1379
26. Sweeny, E. A., and Shorter, J. (2015) Mechanistic and Structural Insights into the Prion-Disaggregase Activity of Hsp104. *Journal of molecular biology*
27. Plumier, J. C., Ross, B. M., Currie, R. W., Angelidis, C. E., Kazlaris, H., Kollias, G., and Pagoulatos, G. N. (1995) Transgenic mice expressing the human heat shock protein 70 have improved post-ischemic myocardial recovery. *The Journal of clinical investigation* **95**, 1854-1860
28. Kakimura, J., Kitamura, Y., Takata, K., Umeki, M., Suzuki, S., Shibagaki, K., Taniguchi, T., Nomura, Y., Gebicke-Haerter, P. J., Smith, M. A., Perry, G., and Shimohama, S. (2002) Microglial activation and amyloid-beta clearance induced by exogenous heat-shock proteins. *FASEB journal : official publication of the Federation of American Societies for Experimental Biology* **16**, 601-603
29. Prusiner, S. B. (1998) Prions. *Proc Natl Acad Sci U S A* **95**, 13363-13383
30. Naslavsky, N., Stein, R., Yanai, A., Friedlander, G., and Taraboulos, A. (1997) Characterization of detergent-insoluble complexes containing the cellular prion protein and its scrapie isoform. *The Journal of biological chemistry* **272**, 6324-6331

31. Caughey, B., Baron, G. S., Chesebro, B., and Jeffrey, M. (2009) Getting a grip on prions: oligomers, amyloids, and pathological membrane interactions. *Annual review of biochemistry* **78**, 177-204
32. Broquet, A. H., Thomas, G., Masliah, J., Trugnan, G., and Bachelet, M. (2003) Expression of the molecular chaperone Hsp70 in detergent-resistant microdomains correlates with its membrane delivery and release. *The Journal of biological chemistry* **278**, 21601-21606
33. Bian, J., Napier, D., Khaychuck, V., Angers, R., Graham, C., and Telling, G. (2010) Cell-based quantification of chronic wasting disease prions. *Journal of virology* **84**, 8322-8326
34. Klohn, P. C., Stoltze, L., Flechsig, E., Enari, M., and Weissmann, C. (2003) A quantitative, highly sensitive cell-based infectivity assay for mouse scrapie prions. *P Natl Acad Sci USA* **100**, 11666-11671

CHAPTER 2:
Early Prion Distribution in Deer Exposed to Chronic Wasting Disease

Summary

Natural exposure of deer to the misfolded infectious prion (PrP^{CWD}) in chronic wasting disease (CWD) is believed to occur through environmental exposure by aerosol or oral routes. Studies in white-tailed deer mimicking these exposure routes with (in retrospect) relatively large challenge doses detected PrP^{CWD} in the retropharyngeal lymph node at 1.5 months and tonsil at 3 months by western blotting and immunohistochemistry. However, the full extent of PrP^{CWD} distribution prior to these time points and the chronological progression of disease during early infection remains unknown. To address this knowledge gap in pathogenesis, we challenged white-tailed deer with CWD prions by intravenous or mucosal exposure routes (oral and oro-nasal) and performed necropsies at 1 and 3 days and 1, 2, 3, and 4 months to assess the tissue distribution of PrP^{CWD}. To enhance PrP^{CWD} detection at early post-infection time points, tissues were assayed using several amplification techniques: real-time quaking induced conversion assay (RT-QuIC) and tyramide signal amplification immunohistochemistry (TSA-IHC). Although we were unable to detect PrP^{CWD} in the immediate period following mucosal exposure, we detected PrP^{CWD} seeding activity in vascular organs 15 minutes and 72 hours post-IV exposure. In an extended survey following mucosal exposure, PrP^{CWD} was first detected in the oropharyngeal-associated lymph nodes at 1 month post-exposure (MPE). Expanding PrP^{CWD} replication was detected at 2 MPE in oropharyngeal lymph nodes and by 3 MPE, PrP^{CWD} had spread to all systemic lymphoid tissues. At 4 MPE, PrP^{CWD} detection remained confined to lymphoid tissues and was not yet evident in central nervous system tissues. These results indicate that the earliest trans-mucosal entry by CWD prions is in the upper alimentary tract and replication in the

lymphoid tissues draining the oropharyngeal cavity followed by rapid dissemination to systemic lymphoid tissues prior to neuroinvasion.

Background

Chronic wasting disease (CWD) is a naturally occurring TSE of cervids, including deer, elk, and moose (1). CWD was first recognized in Colorado in 1967 and has since spread to captive and free-ranging cervid populations in 24 states and three additional countries, Canada, the Republic of Korea, and Norway (2,3). Clinical signs include progressive wasting despite polyphagia, bruxism, head tremors, and ataxia (1,4). Like other transmissible spongiform encephalopathies, clinical disease is associated with spongiform change and accumulation of the infectious prion isoform, PrP^{CWD}, in the central nervous system, most consistently observed affecting the nucleus of the vagus nerve in the obex region of the medulla oblongata (5-7).

Natural horizontal CWD transmission is predicted to occur through direct contact with infected animals or by indirect environmental exposure associated with foraging activities (8). Infectious CWD prions have been demonstrated in body fluids and excreta, including saliva, urine, feces, contaminated fomites, and pasture (8-12). Once CWD has contaminated the environment it has been shown to persist and remain infectious for years, potentially through complexing with soil (13). Vertical transmission has also been described, however, it is unclear what degree it plays in the spread of CWD (14).

Like other TSEs, the pathogenesis of CWD is influenced by the *PRNP* gene sequence and four polymorphisms have been identified in white-tailed deer: Q95H, G96S, A116G, and Q226K (15). Of the identified polymorphisms, 95Q, 96G, and 116A, are more commonly represented in the deer population and reported with higher frequency in field-cases of CWD (16). Research

has demonstrated at least one copy of the 96S allelic variation prolongs the CWD incubation period in deer, up to 230%, and potentially impedes PrP^{CWD} conversion (2,17,18).

Evidence suggests CWD pathogenesis has many similarities to scrapie, including a lymphoid replication phase prior to neuroinvasion (19). A survey of mule deer from CWD endemic areas identified PrP^{CWD} in tonsil biopsies without overt clinical signs of disease (20). Experimental studies of CWD transmission following relatively large oral challenge with CWD+ brain homogenate, have demonstrated PrP^{CWD} in gastrointestinal-associated lymphoid tissues as early as 42 days (21) and spread to systemic lymphoid tissues by 90 days post-exposure (22). However, there remains relatively little information regarding the chronological progression of PrP^{CWD} in deer tissues during the early post-exposure period.

To reveal features of the early CWD pathogenesis, we examined the distribution and accumulation of PrP^{CWD} after oral and intravenous exposure in white-tailed deer using both traditional and modern amplification methods. Prions rapidly disseminated to highly vascularized organs within 15 minutes and remained within these tissues at 3 days post-exposure. Following mucosal exposure, we found the earliest evidence of trans-mucosal prion entry in the upper alimentary tract in the lymphoid tissues draining the oropharyngeal cavity, followed by rapid dissemination to systemic lymphoid tissues prior to neuroinvasion. This study highlights the contribution of the lymphoid system in early CWD pathogenesis following mucosal exposure.

Methods

Animal care and study design

Indoor housed, hand-raised white-tailed deer (WTD) (*Odocoileus virginianus*) were provided through long collaboration with Sally Dahmes and David Osborn. WTD were

maintained in strict accordance with Colorado State University Animal Care and Use Committee. PrP^C genotype sequence at codon 96 was determined as previously described (14,23,24).

Intravenous-inoculation:

Four WTD were intravenously inoculated with 0.55 grams of CWD-positive (CWD+) brain homogenate. One WTD was inoculated with CWD-negative (CWD-) brain homogenate following similar route as a negative control. The brain inocula were prepared in sterile 1xPBS containing 2.0% penicillin-streptomycin (Life Technologies). WTD were inoculated into the jugular vein over a period of 5 minutes while under sedation. Two CWD+ deer were sacrificed 15 minutes post-inoculation and the remaining 2 CWD+ and 1 CWD- animals were collected 72 hours post-inoculation. No signs of clinical disease were detected throughout the course of study.

Mucosal-inoculation:

WTD identified by 900-series were inoculated with a combined oro-nasal inoculation of homogenate consisting of 0.55 grams pooled cervid brain that was confirmed CWD positive by western blot. Oral inoculation was performed by instilling 0.5g of brain directly into the animal's mouth using a syringe. Aerosol inoculation was performed by atomizing brain homogenate corresponding to 0.05 g of brain using a Nasonex™-style sprayer directly in the nostrils. Negative control WTD were inoculated with a similar dose and route of pooled CWD-negative cervid brain homogenate. WTD were sacrificed at either 24 hours or 72 hours post-inoculation. WTD identified by 1100 or 1200-series were inoculated with either 0.5 grams of CWD positive or CWD negative brain homogenate and sacrificed at 1, 2, 3, or 4 months post-inoculation. *PRNP* genotype at codon 96 was evenly distributed throughout the collection time-

points to ensure equal genetic representation (Figure 2.1). No signs of clinical disease were detected throughout the course of study.

Figure 2.1 Overview of WTD *PRNP* genotype distribution of mucosal-exposure cohort. White tailed deer were collected at 1 and 3 days or 1, 2, 3, and 4 months. PRNP codon 96 genotypes, 96G or 96S, were distributed throughout the collections to ensure adequate genetic representation.

Tissue processing

Complete necropsy and tissue collection of each WTD was performed at time of sacrifice. Lymphoid tissues, obex, ileum and vomeronasal organ (VNO) were analyzed for PrP^{CWD} amyloid seeding activity by RT-QuIC and PrP^{CWD} immunoreactivity by IHC. Many other tissues were collected from deer at necropsy but were not analyzed for the present report. Each tissue was collected with an individual, clean, prion-free instrument to avoid cross-contamination. Tissues were split into two with half frozen and stored at -80 C until use. The other half of tissue was fixed in periodate-lysine-paraformaldehyde (PLP) for 4 days before changing to sterile 1xPBS until trimming and histology tissue cassetting, followed by 70% ethanol for long-term storage. Tissue cassettes were processed into paraffin-embedded blocks following routine histologic techniques. Frozen tissues were processed into ten percent weight-per-volume tissue homogenates using 1xPBS (Life Technologies) and a Bullet Blender™ tissue homogenizer (Next Advance).

Immunohistochemistry

PrP^{CWD} was detected following a two-step immunostaining procedure with tyramide-signal (TSA) enhancement as previously described with minor modifications (25). Briefly, 5 μm tissue sections were mounted on positively charged glass slides. Following routine deparaffinization with xylene and rehydration with graded alcohols, tissues were subjected to 1 μg/mL proteinase K digestion at 37 C to remove native PrP^{C}. Epitope exposure was performed using hydrated autoclaving antigen retrieval in 10 mM EDTA, pH 6.0. Tissues were briefly exposed to 88% formic acid prior to quenching endogenous peroxide activity with 3.0% hydrogen peroxide in methanol. Tissue sections were blocked with proprietary protein block, TNB (Perkin-Elmer), followed by sequential application of primary anti-prion protein antibody BAR224 (Cayman chemical) at 0.5μg/mL, a 1:2000 dilution and secondary anti-mouse antibody conjugated to horseradish peroxidase (HRP) (Envision+™, Dako). Antibody signal was enhanced with Tyramide Signal Amplification™ (Perkin Elmer) following the suggested protocol. Immunoreactivity was detected using AEC substrate-chromogen (Dako). Coverslips were mounted using aqueous mounting media and staining visualized by light microscopy.

RT-QuIC protein purification

RT-QuIC experiments were performed with recombinant truncated Syrian hamster PrP^{C} (SHrPrP) encoding residues 90-231, which was expressed and purified as previously described (26,27). Briefly, SHrPrP was expressed in BL21 Rosetta *Escherichia coli* (Novagen). Bacteria were cultured at 37°C in lysogeny broth (LB) media in the presence of selection antibiotics kanamycin and chloramphenicol until the final OD^{600} was at least 2.5. Cell lysis was performed using Bugbuster™ reagent supplemented with Lysonase™ (EMD Biosciences) and inclusion bodies harvested by centrifugation at 15,000 x g. The inclusion body pellet was solubilized (8M

guanidine hydrochloride, 100mM Na_2PO_4) prior to application to NiNTA superflow resin (Qiagen) that had been previously equilibrated with denaturation buffer (6M guanidine hydrochloride, 100 mM Na_2PO_4, 10mM Tris). The resin-SHrPrP was applied to a XK16-60 column (GE Healthcare) and purified using a Bio-Rad Duoflow^{TM} FPLC using a gradient from denaturation buffer to refolding buffer (100mM Na_2HPO_4, 10mM Tris) to induce protein refolding. Refolding was followed by a gradient from refolding to elution buffer (100mM NaH_2PO_4, 10mM Tris, 0.5 M imidazole) with all fractions being collected. Fractions from the elution peak were combined and dialyzed against 4L of buffer (20mM NaH_2PO_4) overnight. Final protein concentration was determined using the A_{280} and a coefficient of extinction of 25,900 in Beer's Law.

RT-QuIC assay

Lymphoid and parenchymal tissues

Tissue homogenates were treated to sodium phosphotungstic acid (NaPTA) precipitation to enhance detection by RT-QuIC. Briefly, 100 µL of a 1% tissue homogenate solution was incubated and shaken with 7 µL NaPTA solution (0.5g sodium phosphotungstic acid, 0.43g $MgCl_2$-6-hydrate, pH 4.0) for 1 hour at 37° C and 1400 rpm. The solution was pelleted by centrifugation at 21,130 rcf for 30 minutes. The supernatant was removed and remaining pellets were resuspended in RT-QuIC dilution buffer (0.1% SDS/1xPBS) corresponding to the original volume of homogenate to maintain consistent protein concentration. Two µL of resuspended NaPTA precipitated tissue sample was used to seed each RT-QuIC reaction.

Nervous tissues

Nervous tissues were alcohol precipitated prior to RT-QuIC assay. Ten µL of a 10% tissue homogenate was incubated at room temperature with 100% ethanol for 5 minutes.

Proteins were pelleted by centrifugation at 21,130 rcf for 5 minutes and the supernatant discarded. The procedure was repeated and the final protein pellet was resuspended in 10 μL of RT-QuIC dilution buffer. Two μL of a 10^{-1} dilution of the precipitated nervous tissue proteins were used to seed the RT-QuIC reaction.

Assay conditions

RT-QuIC was performed as previously described (26,27). Briefly, RT-QuIC experiments were carried out in black, optical bottom 96-well plates (Nunc) with each well containing 0.1 mg/mL SHrPrP substrate and RT-QuIC reaction buffer (20mM NaH_2PO_4, 320mM NaCl, 1.0mM EDTA, 1mM Thioflavin T). RT-QuIC experiments were carried out in a BMG Labtech Polarstar™ fluorometer with each cycle consisting of 1 minute shaking at 700 rpm followed by 1 minute rest, repeated for 15 minutes. Fluorescence readings with an excitation of 450 nm, emission of 480 nm, and gain of 1700 were taken at the completion of each 15 minute shake/rest cycle by measuring each well 20 flashes and an orbital average of 4. Each RT-QuIC experiment consisted of 250 fluorescence readings, a total of 62.5 hours.

RT-QuIC data analysis

Data for each sample was collected by three separate RT-QuIC experiments with 4 replicates each for a total of 12 replicates. Individual replicates were considered to have positive amyloid formation if their fluorescence rose above a pre-determined threshold set at 5 standard deviations above the average of the baseline fluorescence. RT-QuIC rates of amyloid formation were calculated as previously described (26,28). Rates of amyloid formation were normalized to the plate positive control minimize any individual experiment variation by dividing each sample rate of amyloid formation by the fastest positive control rate of amyloid formation. Sample data was statistically evaluated using GraphPad software. RT-QuIC replicate distributions were

determined to be normally distributed using D'Agostino test for normality and a p-value <0.05. The rates of amyloid formation from tissue homogenates from PrP^{CWD} exposed animals were compared to corresponding negative controls by one sample t-test and considered positive if the p-value <0.05.

Results

PrP^{CWD} amplifies in lymphoid tissues during the early course of infection

24 and 72 hours post-mucosal exposure. In WTD collected at 24 and 72 hours post-mucosal CWD exposure, occasional RT-QuIC sample replicates of the prescapular, mandibular, and hepatogastric lymph nodes displayed amyloid seeding activity, however, the average rates of amyloid seeding for these samples were not significantly different than corresponding negative control tissues (Figure 2.2). IHC analysis of tissues from these early time points did not display any PrP^{CWD} immunoreactivity.

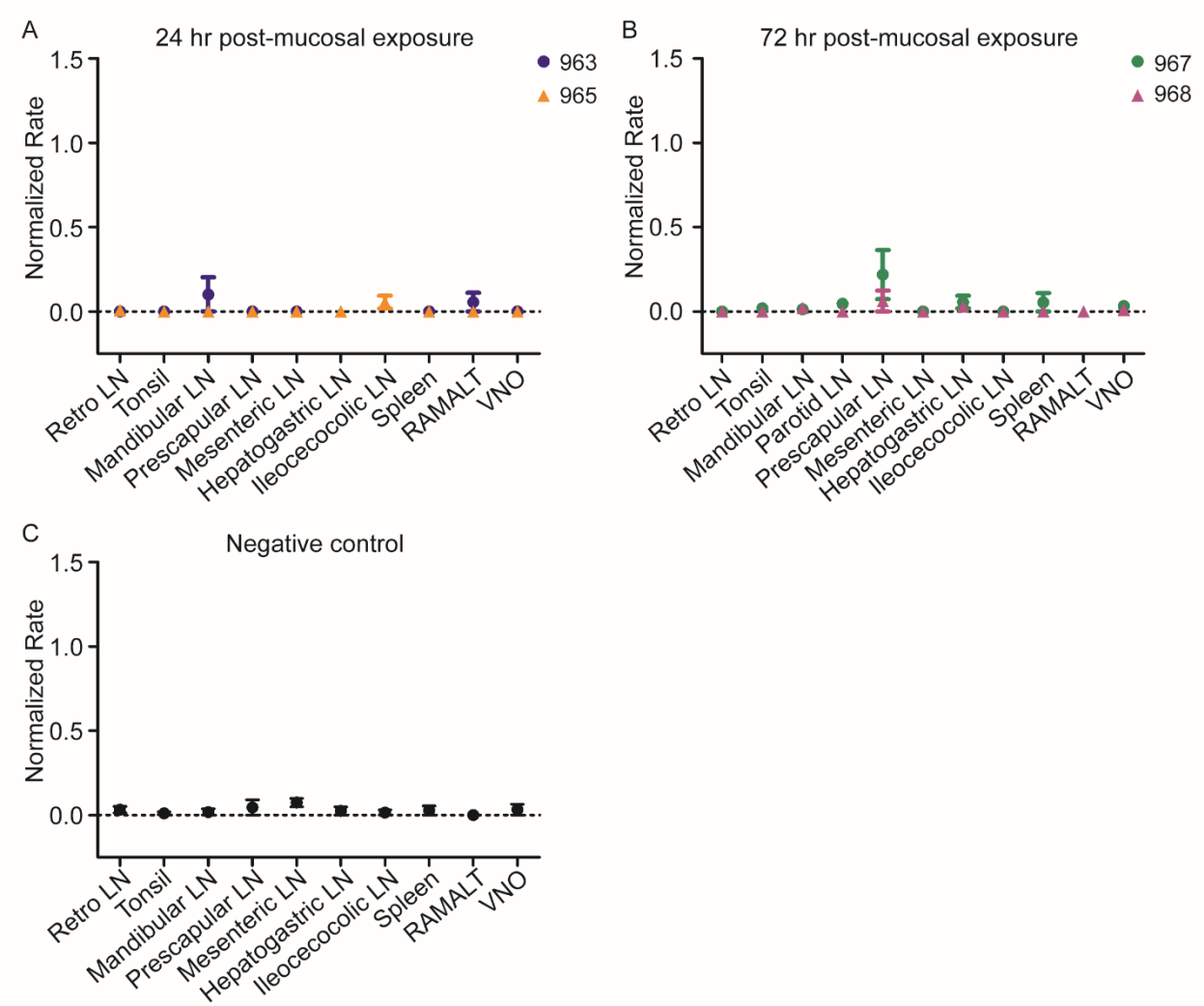

Figure 2.2 24 and 72 hours post-mucosal exposure.
A. RT-QuIC of tissues collected 24 hours post-mucosal exposure. Rare tissues, such as the prescapular LN, mandibular LN and RAMALT, displayed minor rPrP^{C} amyloid conversion, however rates of amyloid formation were not statistically different than corresponding negative control tissues. Data displayed is mean and standard error of mean (SEM) from 8 replicates representing 2 separate experiments. (LN= lymph node; Retro LN = Retropharyngeal lymph node; RAMALT= rectoanal mucosal associated lymphoid tissue; VNO= vomeronasal organ)
B. RT-QuIC of tissues collected 72 hours post-mucosal exposure. Rare tissues, such as the prescapular LN and spleen, displayed minor rPrP^{C} amyloid conversion, however rates of amyloid formation were not statistically different than corresponding negative control tissues ($p>0.05$, one-sample t-test). Data displayed is mean and SEM from 8 replicates representing 2 separate experiments.
C. RT-QuIC of negative control tissues collected at 72 hours post-mucosal exposure. Rare tissues displayed minor elevated rates consistent with spontaneous amyloid formation of SHrPrP substrate. Data displayed is mean and SEM from a minimum of 8 replicates and 2 separate experiments.

15 minutes and 72 hours post-intravenous exposure. To contrast PrP^{CWD} tissue distribution with mucosal exposure, deer were inoculated IV with CWD+ or CWD- brain homogenate and collected 15 minutes or 72 hours post-inoculation. We observed variable amyloid seeding in highly vascularized organs at both 15 minutes and 72 hours post-exposure, including the lung and liver (Figure 2.3). No PrP^{CWD} immunoreactivity was observed on TSA-IHC examination of the corresponding tissues.

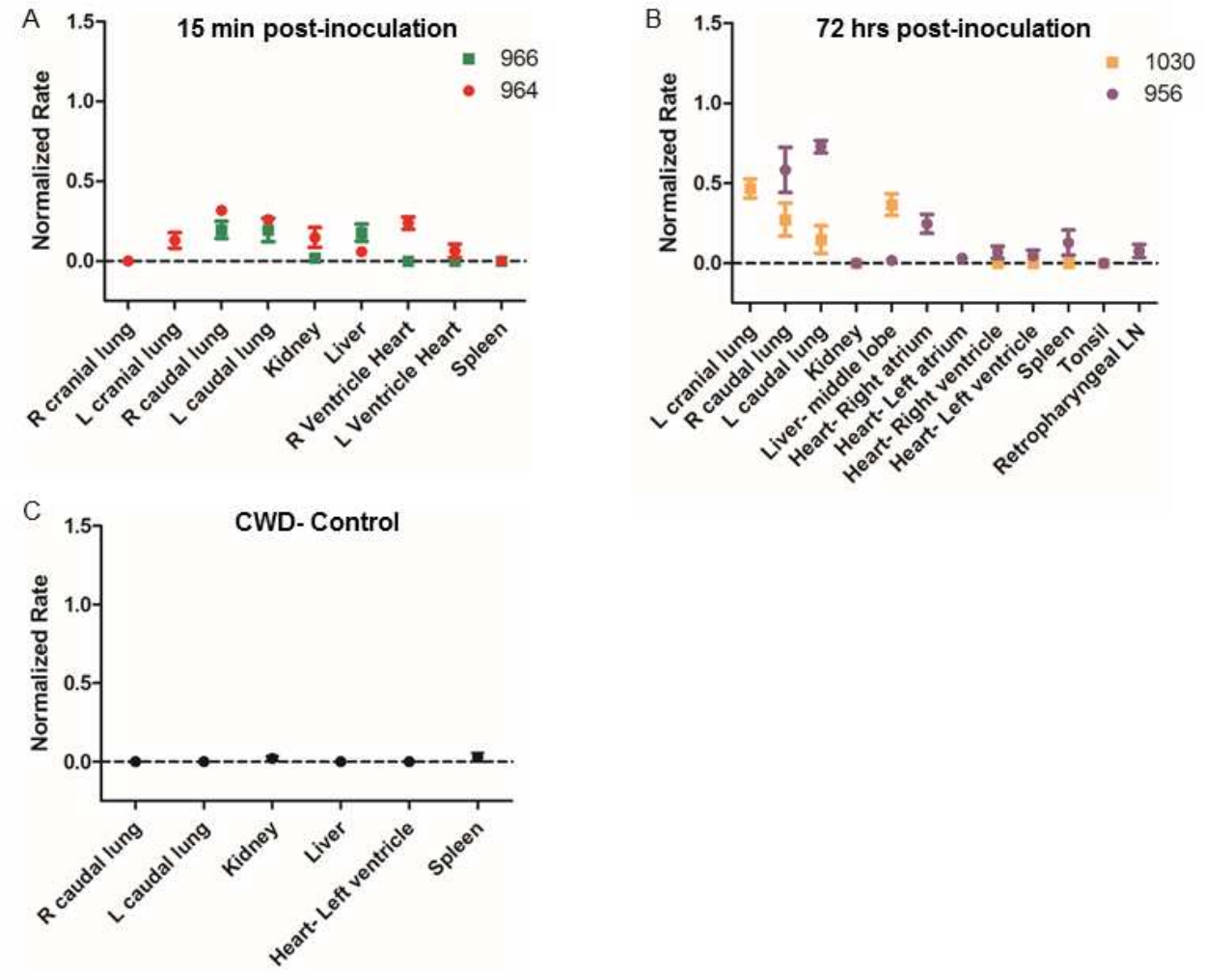

Figure 2.3 15 minutes and 72 hours post-IV inoculation.
A. PrP^{CWD} detection 15 minutes post-IV inoculation. PrP^{CWD} amyloid seeding was variably detected in the lung, kidney, liver, and right ventricle of the heart 15 minutes following IV inoculation. Of those tested, the right caudal lung, left caudal lung, and right ventricle samples from animal 964 had amyloid formation rates significantly different than the corresponding negative control (*, $p<0.05$, Wilcoxon signed rank test). Data represents mean and SEM of 8

replicates and 2 separate experiments.
B. PrP^{CWD} detection 72 hours post-IV inoculation. Variable PrP^{CWD} amyloid seeding was detected in all lung lobes, liver, and right atrium. The samples from deer 956 that displayed significant rates of amyloid formation included: the right atrium of the heart, and the right and left caudal lung lobes (**, $p<0.01$, Wilcoxon signed rank test). From deer 1030, only the liver sample displayed significant rate of amyloid seeding (*, $p<0.05$, Wilcoxon signed rank test). Data represents mean and SEM of 8 replicates and 2 separate experiments.
C. No PrP^{CWD} amyloid seeding detected in the negative control deer.

One month post exposure (MPE). At 1 MPE, significant PrP^{CWD} amyloid seeding activity ($p<0.01$, one sample t-test) was detected in the retropharyngeal lymph nodes from two 96G WTD and the parotid lymph node from one 96G WTD when compared to corresponding negative controls (Figure 2.4A). By comparison, no significant amyloid seeding was observed in tissues from 96S WTD at 1 MPE. This indicates the amyloid seeding detected in 96G tissues is consistent with *de novo* prion generation in these tissues and not residual inoculum.

TSA-IHC evaluation of lymphoid tissues at 1 MPE demonstrated faint granular PrP^{CWD} immunoreactivity in rare germinal centers of tonsils in two of the three 96G WTD (Figure 2.4B). Similar faint granular PrP^{CWD} immunoreactivity was detected in the parotid lymph node with corresponding amyloid seeding detected by RT-QuIC. Despite significant RT-QuIC amyloid seeding, TSA-IHC failed to demonstrate PrP^{CWD} immunoreactivity in retropharyngeal lymph nodes. The variation in PrP^{CWD} tissue detection at this early disease time point is likely due to unequal tissue distribution and sectioning differences. No PrP^{CWD} immunoreactivity was observed in 96S tissues.

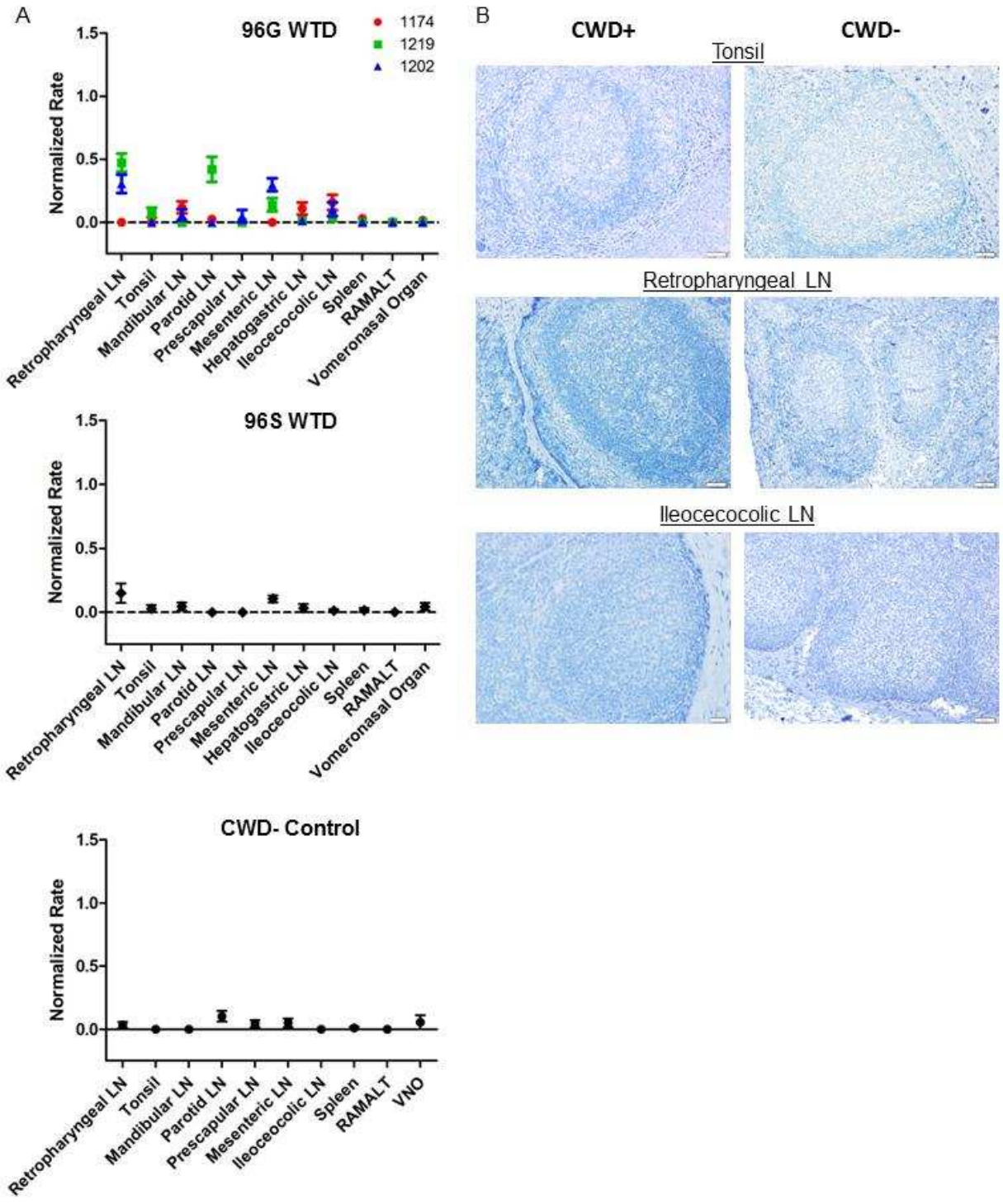

Figure 2.4. 1 MPE collection.
A. RT-QuIC of 96G, 96S, and negative control tissues collected at 1 MPE. Three tissues displayed significant RT-QuIC amyloid seeding: 1219 retropharyngeal lymph node, 1202 retropharyngeal lymph node, and 1219 parotid lymph node (one sample t-test, $p<0.05$). No significant PrP^{CWD} amyloid seeding formation was observed in 96S WTD tissues. Data represents mean rate of amyloid formation and standard error of mean (SEM) of 12 replicates

from 3 separate experiments.
B. Representative TSA-IHC from 96G WTD collected at 1 MPE. Minimal to no PrP^{CWD} immunoreactivity was detected in tonsils from WTD at 1 MPE. All images 200x magnification; scale bar = 50μm.

Two MPE. At 2 MPE, significant PrP^{CWD} seeding activity ($p<0.01$, one sample t-test) was consistently detected in lymph nodes draining the head and neck including the tonsil, retropharyngeal lymph node, and mandibular lymph node (Figure 2.5A). In addition, one 96G WTD had significant seeding activity in the parotid lymph node. Compared to 1 MPE (Figure 2.4A), the tonsil and retropharyngeal lymph node at 2 MPE displayed a faster amyloid formation rate, consistent with greater accumulation of PrP^{CWD} in these tissues. As at 1 MPE, lymphoid tissues from 96S WTD at 2 MPE contained no detectable PrP^{CWD} amyloid seeding activity.

TSA-IHC evaluation of lymphoid tissues from 96G WTD revealed PrP^{CWD} immunoreactivity in tonsils with greater distribution of staining when compared with 1 MPE tissues (Figure 2.5B)(summarized in Table 1). In addition, PrP^{CWD} immunoreactivity was observed in retropharyngeal lymph nodes from two 96G WTD. No PrP^{CWD} immunoreactivity was observed in 96S tissues.

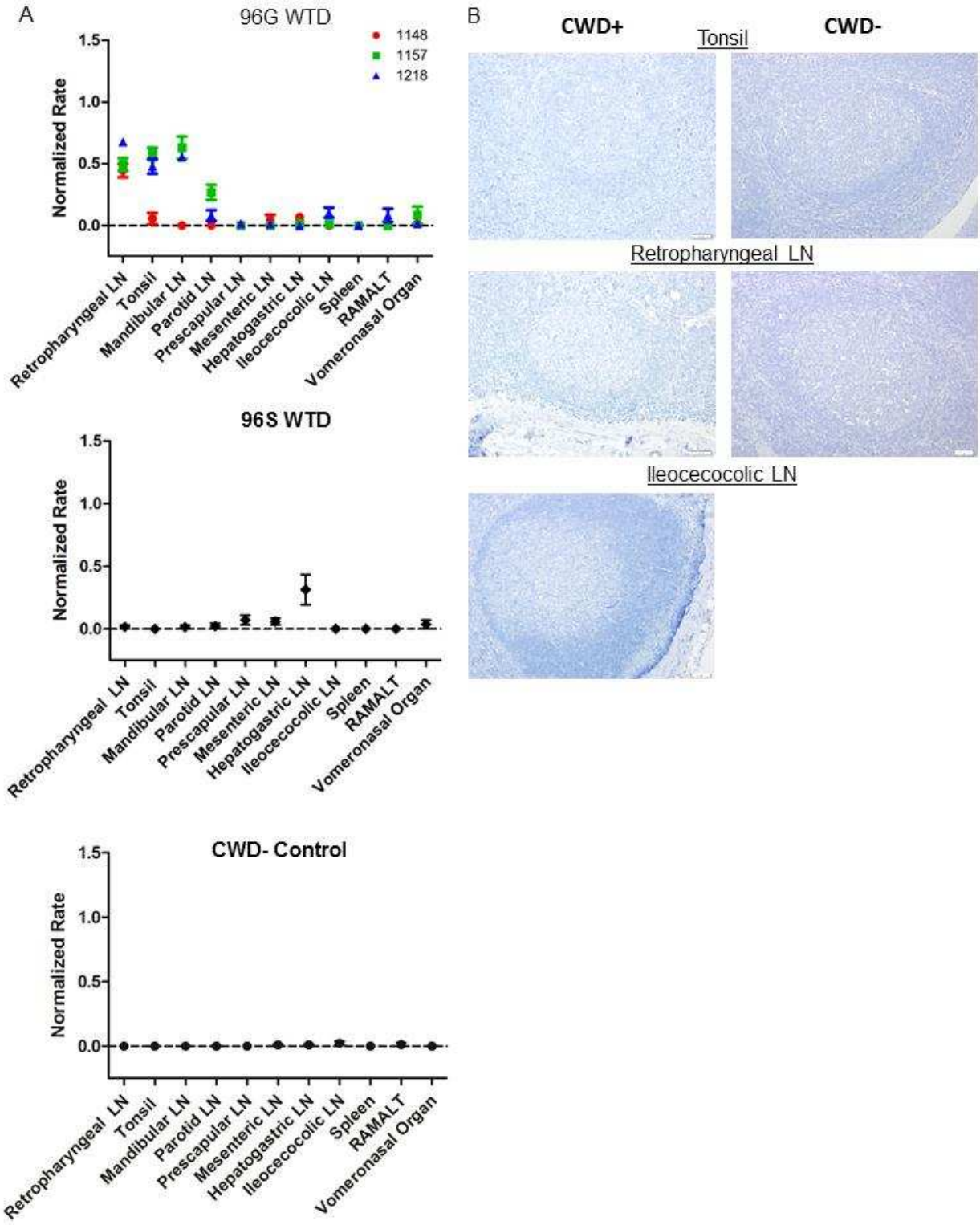

Figure 2.5 2 MPE collection.
A. RT-QuIC of 96G WTD, 96S WTD, and negative control tissues collected at 2 MPE. PrP^{CWD} amyloid seeding was detected in oropharyngeal lymphoid tissues from at least 1 96G WTD collected at 2 MPE, including the tonsil, retropharyngeal, mandibular, and parotid lymph nodes

(one sample t-test, $p<0.01$). Amyloid formation rates from 96S WTD tissues were not significantly different than the negative control. Data represents mean and SEM of 12 replicates from 3 separate experiments.
B. Representative TSA-IHC from 96G WTD collection at 2 MPE. Mild PrP^{CWD} immunoreactivity was detected in a small number of germinal center lymphoid follicles in tonsil and retropharyngeal lymph nodes. Images are 200x magnification; scale bar = 50 μm.

Three MPE. Following 3 MPE, significant PrP^{CWD} seeding activity expanded from lymph nodes associated with the head and neck detected at earlier collection times to include all systemic lymphoid tissues examined (Figure 2.6A) from at least one of the two 96G WTD. The lymphoid tissues draining the head and neck had the highest rates of amyloid seeding activity consistent with a greater PrP^{CWD} burden. The PrP^{CWD} seeding activity in spleen is consistent with systemic spread of prions, either through lymphoid cell trafficking or blood.

TSA-IHC analysis of tissues at 3MPE collection identified PrP^{CWD} immunoreactivity in the majority of systemic lymphoid tissues in addition to oropharyngeal lymphoid tissues (Figure 2.6B) (summarized in Table 2.1). Lymph nodes draining the head and neck had the greatest PrP^{CWD} staining distribution and intensity.

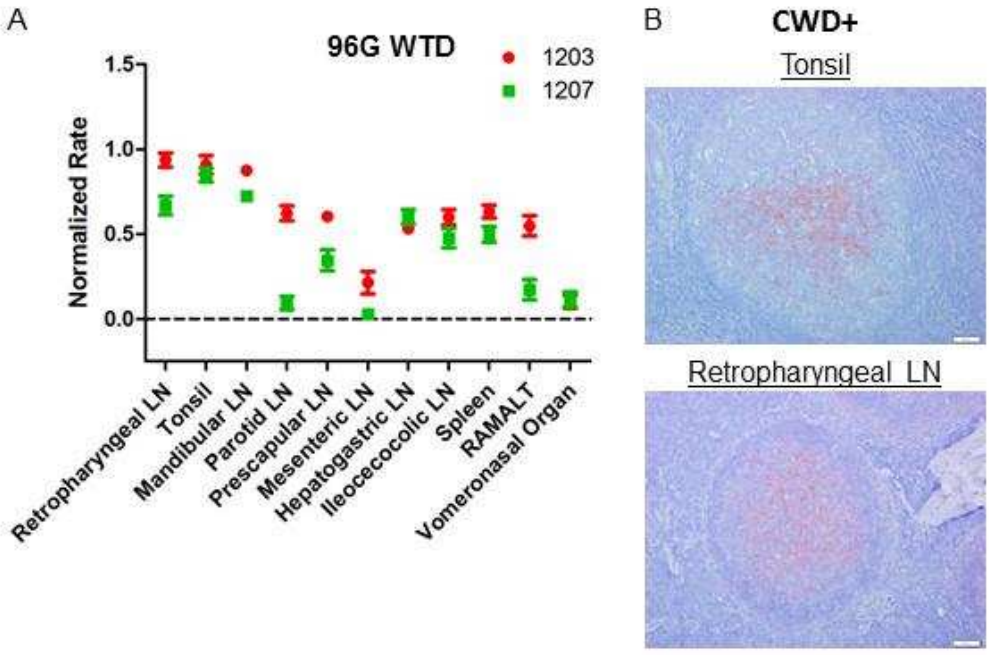

Figure 2.6 3 MPE collection.
A. RT-QuIC of 96G WTD tissues collected at 3 MPE. The majority of tissues display positive rates of amyloid formation that are statistically different than the corresponding negative control tissues (one sample t-test, $p<0.05$). The two tissues that are not significant are: 1207 mesenteric lymph node and 1207 parotid lymph node. The increase in lymphoid tissue distribution at 3 MPE is consistent with systemic prion spread. Amyloid formation rates in the oropharyngeal lymphoid tissues are higher at 3 MPE when compared with 2 MPE (Figure 2.5A) consistent with an accumulation of PrP^{CWD} with the longer incubation time. Data represents mean and SEM of 12 replicates from 3 separate experiments. 3 MPE tissues were compared with 4 MPI negative control tissues for statistical analysis.
B. Representative TSA-IHC from 96G WTD collected at 3 MPE. Increased PrP^{CWD} immunoreactivity staining was identified in oropharyngeal lymphoid tissues in lymphoid follicle germinal centers. TSA-IHC additionally detected PrP^{CWD} immunoreactivity in the majority of systemic lymphoid tissues (not pictured). IHC images are 200x magnification.

Four MPE. Tissues from 96G WTD sacrificed at 4 MPE had significant PrP^{CWD} amyloid seeding activity in the majority of tissues evaluated with only RAMALT and VNO displaying variable seeding activity (Figure 2.7A). Overall, tissues had a faster rate of amyloid formation when compared with 3 MPE consistent with greater PrP^{CWD} tissue accumulation. The first identification of amyloid seeding activity in a 96S WTD was detected in the tonsil at this time point.

TSA-IHC analysis of 4 MPE tissues revealed PrP^{CWD} immunoreactivity in all tissues from at least 2 of the 3 96G WTD examined (Figure 2.7B). The tonsil and retropharyngeal lymph nodes had extensive PrP^{CWD} immunoreactivity in lymphoid follicle germinal centers. Other tissues had increased PrP^{CWD} follicle distribution compared to 3 MPE tissues and greater staining intensity consistent with increased prion accumulation. No PrP^{CWD} immunoreactivity was observed in tissues from 96S WTD.

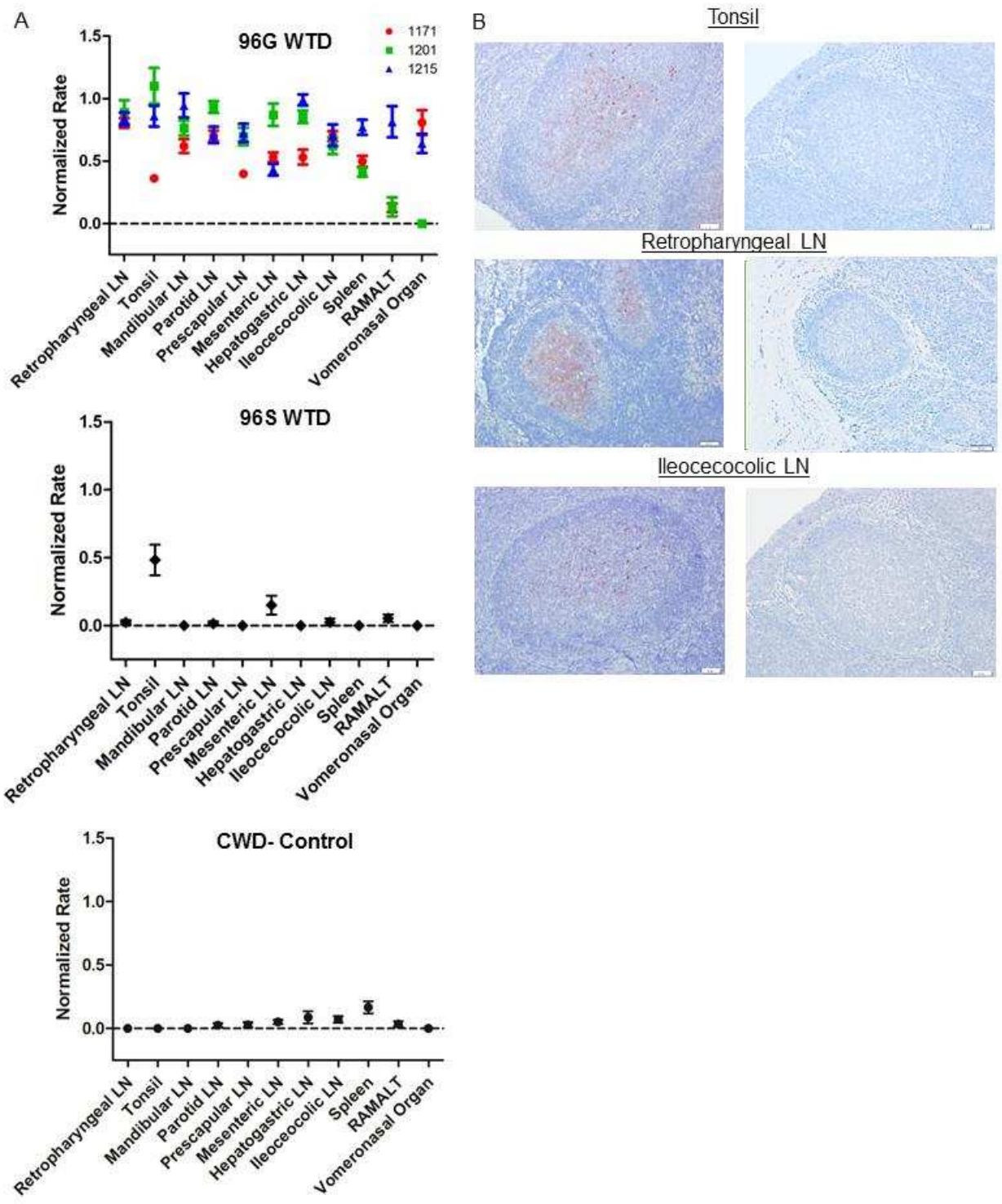

Figure 2.7 4 MPE collection.
A. RT-QuIC of WTD tissues collected at 4 MPE. All tissues examined displayed PrP^{CWD} amyloid formation detected in at least two of the three 96G WTD (one sample t-test, $p<0.05$). The two tissues that did not have significant rates of amyloid formation are 1201 vomeronasal organ and 1201 RAMALT. Compared with 3 MPE (Figure 2.6), 4 MPI tissues have greater rates of amyloid formation consistent with a larger PrP^{CWD} tissue burden. Tonsil from 96S WTD had

detectable amyloid formation at this collection time (one sample t-test, $p<0.01$). Data represents mean and SEM of 12 replicates from 3 separate experiments.
B. Representative TSA-IHC from 96G WTD collected at 4 MPE. All lymphoid tissues displayed PrP^{CWD} immunoreactivity in the germinal centers of follicles. The greatest staining was observed in oropharyngeal lymphoid tissues. No staining was observed in corresponding negative control tissues.

Evaluation of PrP^{CWD} in the obex. The obex region of the medulla oblongata was evaluated for evidence of PrP^{CWD} neuroinvasion by RT-QuIC and TSA-IHC. No PrP^{CWD} RT-QuIC seeding was detected at any collection time (Figure 2.8A). No PrP^{CWD} immunoreactivity was observed by TSA-IHC (Figure 2.8B). This demonstrates that there is no detectable evidence of neuroinvasion in the time period we evaluated following mucosal prion exposure.

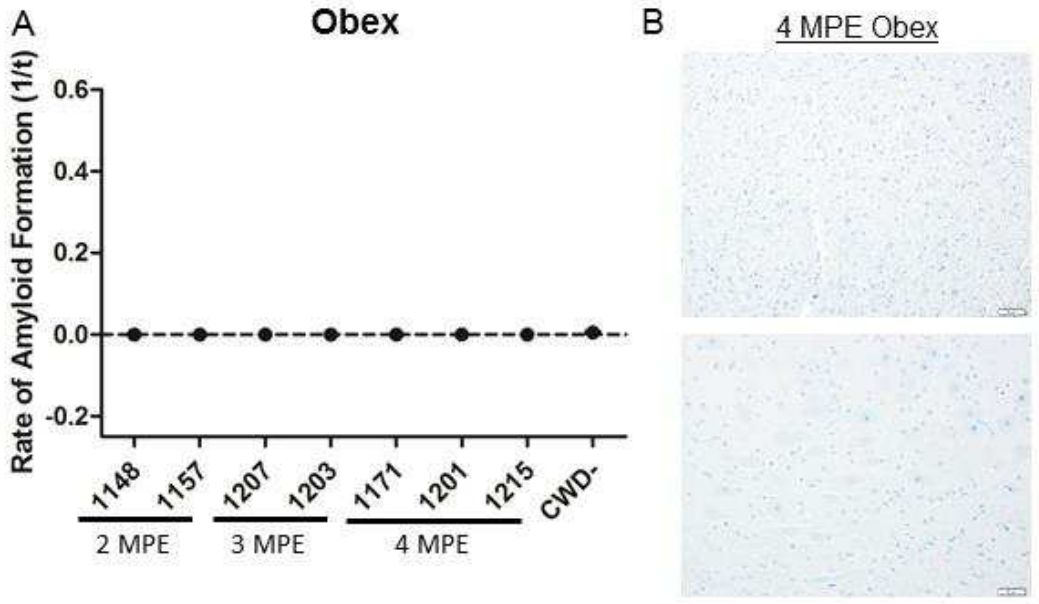

Figure 2.8 No evidence of neuroinvasion at 4 MPE.
A. RT-QuIC evaluation of obex samples collected from 2MPE to 4 MPE. No evidence of PrP^{CWD} amyloid seeding was detected in the obexes evaluated from early infection time points.
B. Representative TSA-IHC of the obex collected at 4 MPE. No PrP^{CWD} immunoreactivity was observed in sections of the obex from the 4 MPE collection.

Table 2.1 Summary of PrP^{CWD} detection by RT-QuIC and IHC following mucosal exposure.
RT-QuIC and TSA-IHC detected similar patterns of PrP^{CWD} accumulation during early infection: initial detection in oropharyngeal lymph nodes prior to systemic lymphoid dissemination. Although the two assays displayed similar lymphoid distribution patterns, RT-QuIC analysis identified more positive tissues when compared with TSA-IHC. Data for each tissue displayed as number of animals positive by detection method out of total number of animals examined. (Abbreviations: QuIC = RT-QuIC; IHC = TSA-IHC; Retro. LN = Retropharyngeal lymph node; LN= lymph node; VNO = Vomeronasal organ)

Tissue	**1 MPE**		**2 MPE**		**3 MPE**		**4 MPE**	
	QuIC	IHC	QuIC	IHC	QuIC	IHC	QuIC	IHC
Retro. LN	2/3	0/3	3/3	2/3	2/2	2/2	3/3	3/3
Tonsil	0/3	2/3	2/3	3/3	2/2	2/2	3/3	3/3
Mandibular LN	0/3	0/3	2/3	0/3	2/2	2/2	3/3	3/3
Parotid LN	1/3	1/3	1/3	0/3	1/2	1/2	3/3	2/3
Prescapular LN	0/3	0/3	0/3	0/3	2/2	1/2	3/3	2/3
Mesenteric LN	1/3	0/3	0/3	0/1	1/2	0/2	3/3	2/3
Hepatogastric LN	0/3	0/3	0/3	0/3	2/2	2/2	3/3	3/3
Ileocecocolic LN	0/3	0/2	0/3	0/3	2/2	1/2	3/3	3/3
Spleen	0/3	0/2	0/3	0/2	2/2	1/2	3/3	2/3
RAMALT	0/3	0/3	0/3	0/2	2/2	0/2	2/3	2/3
VNO	0/3	N/A	0/3	N/A	2/2	N/A	2/3	N/A
Ileum	N/A	0/2	N/A	0/2	N/A	1/2	N/A	2/2
Obex	0/3	0/3	0/3	0/3	0/2	0/2	0/3	0/3

Estimation of prion burden during early CWD infection

We have previously reported the prion concentration in the sample used to seed the RT-QuIC reaction directly correlates with the rate of amyloid formation (26,27). To explore the kinetics of PrP^{CWD} accumulation in lymphoid tissues over the course of early infection, we compared the average rates of amyloid formation in lymphoid tissues from the 1-4 MPE collection times with those collected from 3 white-tailed deer with terminal disease (20-24 months post-infection). Evaluation of lymphoid tissues over time revealed two patterns. First, the oropharyngeal lymph nodes, including the tonsil, retropharyngeal lymph node, and mandibular lymph node displayed a rapid accumulation of PrP^{CWD}, approximating terminal tissue levels by 3 MPI, with no statistical difference observed between 3 MPI, 4 MPE, and the

terminal disease states ($p < 0.05$, one sample t-test) (Figure 2.9A). Second, the parotid lymph node, distal gastrointestinal lymph nodes, and spleen displayed a later accumulation of PrP^{CWD} and did not reach peak tissue burdens during the time course of our study (4 MPE tissues compared with terminal, $p<0.05$, one sample t-test) (Figure 2.9B). We approximated the PrP^{CWD} amyloid formation kinetics of these two lymphoid patterns by linear regression analysis and found no statistical difference between the rates by slope analysis of best-fit linear regression lines ($p=0.4229$, linear regression analysis). This data confirms the lymphoid tissues examined have similar prion replication kinetics and that the difference in lymphoid tissue prion levels at 4 MPE is due to the sequence of PrP^{CWD} tissue infection, i.e. the oropharyngeal tissues were infected earlier than systemic lymphoid tissues, and not due to a difference in prion replication kinetics.

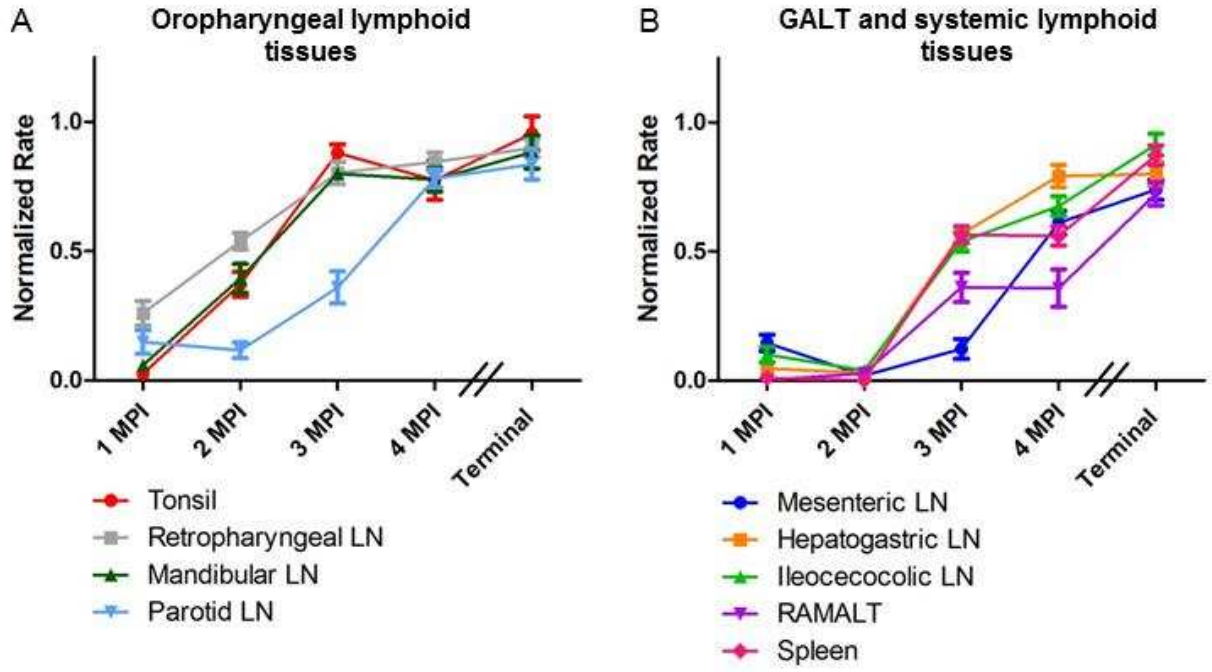

Figure 2.9. Estimation of lymphoid tissue prion accumulation during the course of early CWD infection.

A. Estimation of prion replication kinetics in oropharyngeal lymphoid tissues during early CWD infection. The prion concentration in tissues was estimated by averaging the rates of amyloid formation collection time point. Two lymphoid PrP^{CWD} accumulation patterns were observed. A) In orophargyneal lymph nodes, the tonsil, retropharyngeal and mandibular lymph nodes displayed a rapid PrP^{CWD} accumulation and reached tissue PrP^{CWD} tissue levels comparable with terminal disease burden by 3 MPE ($p<0.05$, one sample t-test). The parotid lymph node had a slower prion accumulation but reached prion levels comparable with terminal disease by 4 MPE ($p<0.01$, one sample t-test).

B. Estimation of prion replication kinetics in gastrointestinal-associated lymphoid tissues (GALT) and systemic lymphoid tissues during early CWD infection. Distal GALT tissues and the spleen did not display PrP^{CWD} seeding until 3 MPE, later than oropharyngeal lymphoid tissues (in A). At 4 MPE, all tissues had significantly lower rates of amyloid formation than corresponding terminal tissues ($p<0.01$, one sample t-test), indicating these lymphoid tissues did not reach maximum prion burdens during the time course of our study.

Discussion

We analyzed PrP^{CWD} distribution in WTD at early time points following oral exposure. Although we were unable to identify the sites of mucosal entry following PrP^{CWD} ingestion, we demonstrated early PrP^{CWD} accumulation in oropharyngeal lymph nodes at 1 MPE and rapid

systemic accumulation of PrP^{CWD} in lymphoid tissues by 4 MPE with tissue prion levels comparable to terminal disease. Our findings are consistent with previous investigations of early CWD pathogenesis (21,22) despite the exposure dose given in our study being 10-fold lower. This suggests either the dose of PrP^{CWD} does not impact infection kinetics or that in all of these studies the given dose far surpassed the natural infectious dose resulting in the same experimental disease course. A recent report determined the minimal effective oral dose of sheep-adapted BSE to be 0.05g and did not observe alterations in the disease course at higher inoculation doses (29). Investigations into the minimum infectious oral dose required for CWD in the natural host are on-going.

Similar to other ingested TSEs, such as scrapie and variant Creutzfeldt-Jakob disease, our results demonstrate CWD displays and early and sustained lymphoid replication phase prior to neuroinvasion (30,31). Temporal investigations of scrapie identified gastrointestinal-associated lymphoid tissues, including tonsil, retropharyngeal lymph node, Peyer's patches, and ileocecocolic lymph nodes, as the first sites of PrP^{Sc} detection (32,33). The pattern of lymphoid accumulation observed in our study is consistent with two phases. First, the lymphoid tissues draining the head and neck displayed PrP^{CWD} amyloid seeding activity and IHC immunoreactivity. This is consistent with either a larger initial PrP^{CWD} dose in these tissues due to direct drainage from the oral mucosa or faster PrP^{CWD} replication kinetics. This initial lymphoid replication phase was followed by widespread systemic lymphoid PrP^{CWD} replication, as evidenced by PrP^{CWD} detection in the spleen. PrP^{CWD} may be trafficked from initial lymphoid replication sites through either blood or lymphoid cells. Blood has been previously shown to harbor CWD infectivity (10) with B cells and platelets being identified as the infectious components (34). In contrast, a mouse study identified macrophages as the cell responsible for

transporting prions from intestinal mucosa to draining lymph nodes (35). Further studies are needed to illuminate which lymphoid cell or cells are responsible for systemic prion trafficking in subclinical chronic wasting disease. A surprising finding was the early detection of PrP^{CWD} seeding activity in the vomeronasal organ at 3 MPE. Nasal brushings in conjunction with RT-QuIC have recently been investigated as a potential pre-clinical diagnostic tool in humans with CJD and cervids (36-38). The early PrP^{CWD} distribution to the nasal cavity may provide a route of environmental shedding in preclinical animals.

Given the transmission of TSEs following oral exposure, investigations have focused on how prions cross gastrointestinal mucosal barriers. Studies on intestinal uptake have identified M cells of the follicle-associated epithelium of Peyer's patches as a site of prion entry (39,40). Additionally, GALT uptake appears to be required for neuroinvasion as depletion of M cells or decreased numbers of Peyer's patches, but not lymphocytes, in mice blocked the development of prion disease (35,41-43). Other imaging studies have suggested prions can use a paracellular route across the epithelial mucosa by identifying prions in between cells (40). Our study identified the oropharyngeal lymph nodes, tonsil, retropharyngeal, and mandibular lymph nodes as an initial site of PrP^{CWD} lymphoid accumulation after oral exposure suggesting a pathway of mucosal uptake in the oral cavity plays an important role in early pathogenesis. It is possible that intestinal mucosal uptake also contributes to prion uptake, similar to other orally transmitted TSEs, but it remains unclear where the primary mucosal entry site is located and how prions cross oral mucosal barriers in CWD.

At early CWD disease stages, the low prion tissue burden limits PrP^{CWD} identification by traditional immunoblotting techniques. Here, we have demonstrated both RT-QuIC and a modified immunohistochemistry technique, TSA-IHC, can enhance PrP^{CWD} detection.

Comparison of RT-QuIC and TSA-IHC as a detection method during early infection time points demonstrated RT-QuIC consistently identified PrP^{CWD} amyloid seeding in tissues approximately 1 month prior to IHC detection. This finding is consistent with recent literature that reported RT-QuIC has at least equal sensitivity as IHC in detecting PrP^{CWD} in RAMALT biopsies from WTD and elk (36,37). A larger sample size is necessary to evaluate the sensitivity and specificity of RT-QuIC as a diagnostic tool for PrP^{CWD} detection in terminal lymphoid tissues. The variation in PrP^{CWD} tissue detection among 96G WTD from the same collection time is consistent with individual animal variation and tissue sectioning differences.

In regards to influence of the PRNP genotype on susceptibility to CWD, our study is consistent with previous investigations on codon 96 (17). Lymphoid tissues from 96S WTD did not display the same RT-QuIC amyloid seeding activity as 96G WTD tissues and PrP^{CWD} was only detected in tonsil collected at 4 MPI. The slower disease course in 96S WTD may be better able to distinguish the chronological sequence of PrP^{CWD} lymphoid replication that is otherwise masked in the faster 96G WTD disease course. Thus, identification of amyloid seeding in tonsil suggests this tissue might be the first location of PrP^{CWD} seeding and replication following oral exposure. However, the small number of animals available for our study makes these conclusions tentative.

In summary, we used RT-QuIC and TSA-IHC to illustrate lymphoid seeding and replication in oropharyngeal lymphoid tissues as early as 1 month following oral CWD exposure. This initial lymphoid replication phase was followed by PrP^{CWD} replication in systemic lymphoid tissues with tissue burdens approximating terminal disease levels by 4 months post-exposure. Similar to other orally acquired TSEs, prion lymphoid amplification appears to occur prior to neuroinvasion.

Future Directions

Future studies will examine the remaining systemic and lymphoid tissues collected at 4 MPE to determine the full-body distribution of PRP^{CWD} at this early time point. We will use a new end-point RT-QuIC technique for this whole-animal survey. In addition, we plan on evaluating excreta, including saliva and urine, from these early collection time points to determine the extent of environmental shedding during early disease.

CHAPTER 2 REFERENCES

1. Williams, E. S. (2005) Chronic wasting disease. *Veterinary pathology* **42**, 530-549
2. Haley, N. J., and Hoover, E. A. (2015) Chronic wasting disease of cervids: current knowledge and future perspectives. *Annu Rev Anim Biosci* **3**, 305-325
3. ProMED-mail. (2016) Chronic Wasting Disease, Cervid - Europe: (Norway). *ProMED-mail* **20160410.4149651**
4. Williams, E. S., and Young, S. (1980) Chronic wasting disease of captive mule deer: a spongiform encephalopathy. *Journal of wildlife diseases* **16**, 89-98
5. Spraker, T. R., Miller, M. W., Williams, E. S., Getzy, D. M., Adrian, W. J., Schoonveld, G. G., Spowart, R. A., O'Rourke, K. I., Miller, J. M., and Merz, P. A. (1997) Spongiform encephalopathy in free-ranging mule deer (Odocoileus hemionus), white-tailed deer (Odocoileus virginianus) and Rocky Mountain elk (Cervus elaphus nelsoni) in northcentral Colorado. *Journal of wildlife diseases* **33**, 1-6
6. Williams, E. S., and Young, S. (1993) Neuropathology of chronic wasting disease of mule deer (Odocoileus hemionus) and elk (Cervus elaphus nelsoni). *Veterinary pathology* **30**, 36-45
7. Spraker, T. R., Zink, R. R., Cummings, B. A., Wild, M. A., Miller, M. W., and O'Rourke, K. I. (2002) Comparison of histological lesions and immunohistochemical staining of proteinase-resistant prion protein in a naturally occurring spongiform encephalopathy of free-ranging mule deer (Odocoileus hemionus) with those of chronic wasting disease of captive mule deer. *Veterinary pathology* **39**, 110-119
8. Miller, M. W., Williams, E. S., Hobbs, N. T., and Wolfe, L. L. (2004) Environmental sources of prion transmission in mule deer. *Emerg Infect Dis* **10**, 1003-1006
9. Mathiason, C. K., Hays, S. A., Powers, J., Hayes-Klug, J., Langenberg, J., Dahmes, S. J., Osborn, D. A., Miller, K. V., Warren, R. J., Mason, G. L., and Hoover, E. A. (2009) Infectious prions in pre-clinical deer and transmission of chronic wasting disease solely by environmental exposure. *PloS one* **4**, e5916
10. Mathiason, C. K., Powers, J. G., Dahmes, S. J., Osborn, D. A., Miller, K. V., Warren, R. J., Mason, G. L., Hays, S. A., Hayes-Klug, J., Seelig, D. M., Wild, M. A., Wolfe, L. L., Spraker, T. R., Miller, M. W., Sigurdson, C. J., Telling, G. C., and Hoover, E. A. (2006) Infectious prions in the saliva and blood of deer with chronic wasting disease. *Science* **314**, 133-136
11. Tamguney, G., Miller, M. W., Wolfe, L. L., Sirochman, T. M., Glidden, D. V., Palmer, C., Lemus, A., DeArmond, S. J., and Prusiner, S. B. (2009) Asymptomatic deer excrete infectious prions in faeces. *Nature* **461**, 529-532
12. Haley, N. J., Seelig, D. M., Zabel, M. D., Telling, G. C., and Hoover, E. A. (2009) Detection of CWD prions in urine and saliva of deer by transgenic mouse bioassay. *PloS one* **4**, e4848
13. Johnson, C. J., Phillips, K. E., Schramm, P. T., McKenzie, D., Aiken, J. M., and Pedersen, J. A. (2006) Prions adhere to soil minerals and remain infectious. *PLoS pathogens* **2**, e32
14. Nalls, A. V., McNulty, E., Powers, J., Seelig, D. M., Hoover, C., Haley, N. J., Hayes-Klug, J., Anderson, K., Stewart, P., Goldmann, W., Hoover, E. A., and Mathiason, C. K.

(2013) Mother to offspring transmission of chronic wasting disease in reeves' muntjac deer. *PloS one* **8**, e71844
15. Robinson, S. J., Samuel, M. D., O'Rourke, K. I., and Johnson, C. J. (2012) The role of genetics in chronic wasting disease of North American cervids. *Prion* **6**, 153-162
16. Johnson, C., Johnson, J., Clayton, M., McKenzie, D., and Aiken, J. (2003) Prion protein gene heterogeneity in free-ranging white-tailed deer within the chronic wasting disease affected region of Wisconsin. *Journal of wildlife diseases* **39**, 576-581
17. Johnson, C. J., Herbst, A., Duque-Velasquez, C., Vanderloo, J. P., Bochsler, P., Chappell, R., and McKenzie, D. (2011) Prion protein polymorphisms affect chronic wasting disease progression. *PloS one* **6**, e17450
18. Race, B., Meade-White, K., Miller, M. W., Fox, K. A., and Chesebro, B. (2011) In vivo comparison of chronic wasting disease infectivity from deer with variation at prion protein residue 96. *Journal of virology* **85**, 9235-9238
19. van Keulen, L. J., Vromans, M. E., and van Zijderveld, F. G. (2002) Early and late pathogenesis of natural scrapie infection in sheep. *APMIS : acta pathologica, microbiologica, et immunologica Scandinavica* **110**, 23-32
20. O'Rourke, K. I., Zhuang, D., Lyda, A., Gomez, G., Williams, E. S., Tuo, W., and Miller, M. W. (2003) Abundant PrP(CWD) in tonsil from mule deer with preclinical chronic wasting disease. *Journal of veterinary diagnostic investigation : official publication of the American Association of Veterinary Laboratory Diagnosticians, Inc* **15**, 320-323
21. Sigurdson, C. J., Williams, E. S., Miller, M. W., Spraker, T. R., O'Rourke, K. I., and Hoover, E. A. (1999) Oral transmission and early lymphoid tropism of chronic wasting disease PrPres in mule deer fawns (Odocoileus hemionus). *The Journal of general virology* **80 (Pt 10)**, 2757-2764
22. Fox, K. A., Jewell, J. E., Williams, E. S., and Miller, M. W. (2006) Patterns of PrPCWD accumulation during the course of chronic wasting disease infection in orally inoculated mule deer (Odocoileus hemionus). *The Journal of general virology* **87**, 3451-3461
23. Hunter, N., Houston, F., Foster, J., Goldmann, W., Drummond, D., Parnham, D., Kennedy, I., Green, A., Stewart, P., and Chong, A. (2012) Susceptibility of young sheep to oral infection with bovine spongiform encephalopathy decreases significantly after weaning. *Journal of virology* **86**, 11856-11862
24. Stewart, P., Campbell, L., Skogtvedt, S., Griffin, K. A., Arnemo, J. M., Tryland, M., Girling, S., Miller, M. W., Tranulis, M. A., and Goldmann, W. (2012) Genetic predictions of prion disease susceptibility in carnivore species based on variability of the prion gene coding region. *PloS one* **7**, e50623
25. Seelig, D. M., Nalls, A. V., Flasik, M., Frank, V., Eaton, S., Mathiason, C. K., and Hoover, E. A. (2015) Lesion profiling and subcellular prion localization of cervid chronic wasting disease in domestic cats. *Veterinary pathology* **52**, 107-119
26. Henderson, D. M., Davenport, K. A., Haley, N. J., Denkers, N. D., Mathiason, C. K., and Hoover, E. A. (2015) Quantitative assessment of prion infectivity in tissues and body fluids by real-time quaking-induced conversion. *The Journal of general virology* **96**, 210-219
27. Henderson, D. M., Denkers, N. D., Hoover, C. E., Garbino, N., Mathiason, C. K., and Hoover, E. A. (2015) Longitudinal Detection of Prion Shedding in Saliva and Urine by Chronic Wasting Disease-Infected Deer by Real-Time Quaking-Induced Conversion. *Journal of virology* **89**, 9338-9347

28. Davenport, K. A., Henderson, D. M., Bian, J., Telling, G. C., Mathiason, C. K., and Hoover, E. A. (2015) Insights into Chronic Wasting Disease and Bovine Spongiform Encephalopathy Species Barriers by Use of Real-Time Conversion. *Journal of virology* **89**, 9524-9531
29. McGovern, G., Martin, S., Jeffrey, M., Dexter, G., Hawkins, S. A., Bellworthy, S. J., Thurston, L., Algar, L., and Gonzalez, L. (2016) Minimum Effective Dose of Cattle and Sheep BSE for Oral Sheep Infection. *PloS one* **11**, e0151440
30. Mabbott, N. A., and MacPherson, G. G. (2006) Prions and their lethal journey to the brain. *Nat Rev Microbiol* **4**, 201-211
31. Beekes, M., and McBride, P. A. (2007) The spread of prions through the body in naturally acquired transmissible spongiform encephalopathies. *The FEBS journal* **274**, 588-605
32. van Keulen, L. J., Schreuder, B. E., Vromans, M. E., Langeveld, J. P., and Smits, M. A. (2000) Pathogenesis of natural scrapie in sheep. *Archives of virology. Supplementum*, 57-71
33. Hadlow, W. J., Kennedy, R. C., and Race, R. E. (1982) Natural infection of Suffolk sheep with scrapie virus. *The Journal of infectious diseases* **146**, 657-664
34. Mathiason, C. K., Hayes-Klug, J., Hays, S. A., Powers, J., Osborn, D. A., Dahmes, S. J., Miller, K. V., Warren, R. J., Mason, G. L., Telling, G. C., Young, A. J., and Hoover, E. A. (2010) B cells and platelets harbor prion infectivity in the blood of deer infected with chronic wasting disease. *Journal of virology* **84**, 5097-5107
35. Takakura, I., Miyazawa, K., Kanaya, T., Itani, W., Watanabe, K., Ohwada, S., Watanabe, H., Hondo, T., Rose, M. T., Mori, T., Sakaguchi, S., Nishida, N., Katamine, S., Yamaguchi, T., and Aso, H. (2011) Orally administered prion protein is incorporated by m cells and spreads into lymphoid tissues with macrophages in prion protein knockout mice. *The American journal of pathology* **179**, 1301-1309
36. Haley, N. J., Siepker, C., Hoon-Hanks, L. L., Mitchell, G., Walter, W. D., Manca, M., Monello, R. J., Powers, J. G., Wild, M. A., Hoover, E. A., Caughey, B., and Richt, J. A. (2016) Seeded amplification of chronic wasting disease prions in nasal brushings and recto-anal mucosa associated lymphoid tissues from elk by real time quaking-induced conversion. *Journal of clinical microbiology*
37. Haley, N. J., Siepker, C., Walter, W. D., Thomsen, B. V., Greenlee, J. J., Lehmkuhl, A. D., and Richt, J. A. (2016) Antemortem detection of chronic wasting disease prions in nasal brush collections and rectal biopsies from white-tailed deer by real time quaking-induced conversion. *Journal of clinical microbiology*
38. Orru, C. D., Bongianni, M., Tonoli, G., Ferrari, S., Hughson, A. G., Groveman, B. R., Fiorini, M., Pocchiari, M., Monaco, S., Caughey, B., and Zanusso, G. (2014) A test for Creutzfeldt-Jakob disease using nasal brushings. *The New England journal of medicine* **371**, 519-529
39. Kujala, P., Raymond, C. R., Romeijn, M., Godsave, S. F., van Kasteren, S. I., Wille, H., Prusiner, S. B., Mabbott, N. A., and Peters, P. J. (2011) Prion uptake in the gut: identification of the first uptake and replication sites. *PLoS pathogens* **7**, e1002449
40. Kincaid, A. E., Hudson, K. F., Richey, M. W., and Bartz, J. C. (2012) Rapid transepithelial transport of prions following inhalation. *Journal of virology* **86**, 12731-12740

41. Donaldson, D. S., Kobayashi, A., Ohno, H., Yagita, H., Williams, I. R., and Mabbott, N. A. (2012) M cell-depletion blocks oral prion disease pathogenesis. *Mucosal Immunol* **5**, 216-225
42. Prinz, M., Huber, G., Macpherson, A. J., Heppner, F. L., Glatzel, M., Eugster, H. P., Wagner, N., and Aguzzi, A. (2003) Oral prion infection requires normal numbers of Peyer's patches but not of enteric lymphocytes. *The American journal of pathology* **162**, 1103-1111
43. Glaysher, B. R., and Mabbott, N. A. (2007) Role of the GALT in scrapie agent neuroinvasion from the intestine. *J Immunol* **178**, 3757-3766

CHAPTER 3:
Detection and Quantification of CWD Prions in Fixed Paraffin Embedded Tissues by Real-Time Quaking-Induced Conversion[1]

Summary

Traditional diagnostic detection of chronic wasting disease (CWD) relies on immunodetection of misfolded CWD prion protein (PrP^{CWD}) by western blotting, ELISA, or immunohistochemistry (IHC). These techniques require separate sample collections (frozen and fixed) which may result in discrepancies due to variation in prion tissue distribution and assay sensitivities that limit detection especially in early and subclinical infections. Here, we harness the power of real-time quaking induced conversion (RT-QuIC) to amplify, detect, and quantify prion amyloid seeding activity in fixed paraffin-embedded (FPE) tissue sections. We show that FPE RT-QuIC has greater detection sensitivity than IHC in tissues with low PrP^{CWD} burdens, including those that are IHC-negative. We also employ amyloid formation kinetics to yield a semi-quantitative estimate of prion concentration in a given FPE tissue. We report that FPE RT-QuIC has the ability to enhance diagnostic and investigative detection of disease-associated PrP^{RES} in prion, and potentially other, protein misfolding disease states.

Background

Prion diseases, or transmissible spongiform encephalopathies, are fatal neurodegenerative diseases that include Creutzfeldt-Jakob disease (CJD) in humans, bovine spongiform encephalopathy (BSE), sheep scrapie, and cervid chronic wasting disease (CWD).

---

[1]Chapter published as: Hoover CE, Davenport KA, Henderson DM, Pulscher LA, Mathiason CK, Zabel MD, Hoover EA. Detection and Quantification of CWD Prions in Fixed Paraffin Embedded Tissues by Real-Time Quaking-Induced Conversion. *Sci Rep*. May 9, 2016. 6:25098

Disease is initiated when a misfolded isoform (designated PrP^{Sc}, PrP^{RES}, PrP^{CWD}, or PrP^{D}) induces templated misfolding of the normal cellular prion protein (PrP^{C}) to propagate via a process of seeded polymerization (1,2). Prions are characterized by increased formation of β sheets, propensity to aggregate into amyloid fibrils, and resistance to protease and acid digestion (3-5). Typical histologic lesions include spongiform neuropathology and neurodegeneration associated with deposition of PrP^{Sc}, and reactive astrogliosis (4).

Definitive diagnosis of CWD traditionally relies on detection of PrP^{CWD} by immunohistochemistry (IHC), western blot (WB), enzyme-linked immunosorbent assay (ELISA), or animal bioassay. The tissues tested typically include antemortem biopsies of tonsil or rectal associated mucosal lymphoid tissue (RAMALT) or postmortem sampling of the obex region of the brainstem. Analysis by these techniques requires a minimum of two separate tissue samples, formalin fixed tissues for IHC and fresh or frozen tissues for WB and ELISA that can create result disparity in results if PrP^{CWD} is not homogenously distributed or at low levels. While immunodetection methods can provide qualitative estimation of prion concentration, calculating the infectious titer of a prion tissue sample requires an end-point dilution bioassay, which relies on disease incubation time to determine infectivity levels. Bioassay limitations include animal availability, cost, and time required (often greater than one year to complete). Cell culture based assays have been developed to supplant animal bioassays (6,7), but remain relatively time consuming, may be limited to specific prion strains, and are not suitable for fixed tissue samples.

Previous studies have established protocols for the isolation of disease associated prion proteins from formalin-fixed paraffin-embedded tissue sections [8-10]. Transgenic mice expressing hamster PrP^{C} intracerebrally inoculated with prions isolated from formaldehyde fixed paraffin-

embedded 263K scrapie strain terminal brains developed clinical disease(8). Prion protein can be demonstrated in some archived formalin-fixed paraffin-embedded tissues and detected by western blotting, albeit with lower levels of sensitivity, typically limiting this method to terminal samples (9,10). A separate protein blotting technique, the paraffin embedded tissue blot, can detect PrP^{D} deposition in the brain of pre-clinical animals by using harsh epitope retrieval and immunostaining; however, the multi-step process is labor intensive and cannot provide quantitative data (11).

In most samples collected prior to terminal disease, PrP^{CWD} levels are often below the threshold of detection by IHC or WB; thus detection at these time points requires *in vitro* amplification methods for detection (12-15). One amyloid amplification method is real time quaking induced conversion (RT-QuIC), which utilizes templated prion seeded conversion of bacterially expressed recombinant PrP^{C} into amyloid structures that are measured by thioflavin T (ThT) fluorescence (15). Repeated cycles of shaking are used to exponentially increase initial low levels of PrP^{CWD}, potentially facilitating a greater sensitivity of detection. In addition, RT-QuIC amyloid formation kinetics have been adapted to estimate the low quantity of prions in samples of body fluids and excreta (16,17) with a sensitivity approaching bioassay (14).

Here, we describe a simple and rapid technique to detect and quantify PrP^{CWD} prion seeding activity from fixed paraffin-embedded (FPE) tissues by RT-QuIC. Assessment of RT-QuIC amyloid formation rate kinetics enabled quantification of PrP^{CWD}, providing a useful estimation of prion infectivity in IHC positive tissues. The combination of IHC and FPE RT-QuIC makes possible the description of PrP^{CWD} distribution and estimation of the infectious titer in tissues, including those with minimal or absent PrP^{CWD} detection by IHC.

Methods

Animals

Hand-raised, indoor-adapted white-tailed deer (WTD) (*Odocoileus virginianus*) were provided through long-standing collaboration of David Osborn, Sallie Dahmes, Karl Olsen, and Robert Warren, at the Warnell School of Forestry and Natural Resources, University of Georgia. Deer were housed in an indoor research facility at Colorado State University. Institutional Animal Care and Use Committee (IACUC) protocols for animal treatment and handling were followed. All animal studies were approved by Colorado State University IACUC. Archived tissues from CWD-infected WTD were used to optimize these techniques. All WTD with 800-series ID numbers were intranasally inoculated with two 1 mL doses of a 5% CWD positive brain homogenate (18). Deer were allowed to develop clinical disease and tissues were collected at terminal necropsy. All deer with 11-series and 12-series ID numbers were inoculated *per os* with 0.5 grams of a CWD positive pool of cervid brain. Deer were sacrificed, necropsied, and tissues collected at scheduled monthly intervals post-inoculation prior to development of clinical signs associated with CWD infection.

Tissue processing

At necropsy, all tissues were individually collected with a prion-free instruments to prevent cross contamination and were divided in half with one half stored at -80°C until use and the other half fixed for a minimum of 48 hours in periodate-lysine-paraformaldehyde (PLP) fixative. After 48 hours tissues were transferred to sterile 1xPBS until trimming and then stored in 70% ethanol. Sections of the obex region of the medulla oblongata, retropharyngeal lymph node, and tonsil were trimmed and subjected to routine paraffin embedding. Frozen tissues were homogenized in 1xPBS at 10% weight per volume with a Blue Bullet™ bead-beater

homogenizer (Next Advance) with care to avoid any cross contamination among tissue homogenates.

Protein extraction from FPE blocks

Eight to 10 μm thick paraffin-embedded tissue wax curls were cut from paraffin blocks using a microtome (Leica) with a prion-free microtome blade and prion-free forceps for every FPE sample to avoid cross contamination. Paraffin-tissue curls were subjected to a series of xylene and graded alcohol washes (100%, 95%, and 70%) to remove paraffin and rehydrate tissues similar to standard histological methods. Following alcohol treatments rehydrated FPE tissues were washed with 1xPBS. Rehydrated FPE tissue was homogenized in at 10% weight per volume by manual disruption or a bead homogenizer as described above.

Immunohistochemistry for PrP^{CWD}

Following routine paraffin embedding, 5 μm microtome tissue sections were placed on positively charged glass slides. Tissues were deparaffinized, rehydrated with graded alcohols, and treated with 88% formic acid digestion prior to heat-induced epitope antigen retrieval in the 2100-Retriever™ (Prestige Medical). Following retrieval, endogenous peroxidase activity was quenched prior to prion epitope detection with anti-prion antibody BAR224 (Cayman chemical) at 2 μg/mL concentration and Envision+™ anti-mouse HRP-labeled polymer (Dako). Following antibody treatment, antigen was visualized with 3-amino-9-ethylcarbazole (AEC) substrate chromogen (Dako). Tissue sections were counterstained with Meyer's hematoxylin (Dako) and 0.1% bicarbonate bluing reagent prior to coverslipping with aqueous mounting media (Dako).

Recombinant Syrian hamster PrP^{C} protein purification

Purification was performed as previously described (14,16,19). Briefly, recombinant truncated Syrian hamster PrP^{C} (90-231) (SHrPrP) was expressed and purified from BL21 Rosetta

(Novagen) *Escherichia coli*. Cells from a glycerol stock were cultured at 37°C in lysogeny broth (LB) media with selection antibiotics kanamycin and chloramphenicol until the final OD_{600} was at least 2.5. Cell lysis was performed using Bugbuster™ reagent, supplemented with Lysonase™ (EMD Biosciences) and inclusion bodies harvested by centrifugation at 15,000 x g. Inclusion bodies were dissolved in solubilization buffer (8M guanidine hydrochloride, 100mM Na_2HPO_4) and applied to NiNTA superflow resin (Qiagen) that had been equilibrated with denaturation buffer (6M guanidine hydrochloride, 100mM Na_2HPO_4, 10mM Tris). The resin-SHrPrP was loaded on to a XK16-60 column (GE Healthcare) and purified using a Bio-Rad Duoflow™ FPLC. A gradient from denaturation buffer to refolding buffer (100mM Na_2HPO_4, 10mM Tris) was applied to induce protein refolding prior to a wash with refolding buffer. Refolding was followed by a gradient from refolding to elution buffer (100mM NaH_2PO_4, 10mM Tris, 0.5 M imidazole) and all fractions were collected. The fractions from the elution peak were pooled and dialyzed (20mM NaH_2PO_4) overnight. Protein concentration was calculated by measuring the A_{280} and using a coefficient of extinction of 25,900 in Beer's Law.

RT-QuIC assay

Assay conditions were as previously described (16,17). FPE tissue homogenates or 10% frozen tissue homogenates were diluted in 0.1% sodium dodecyl sulfate (SDS)/ 1xPBS buffer as described. For subclinical WTD samples, a 10^{-1} dilution of FPE homogenates was used to seed the RT-QuIC reaction. Two μL of diluted sample was added to the RT-QuIC reaction buffer consisting of 20mM NaH_2PO4, 320mM NaCl, 1.0mM EDTA, 1mM Thioflavin T (ThT) and 0.1 mg/mL SHrPrP. RT-QuIC reactions were carried out in black, optical bottom 96-well plates (Nunc) in a BMG Labtech Polarstar™ fluorometer. RT-QuIC cycles consisted of 1 minute of shaking at 700 rpm followed by 1 minute of rest, repeated for 15 minutes. Fluorescence was

read at the conclusion of each 15 minute shake/rest cycle with an excitation of 450 nm and emission of 480 nm, gain of 1700, and each well was measured with 20 flashes per well with an orbital averaging of 4. Each RT-QuIC assay was performed for 250 cycles, the equivalent of 62.5 hours.

CWD bioassay in transgenic cervidized mice

All mice were bred and maintained at Colorado State University Lab Animal Resources, accredited by the Association for Assessment and Accreditation of Lab Animal Care International in accordance with protocols approved by the Institutional Animal Care and Use Committee at Colorado State University. All animal studies were approved by Colorado State University IACUC. Transgenic mice overexpressing the cervid cellular prion protein were inoculated with 30 µL of a homogenate pooled from six terminal experimentally inoculated WTD brain samples (cervid brain pool 6; CBP6) diluted from 1.0% to 0.00001% concentration. Mice were observed for clinical signs and sacrificed when they reached terminal disease. Mice that did not develop clinical signs were sacrificed at 500 days post inoculation when the study was terminated. Brains were harvested from all animals at time of sacrifice and analyzed for PrP^{CWD} by immunohistochemistry following the above protocol or western blot (20).

RT-QuIC rate analysis and quantification

The time to threshold, or C_t values, were calculated by determining the time (hours) for a positive amyloid seeding reaction to reach a predetermined threshold (established as 5 standard deviations above the average baseline fluorescence of all samples). The rate of amyloid formation was calculated as the inverse of the Ct value (1/h). FPE RT-QuIC amyloid formation

rates for each sample were confirmed to be normally distributed using the D'Agostino-Pearson normality test. RT-QuIC amyloid formation rates were statistically compared with corresponding negative controls using a one-sample t test. An equation relating the amyloid formation rate (1/h) to the LD_{50} for mouse bioassayed material (CBP6) was created by applying a best-fit line to the linear range, 10^{-4} to 10^{-6}, of the RT-QuIC CBP6 dilution. This equation, in the format of y=mlog(x) +b, was used to correlate LD_{50} data (x) to RT-QuIC rates (y).

Results

Detection of PrP^{CWD} in FPE brain samples

RT-QuIC is a prion-seeded amyloid amplification assay that uses recombinant PrP^{C} as the substrate and thioflavin T (ThT) amyloid-binding fluorescence emission as the indicator of prion enciphered amyloid fibril formation (21). RT-QuIC generation of prion seeded amyloid fibril formation follows a logarithmic pattern, with an early lag phase below the level of ThT detection and a rapid exponential phase as amyloid fibrils are formed, analogous to DNA replication in PCR reactions (Fig 3.1a). A positive RT-QuIC reaction is defined as when a ThT fluorescence curve crosses an established baseline threshold, calculated to be five standard deviations above the average initial fluorescence. The time for a reaction to reach the threshold is defined as the C_t value (hours). Since ThT fluorescence is recorded in real time, the rate of amyloid formation can be calculated as the inverse of the C_t value (1/h). Previous studies have demonstrated a direct, linear relationship between the C_t value and concentration of prions in the sample used to seed a reaction. Thus, samples with larger prion burdens have greater amyloid formation rates (14,16).

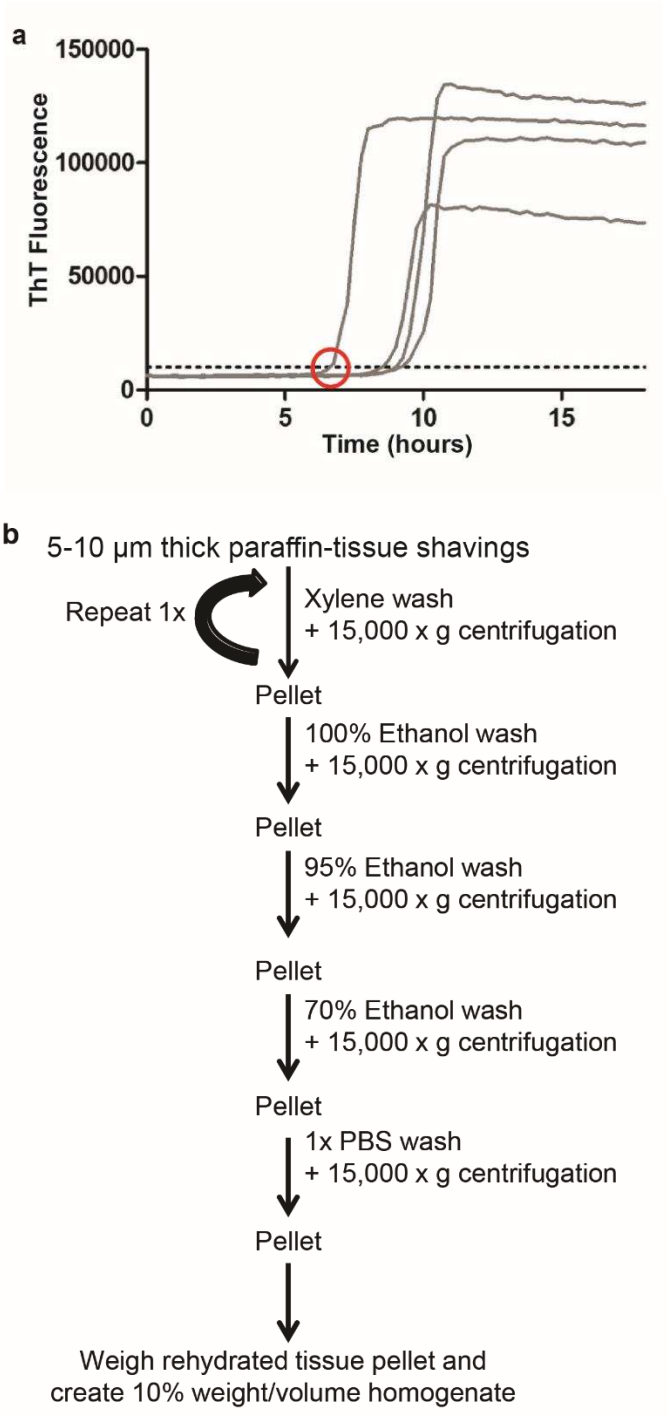

Figure 3.1 Overview of methods.
(a) Representative RT-QuIC fluorescence curve. As prion-enciphered amyloid is formed out of $rPrP^C$ substrate the RT-QuIC reaction transitions from lag phase to exponential phase. Amyloid formation is measured through thioflavin T (ThT) fluorescence emission as it binds amyloid. The Ct value is defined as the time (hours) for a positive RT-QuIC reaction to reach a predefined threshold (horizontal line), indicated by the red circle. The rate of amyloid formation is calculated as the inverse of Ct (1/h).
(b) Schematic of FPE protein extraction method.

To determine if our FPE protein extraction method preserved PrP^{CWD} amyloid seeding activity for RT-QuIC detection, we selected the obex portion of the medulla oblongata region of the brainstem from white-tailed deer (WTD) infected with CWD by an aerosol route. This region had marked PrP^{CWD} deposition demonstrated by IHC (Figure 3.2a) (18). Obex samples from sham-inoculated WTD were processed in parallel as negative controls. Microtome paraffin shavings of 8 to 10 µm thickness from FPE tissue blocks were treated with a series of xylene and alcohol washes to remove paraffin and rehydrate the tissue sections consistent with conventional histologic section processing. Following tissue rehydration, extracted samples were weighed and converted into a 10% weight per volume homogenate to standardize the amount of sample analyzed by RT-QuIC (Fig 3.1b).

Serial dilutions from 10^{-1} to 10^{-8} were analyzed comparing the FPE-extracted obex sample homogenates to the corresponding unfixed, frozen obex sample homogenates collected at necropsy from the same animal. All WTD inoculated with CWD had marked, variably sized PrP^{CWD} plaque accumulation and neuropil vacuolation in the obex by IHC consistent with terminal disease pathology (Figure 3.2a). No PrP^{CWD} immunoreactivity was observed in the corresponding negative control obex samples. RT-QuIC ThT fluorescence readings were converted to rates of amyloid formation by calculating the C_t value. The dilutional series data demonstrated that the FPE obex homogenates maintained prion amyloid seeding activity over a 10^{-1} to 10^{-7} dilution range (Figure 3.2b). By comparison, dilution of parallel frozen unfixed obex homogenates from the same animal contained prion seeding activity from dilutions 10^{-3} to 10^{-8}. The absence of RT-QuIC amyloid seeding activity in 10^{-1} and 10^{-2} dilutions of unfixed frozen samples is well documented and believed to be the result of inhibitors present in high concentrations in nervous tissue homogenates, which must be diluted before amyloid formation

can occur (22). Background, spontaneous unseeded amyloid formation from $rPrP^{C}$ substrate was rare in negative control obex homogenates derived from either FPE or unfixed frozen obex samples and comparable between the two sample preparation techniques. These results demonstrated that the FPE RT-QuIC protocol can consistently and specifically detect PrP^{CWD} amyloid seeding activity in FPE obex homogenates from CWD-infected, but not control, WTD.

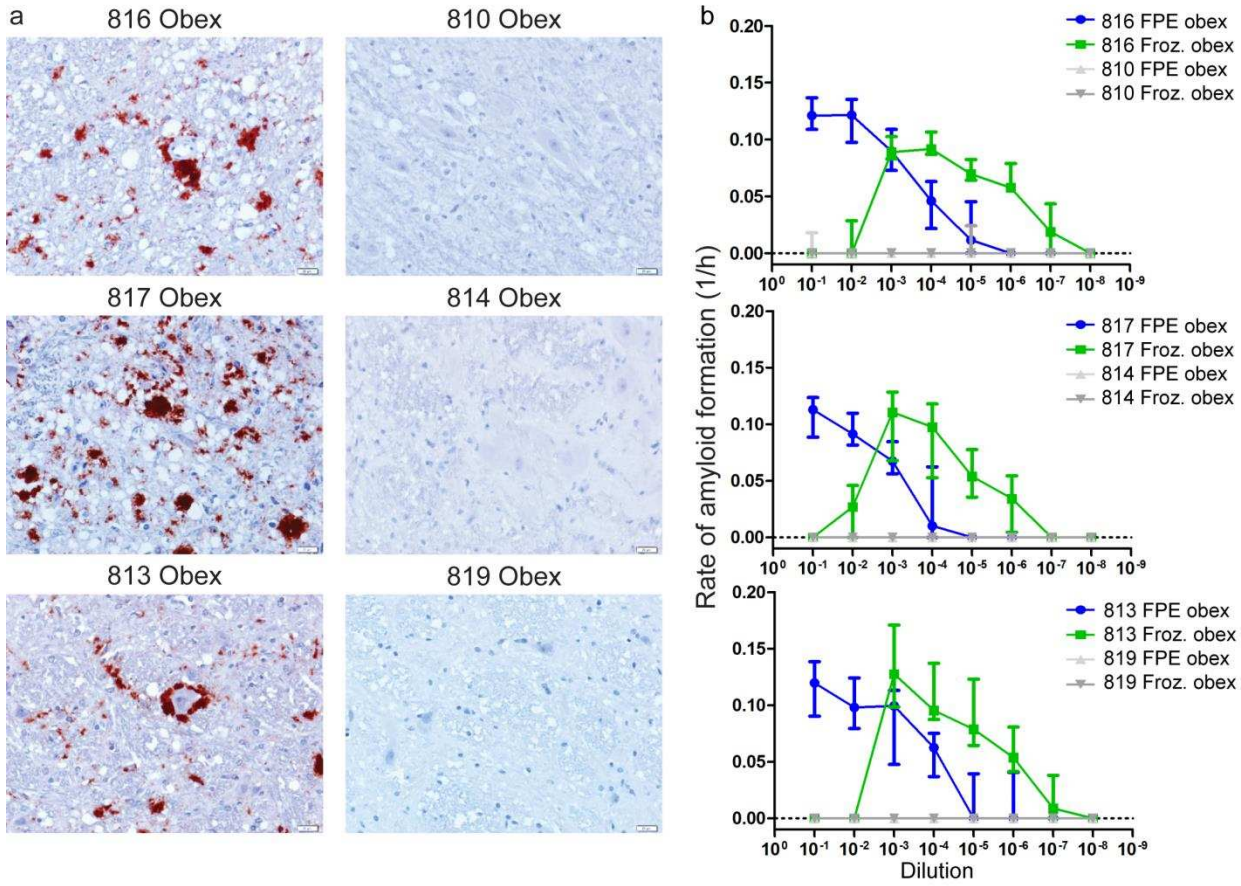

Figure 3.2 Detection of amyloid seeding activity in FPE obex tissue.
(a) Immunohistochemistry of obex from three terminal white-tailed deer. All display variably sized PrP^{CWD} plaque accumulations in the neuropil. The corresponding negative control animals do not display any PrP^{CWD} immunoreactivity. Images are 400x magnification, measurement bars represent 20 μm.
(b) RT-QuIC rates of amyloid formation of serial dilutions of FPE tissues from IHC positive obex and frozen 10% obex tissue homogenate. FPE samples from IHC positive obex are detectable in RT-QuIC from all three white-tailed deer examined. The RT-QuIC linear range in FPE obex samples extends from 10^{-1} to 10^{-6} whereas the linear range in frozen 10% homogenates is from 10^{-4} to 10^{-7}. Spontaneous amyloid formation from $rPrP^{C}$ negative control samples occurred equally rarely in both FPE and frozen homogenates. Each point represents median and interquartile range (IQR) and is derived of 8 replicates from a minimum of two separate experiments.

Detection of PrP^{CWD} seeding activity in FPE retropharyngeal lymph node

Next, we examined retropharyngeal lymph nodes from the same WTD analyzed in Figure 2 using identical FPE protein extraction methodology. Retropharyngeal lymph nodes from WTD inoculated with CWD displayed moderate to marked PrP^{CWD} deposition in germinal centers of

lymphoid follicles by IHC consistent with a CWD disease state (Figure 3a). By comparison, retropharyngeal lymph nodes from corresponding negative control WTD did not display any PrP^{CWD} immunoreactivity. Both FPE and frozen lymph node homogenates displayed amyloid seeding activity over dilutions 10^{-1} to 10^{-5} revealing lower endpoints and less inhibitor activity when compared to nervous tissue (Figure 3.3b). These results confirmed that the FPE protein extraction protocol is applicable to demonstrating amyloid seeding activity in FPE lymphoid tissues of WTD.

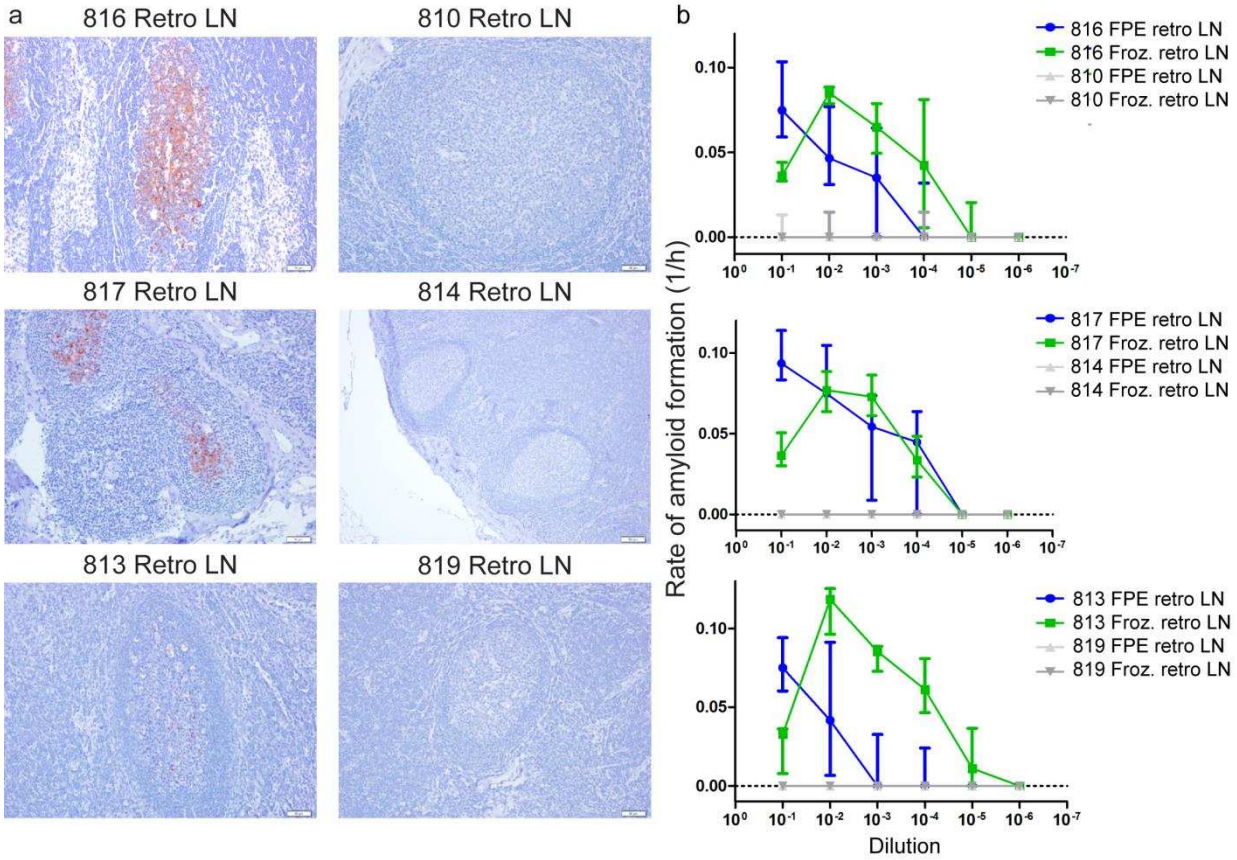

Figure 3.3 Detection of amyloid seeding activity in FPE retropharyngeal lymph node.
(a) Immunohistochemistry of retropharyngeal lymph nodes from three terminal white-tailed deer. Mild to marked PrP^{CWD} immunoreactivity is present in germinal centers of lymphoid follicles. No PrP^{CWD} immunoreactivity is detected in negative control animals. All IHC images are 200x magnification, measurement bars represent 20 μm.
(b) RT-QuIC of serial dilutions of terminal-disease, IHC positive FPE retropharyngeal lymph node and 10% frozen homogenate. Similar to obex samples (see Fig 2), RT-QuIC successfully detected amyloid seeding activity in FPE retropharyngeal lymph node samples. The range of

detection was similar between FPE samples and frozen samples, generally from 10^{-1} to 10^{-5}. Spontaneous amyloid formation was rare in negative controls and did not differ between FPE and frozen samples. Each point represents median and IQR and is derived of 8 replicates from a minimum of two separate experiments.

Sensitivity of RT-QuIC prion seeding activity detection in FPE tissues

We sought to estimate the sensitivity of FPE RT-QuIC seeding and concurrently determine whether prion-related amyloid seeding could be detected in IHC-negative tissues from CWD inoculated WTD due to RT-QuIC amplification of initial prion seeds. We selected tonsil and retropharyngeal lymph node samples from subclinical WTD that were orally inoculated with CWD and sacrificed at either two or four months post-inoculation (MPI). At these collection times, PrP^{CWD} was variably detectable by IHC in retropharyngeal lymph nodes and tonsils (summarized in Table 1). At 2 MPI, minimal or no PrP^{CWD} immunoreactivity was observed in tissues and was characterized by faint granular staining in germinal centers and limited lymphoid follicle distribution (Figure 4a). By contrast, at 4 MPI both lymphoid tissues displayed strong PrP^{CWD} IHC immunoreactivity with dense granular staining affecting the majority of the follicles. FPE RT-QuIC of tonsil and retropharyngeal lymph nodes from both subclinical time points (2 and 4 MPI) demonstrated amyloid seeding activities that were significantly different than corresponding FPE negative control tissues (One sample t-test, $p<0.01$) (Figure 4b). Tissues from 2 MPI had lower rates of amyloid formation, correlating with the minimal or absent PrP^{CWD} deposition observed by IHC. Likewise, higher amyloid formation rates were present in 4 MPI tissues, correlating with the marked PrP^{CWD} distribution noted by IHC. There were no significant differences between the amyloid formation rates of tonsil or retropharyngeal lymph nodes collected at the same MPI from WTD ($p<0.05$, 2 MPI one sample t-test, 4 MPI one-way ANOVA). These results demonstrated correlation of FPE RT-QuIC amyloid formation rates

with PrP^{CWD} detection by IHC. Additionally, we detected prion-related amyloid seeding activity in FPE samples at or below the threshold of IHC detection at 2 MPI.

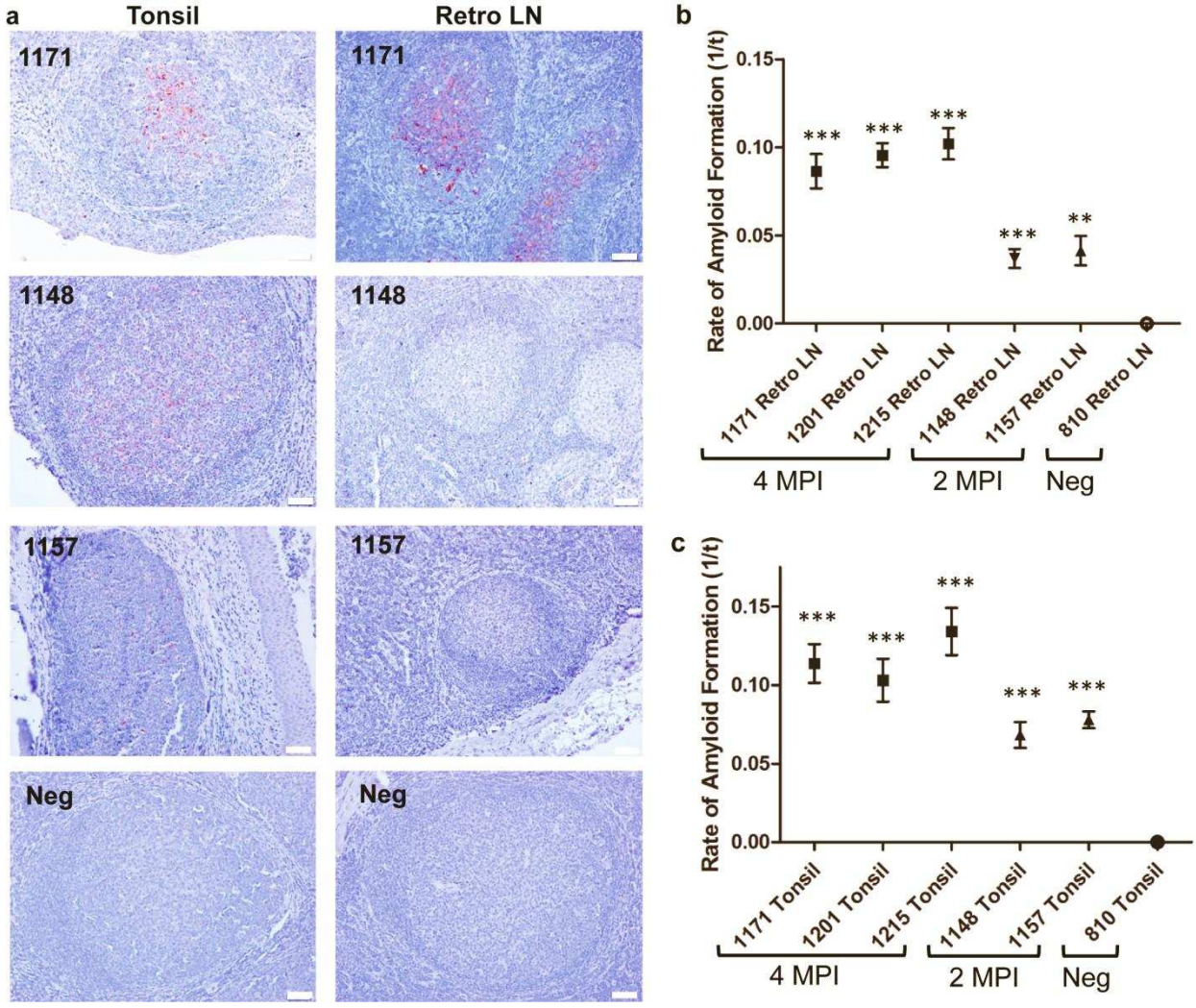

Figure 3.4 Analysis of FPE lymphoid tissues from subclinical CWD-infected WTD by RT-QuIC.

(a) Representative IHC of FPE lymphoid tissues from subclinical, CWD-infected WTD. Tissues collected at 4 MPI have increased density of PrP^{CWD} staining when compared to 2 MPI tissues reflecting a greater prion accumulation over the disease course. The low-level of PrP^{CWD} staining at 2 MPI reflects the early course of disease. RT-QuIC detected amyloid seeding activity in FPE samples that are IHC negative (1148 Retro LN). All IHC images are 200x magnification, measurement bars represent 50 μm.

(b) RT-QuIC of subclinical WTD retropharyngeal lymph nodes. All retropharyngeal lymph nodes from subclinical animals displayed significant amyloid seeding activity (means analyzed by one sample t-test; ** = $p< 0.01$, *** = $p<0.001$) when compared with respective negative control tissues. Lymph nodes collected at 4 MPI had higher RT-QuIC amyloid formation rates than tissues collected at 2 MPI which is consistent with greater PrP^{CWD} amyloid seeding activity. Each point represents the mean and SEM derived from eight replicates and in two

separate experiments. All FPE samples are assayed at a 10^{-1} dilution.
(c) RT-QuIC of subclinical WTD tonsils. All tonsils from subclinical animals displayed significant amyloid seeding activity (means analyzed by one sample t-test; *** = $p < 0.001$) when compared with respective negative control tissues. Similar to the retropharyngeal lymph nodes in b, tonsils collected at 4 MPI had higher RT-QuIC amyloid formation rates than tissues collected at 2 MPI which is consistent with greater PrP^{CWD} amyloid seeding activity. Each point represents the mean and SEM derived from eight replicates and in two separate experiments. All FPE samples are assayed at a 10^{-1} dilution.

Table 3.1 Summary of PrP^{CWD} IHC immunoreactivity in lymphoid tissues of subclinical WTD.
The number of lymphoid follicle germinal centers with PrP^{CWD} immunoreactivity out of the total number of follicles in the sections examined. This gives a general comparison of how much PrP^{CWD} is present in the tissue by IHC analysis. (LN = lymph node)

WTD	Tonsil	Retropharyngeal LN
1171 (4 MPI)	104/129	70/112
1201 (4 MPI)	146/183	177/232
1215 (4 MPI)	151/191	183/216
1148 (2 MPI)	8/134	0/95
1157 (2 MPI)	5/125	1/99

Correlation of RT-QuIC reaction rate with bioassay

To establish a biological correlation between the amyloid formation rate and an estimated tissue prion burden, we analyzed the RT-QuIC rate from a dilutional series of a deer brain homogenate that was assayed by cervid PrP^{C} transgenic mouse end-point dilutional bioassay to yield a calculated prion titer. The bioassay inoculum was a brain homogenate pooled from six terminal experimentally inoculated WTD (cervid brain pool 6; CBP6) that were confirmed PrP^{CWD} positive by western blot prior to pooling. Transgenic mice engineered to express the cellular cervid prion protein were inoculated intracerebrally with a dilution of the CBP6 extending from 1.0% to 0.00001% weight per volume (Figure 5a). Using Reed-Muench calculations, the mouse bioassay LD_{50} was calculated to be a 10^{-5} dilution, the equivalent of 3.33×10^{6} LD_{50}/gram of brain tissue (23). The CBP6 dilutional series linear range of RT-QuIC amyloid formation rates extended from 10^{-4} to 10^{-6} and was fit with a semi-log linear regression

line (Figure 5b). The equation of the semi-log fit line relates RT-QuIC amyloid formation rates on the y-axis to LD_{50} on the x-axis, enabling semi-quantitative estimation of the prion titer for a sample.

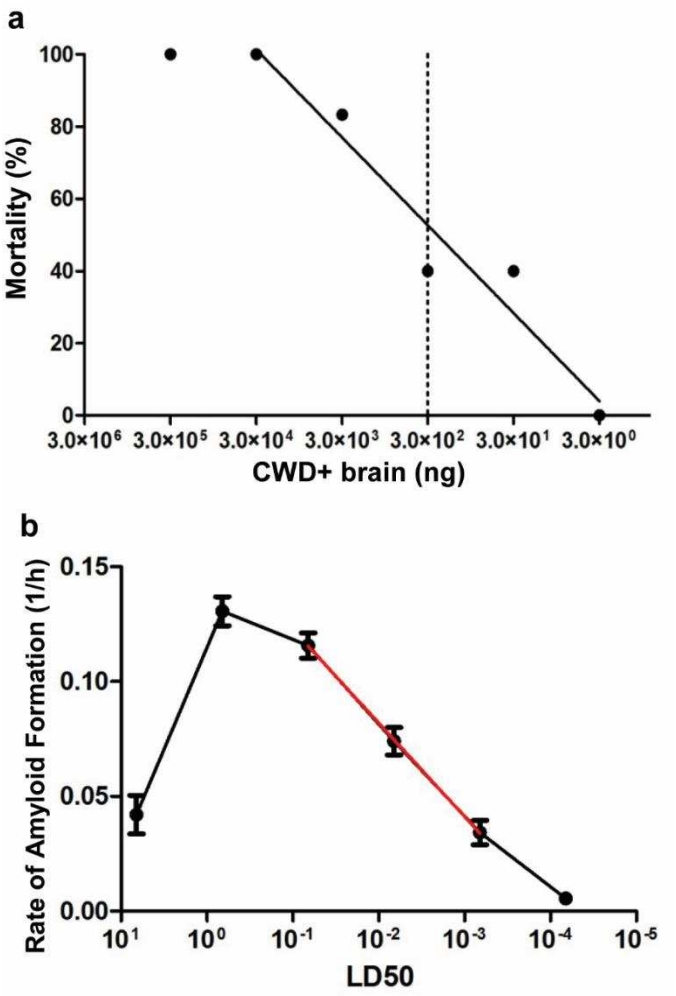

Figure 3.5 Endpoint dilution bioassay and RT-QuIC quantification of a CWD+ brain sample

(a) Percent mortality of cervidized transgenic mice that developed terminal CWD. The dashed vertical line indicates the LD_{50} which is calculated to be a 10^{-5} dilution or 3.33×10^6 LD_{50}/g of brain tissue.

(b) RT-QuIC rates of bioassay inoculum dilutional series. The solid curve represents the RT-QuIC amyloid formation rates (in LD_{50} units). The linear range extended from 10^{-4} to 10^{-6}. A semi-fit log line (red) was extrapolated from the linear range and used to relate y (rate of amyloid formation) to x (LD_{50}). The equation of this line, in the form y=m log(x) + b, was used for FPE quantification displayed in Table 2. Each point represents the mean and SEM of 48 replicates derived from eight separate experiments.

Quantification of prion-related seeding activity in FPE tissues

The correlation of FPE- RT-QuIC rates with PrP^{CWD} immunoreactivity in pre-clinical WTD (Figure 4) led us to estimate prion seeding activity in FPE samples by extrapolation to the RT-QuIC reaction rate standard curve derived from a bioassayed CWD brain pool as previously described (17). To establish the standard curve, we used a semi-log linear regression equation defined as: amyloid formation rate = 0.04073 log (sample LD_{50}) + 0.1633. Based on the RT-QuIC amyloid formation rate we were able to calculate the LD_{50} equivalents in each gram of FPE tissue using the defined equation (16). For example, the estimated PrP^{CWD} prion seeding activity in 1 gram of FPE tonsil from a 4 MPI WTD is calculated to be 3039.6 LD_{50}. The estimated LD_{50} per gram of FPE tissue in the subclinical WTD samples analyzed in Figure 4 are listed in Table 2. By correlating IHC detection and the RT-QuIC seeding rates in the FPE samples tested, we were able to consistently detect moderate IHC staining in samples with greater than 200 LD_{50}/g of FPE tissue. When comparing PrP^{CWD} detection by IHC and RT-QuIC, we determined that RT-QuIC could detect as little as 39 LD_{50}/g of tissue whereas the apparent threshold for detection by IHC examination was 50 LD_{50}/gram. This indicated that FPE RT-QuIC had a greater sensitivity than IHC alone for detecting CWD prion infection; however, a larger data set is needed to make a more definitive comparison and quantify the differences in sensitivity. Estimates of prion burdens in FPE samples also enable biological characterization of early CWD prion infection previously unavailable using IHC analysis alone. For example, FPE tissues collected during subclinical CWD infection (2 MPI to 4 MPI) demonstrated that tonsils consistently accumulated a higher CWD prion burden when compared to retropharyngeal lymph nodes. Likewise, the lymphoid tissues examined at 4 MPI contained at least a 10-fold greater LD_{50}/gram PrP^{CWD} deposition in the same tissues on average when compared to 2 MPI. These

observations suggest interesting insights into the early pathogenesis of CWD; however, a larger sample size is necessary to draw definitive conclusions.

Table 3.2 The estimated LD_{50}/gram of FPE samples.

WTD	Tonsil	Retropharyngeal LN
1171 (4 MPI)	3.04×10^3	6.49×10^2
1201 (4 MPI)	1.66×10^3	1.09×10^3
1215 (4 MPI)	9.60×10^3	1.57×10^3
1148 (2 MPI)	2.32×10^2	3.95×10^1
1157 (2 MPI)	4.00×10^2	5.07×10^1

Discussion

We describe a method for detection and semi-quantification of prion amyloid seeding activity in microtome sections of fixed paraffin-embedded tissues. Consistent with previous formalin fixed paraffin-embedded tissue studies analyzing prions by western blot or paraffin-embedded tissue blot we demonstrate that prion amyloid seeding is maintained throughout the tissue aldehyde cross-linking, dehydrating, lipid extracting, and paraffin embedding histological processes (9,11). The FPE RT-QuIC method makes possible the analysis of archived samples when only fixed paraffin-embedded tissues are available and minimizes the sampling differences encountered when separate fixed and frozen tissue samples are collected and examined. The additional semi-quantitative information provided by FPE RT-QuIC allows more precise investigations into PrP^{CWD} accumulation by tissues compared with subjective IHC scoring of mild/moderate/marked or lymphoid follicle counts. We have demonstrated the application of this method with a small observational study of deer early in their CWD disease progression.

An interesting observation of FPE RT-QuIC analysis of obex samples in Figure 2 was a shift in the range of detection. Previous RT-QuIC studies of frozen brain samples have consistently demonstrated an inability to detect seeding activity in 10^{-1} to 10^{-3} dilutions (16,22).

This is presumed to be due to inhibitors present in brain homogenates that are diluted out or minimized in smaller dilutions, permitting the amyloidogenesis from $rPrP^{C}$ reaction to occur. Investigations identifying the biochemical nature of these amyloid seeding inhibitors in brain are ongoing.

The correlation between IHC deposition, RT-QuIC amyloid seeding rate, and the disease course expressed as MPI is clear. Small differences in tissue amyloid seeding rates between animals collected at the same time point are expected due to biological variability. Importantly, detection of PrP^{CWD} seeding activity in lymphoid tissues of preclinical WTD with no or minimal detectable PrP^{CWD} by IHC suggests either greater sensitivity provided by RT-QuIC amplification or the presence of prion conformers that are sensitive to protease treatments used during IHC to abolish PrP^{C} background (24). Likewise, protein misfolding cyclic amplification analyses of some tissues in CWD-infected WTD have shown a contrast between amplifiable prion enciphering activity and detection of PrP^{CWD} in tissues by IHC (12). Further analysis with a larger data set is needed to accurately compare the diagnostic detection sensitivities and specificities of RT-QuIC and IHC. As with IHC, the degree to which the amyloid seeding activity measured by RT-QuIC is infectious is unknown. Here, we report on FPE RT-QuIC as a means to identify prion-derived amyloid seeding activity in fixed tissue and use this information to detect prion infection. This information can then be used, if desired, to estimate tissue prion burden by extrapolation to a bioassayed reference sample.

Building on previous work, we used the mathematical relationship between PrP^{CWD} seed concentration and the amyloid formation rate to estimate PrP^{CWD} concentration in tissues (16,17). The RT-QuIC quantification method we applied is consistent with previous literature that based quantification on endpoint dilution (14) and quantitative PMCA that demonstrates initial PrP^{CWD}

seed determines the amplification round of detection (25). In addition, the IHC staining results correlated well with RT-QuIC rates, further validating the relationship between amyloid seeding rates and concentration of prions in the sample. The RT-QuIC amyloid seeding reaction, which is consistent across various sample types, requires the presence of a conversion-competent prion seed to initiate amyloid formation. Bioassay data provides information on the lethality of the tested sample that is presumed to correspond to the prion burden of the inoculum. Thus, we can estimate the prion burden and lethality of a sample, such as FPE tissues, by extrapolating to the bioassay data. Of course this remains an approximation since the relationship of seeding activity and infectivity would be expected to vary with tissue, prion strain, RT-QuIC substrate sensitivity, and inhibitors that may be present, especially at low dilutions. Additional studies are needed to more closely quantify the infectivity and lethality of FPE RT-QuIC seeds and amyloid products. Frozen lymphoid tissue homogenates likely contain a variety of prion aggregation states as has previously been demonstrated in brain homogenates (26,27). It is not known whether this aggregation diversity is maintained throughout the FPE extraction process or if a single aggregate type or conformation is preferentially being selected. We included multiple experiments and replicates in our RT-QuIC analysis to mitigate uneven distribution of prion seeds in our samples and assay variability. It is also plausible that a small fraction of prion content is lost through the FPE extraction process. The one log lower upper limit of detection in FPE brain and retropharyngeal lymph nodes (Figures 2 and 3) could reflect these factors. If this is the case, our mathematical calculations may be underestimating the true prion seeding concentration. Despite these limitations, the FPE RT-QuIC quantification method still provides a useful means of estimating prion burden in diverse tissues when animal bioassays are precluded by large sample numbers or financial feasibility.

There is little to no evidence at present that RT-QuIC generates infectious prions. However, Sano et al. have reported bioassay of amyloid fibrils generated by the first round of RT-QuIC reactions seeded with infectious brain homogenate induced prion-specific disease when inoculated into wild-type mice (28). However, amyloid products from additional rounds of RT-QuIC did not demonstrate any infectivity. Lack of infectivity in amyloid fibrils generated from recombinant PrP^{C} is not unique to RT-QuIC. Amyloid fibrils produced by protein misfolding cyclic amplification using recombinant PrP^{C} substrate require polyanionic cofactors, such as RNA or specific lipids, to demonstrate infectivity in mouse bioassay (29,30). Possible reasons for lack of infectivity of RT-QuIC products include the use of truncated $rPrP^{C}$ as the substrate and absence of post-translational modifications, including glycosylation (31).

In summary, we present a rapid and simple method of PrP^{CWD} extraction from fixed paraffin embedded tissues and analysis for prion amyloid seeding activity using RT-QuIC. We believe this method can facilitate quantitative and correlative investigations of kinetics and pathogenesis during early and carrier states of prion diseases and potentially other protein misfolding disorders.

CHAPTER 3 REFERENCES

1. Prusiner, S. B. (1982) Novel proteinaceous infectious particles cause scrapie. *Science* **216**, 136-144
2. Pan, K. M., Baldwin, M., Nguyen, J., Gasset, M., Serban, A., Groth, D., Mehlhorn, I., Huang, Z., Fletterick, R. J., Cohen, F. E., and et al. (1993) Conversion of alpha-helices into beta-sheets features in the formation of the scrapie prion proteins. *Proc Natl Acad Sci U S A* **90**, 10962-10966
3. Prusiner, S. B., Groth, D. F., Bolton, D. C., Kent, S. B., and Hood, L. E. (1984) Purification and structural studies of a major scrapie prion protein. *Cell* **38**, 127-134
4. Aguzzi, A., Sigurdson, C., and Heikenwaelder, M. (2008) Molecular mechanisms of prion pathogenesis. *Annual review of pathology* **3**, 11-40
5. McKinley, M. P., Bolton, D. C., and Prusiner, S. B. (1983) A protease-resistant protein is a structural component of the scrapie prion. *Cell* **35**, 57-62
6. Bian, J., Napier, D., Khaychuck, V., Angers, R., Graham, C., and Telling, G. (2010) Cell-based quantification of chronic wasting disease prions. *Journal of virology* **84**, 8322-8326
7. Klohn, P. C., Stoltze, L., Flechsig, E., Enari, M., and Weissmann, C. (2003) A quantitative, highly sensitive cell-based infectivity assay for mouse scrapie prions. *P Natl Acad Sci USA* **100**, 11666-11671
8. Priola, S. A., Ward, A. E., McCall, S. A., Trifilo, M., Choi, Y. P., Solforosi, L., Williamson, R. A., Cruite, J. T., and Oldstone, M. B. (2013) Lack of prion infectivity in fixed heart tissue from patients with Creutzfeldt-Jakob disease or amyloid heart disease. *Journal of virology* **87**, 9501-9510
9. Nicholson, E. M., Kunkle, R. A., Hamir, A. N., Lebepe-Mazur, S., and Orcutt, D. (2007) Detection of the disease-associated isoform of the prion protein in formalin-fixed tissues by Western blot. *Journal of veterinary diagnostic investigation : official publication of the American Association of Veterinary Laboratory Diagnosticians, Inc* **19**, 548-552
10. Loiacono, C. M., Beckwith, N., Kunkle, R. A., Orcutt, D., and Hall, S. M. (2010) Detection of PrP(Sc) in formalin-fixed, paraffin-embedded tissue by Western blot differentiates classical scrapie, Nor98 scrapie, and bovine spongiform encephalopathy. *Journal of veterinary diagnostic investigation : official publication of the American Association of Veterinary Laboratory Diagnosticians, Inc* **22**, 684-689
11. Schulz-Schaeffer, W. J., Tschoke, S., Kranefuss, N., Drose, W., Hause-Reitner, D., Giese, A., Groschup, M. H., and Kretzschmar, H. A. (2000) The paraffin-embedded tissue blot detects PrP(Sc) early in the incubation time in prion diseases. *The American journal of pathology* **156**, 51-56
12. Haley, N. J., Mathiason, C. K., Carver, S., Telling, G. C., Zabel, M. D., and Hoover, E. A. (2012) Sensitivity of protein misfolding cyclic amplification versus immunohistochemistry in ante-mortem detection of chronic wasting disease. *The Journal of general virology* **93**, 1141-1150
13. Morales, R., Duran-Aniotz, C., Diaz-Espinoza, R., Camacho, M. V., and Soto, C. (2012) Protein misfolding cyclic amplification of infectious prions. *Nat Protoc* **7**, 1397-1409
14. Wilham, J. M., Orru, C. D., Bessen, R. A., Atarashi, R., Sano, K., Race, B., Meade-White, K. D., Taubner, L. M., Timmes, A., and Caughey, B. (2010) Rapid end-point

quantitation of prion seeding activity with sensitivity comparable to bioassays. *PLoS pathogens* **6**, e1001217
15. Atarashi, R., Moore, R. A., Sim, V. L., Hughson, A. G., Dorward, D. W., Onwubiko, H. A., Priola, S. A., and Caughey, B. (2007) Ultrasensitive detection of scrapie prion protein using seeded conversion of recombinant prion protein. *Nature methods* **4**, 645-650
16. Henderson, D. M., Davenport, K. A., Haley, N. J., Denkers, N. D., Mathiason, C. K., and Hoover, E. A. (2015) Quantitative assessment of prion infectivity in tissues and body fluids by real-time quaking-induced conversion. *The Journal of general virology* **96**, 210-219
17. Henderson, D. M., Denkers, N. D., Hoover, C. E., Garbino, N., Mathiason, C. K., and Hoover, E. A. (2015) Longitudinal Detection of Prion Shedding in Saliva and Urine by Chronic Wasting Disease-Infected Deer by Real-Time Quaking-Induced Conversion. *Journal of virology* **89**, 9338-9347
18. Denkers, N. D., Hayes-Klug, J., Anderson, K. R., Seelig, D. M., Haley, N. J., Dahmes, S. J., Osborn, D. A., Miller, K. V., Warren, R. J., Mathiason, C. K., and Hoover, E. A. (2013) Aerosol transmission of chronic wasting disease in white-tailed deer. *Journal of virology* **87**, 1890-1892
19. Henderson, D. M., Manca, M., Haley, N. J., Denkers, N. D., Nalls, A. V., Mathiason, C. K., Caughey, B., and Hoover, E. A. (2013) Rapid antemortem detection of CWD prions in deer saliva. *PloS one* **8**, e74377
20. Denkers, N. D., Telling, G. C., and Hoover, E. A. (2011) Minor oral lesions facilitate transmission of chronic wasting disease. *Journal of virology* **85**, 1396-1399
21. LeVine, H., 3rd. (1999) Quantification of beta-sheet amyloid fibril structures with thioflavin T. *Methods in enzymology* **309**, 274-284
22. Orru, C. D., Wilham, J. M., Raymond, L. D., Kuhn, F., Schroeder, B., Raeber, A. J., and Caughey, B. (2011) Prion disease blood test using immunoprecipitation and improved quaking-induced conversion. *mBio* **2**, e00078-00011
23. Reed, L. J., and Muench, H. (1938) A SIMPLE METHOD OF ESTIMATING FIFTY PER CENT ENDPOINTS. *American Journal of Epidemiology* **27**, 493-497
24. Safar, J. G., Scott, M., Monaghan, J., Deering, C., Didorenko, S., Vergara, J., Ball, H., Legname, G., Leclerc, E., Solforosi, L., Serban, H., Groth, D., Burton, D. R., Prusiner, S. B., and Williamson, R. A. (2002) Measuring prions causing bovine spongiform encephalopathy or chronic wasting disease by immunoassays and transgenic mice. *Nature biotechnology* **20**, 1147-1150
25. Chen, B., Morales, R., Barria, M. A., and Soto, C. (2010) Estimating prion concentration in fluids and tissues by quantitative PMCA. *Nature methods* **7**, 519-520
26. Prusiner, S. B., Groth, D. F., Bildstein, C., Masiarz, F. R., McKinley, M. P., and Cochran, S. P. (1980) Electrophoretic properties of the scrapie agent in agarose gels. *Proc Natl Acad Sci U S A* **77**, 2984-2988
27. Silveira, J. R., Raymond, G. J., Hughson, A. G., Race, R. E., Sim, V. L., Hayes, S. F., and Caughey, B. (2005) The most infectious prion protein particles. *Nature* **437**, 257-261
28. Sano, K., Atarashi, R., Ishibashi, D., Nakagaki, T., Satoh, K., and Nishida, N. (2014) Conformational properties of prion strains can be transmitted to recombinant prion protein fibrils in real-time quaking-induced conversion. *Journal of virology* **88**, 11791-11801

29. Deleault, N. R., Piro, J. R., Walsh, D. J., Wang, F., Ma, J., Geoghegan, J. C., and Supattapone, S. (2012) Isolation of phosphatidylethanolamine as a solitary cofactor for prion formation in the absence of nucleic acids. *Proc Natl Acad Sci U S A* **109**, 8546-8551
30. Wang, F., Wang, X., Yuan, C. G., and Ma, J. (2010) Generating a prion with bacterially expressed recombinant prion protein. *Science* **327**, 1132-1135
31. Caughey, B., Baron, G. S., Chesebro, B., and Jeffrey, M. (2009) Getting a grip on prions: oligomers, amyloids, and pathological membrane interactions. *Annual review of biochemistry* **78**, 177-204

CHAPTER 4:
Brain-derived Lipids Inhibit Prion Amyloid Formation *in vitro*

Summary

The normal cellular prion protein (PrP^C) resides in outer membrane lipid rafts and conversion from PrP^C to the pathogenic misfolded form is believed to occur at this location. Once misfolding occurs, monomers of the pathogenic isoform can polymerize into highly stable amyloid fibrils. *In vitro* assays have demonstrated an intimate association between prion conversion and lipids, specifically phosphatidylethanolamine, which is a critical cofactor in the formation of synthetic infectious prions. In the current work, we demonstrate an opposing property of lipids, the ability to inhibit amyloid formation *in vitro*. The amyloid seeding assay, real-time quaking-induced conversion (RT-QuIC), was used to investigate whole brain lipid effects on prion amyloid formation. An alcohol based extraction technique was used to remove the lipid content from terminal chronic wasting disease (CWD)-infected white tailed deer brain homogenates. Eliminating lipids increased the sensitivity of RT-QuIC detection of CWD in brain samples one hundred-fold. Conversely, addition of brain-derived lipid extracts to CWD prion samples inhibited amyloid formation in a dose-dependent manner. Brain-derived lipids also inhibited prion amyloid formation in RT-QuIC reaction seeds derived from lymphoid tissues. Subsequent lipid analysis demonstrated the inhibitory property was restricted to brain polar lipids. This is the first demonstration that a fraction of brain derived lipids directly inhibit prion amyloid conversion *in vitro* and highlights the diverse roles lipids play in the prion conversion process. Future experiments aim to identify the lipid classes or individual lipid species responsible for this inhibitory activity.

Background

The normal cellular prion protein, PrP^{C}, is intimately associated with the outer lipid bilayer of the plasma membrane. PrP^{C} is located within detergent-resistant lipid rafts and anchored to the outer membrane through a C-terminal GPI anchor (1-3). This cellular location is believed to be crucial for the conformational misfolding that creates the pathogenic isoform of prion diseases (4,5). The PrP^{C} pathogenic conformational change to PrP^{RES} has been shown to occur at the cell surface and disruption of lipid rafts, and thus dispersal of PrP^{C}, prevents prion infection in cultured neurons (6-8). In addition, studies using recombinant PrP^{C} to isolate co-factors to create a *de novo* infectious prion have identified lipids as a facilitating this pathogenic conversion (9). Phosphatidylethanolamine (PE), in particular, has been isolated as an efficient co-factor of prion conversion in every animal species examined (10).

RT-QuIC is an amyloid seeding assay that utilizes prion amyloid oligomers or fibrils as the seed to initiate amyloid formation and elongation with recombinant PrP^{C} ($rPrP^{C}$) as the substrate (11,12). Similar to other assays using $rPrP^{C}$, amyloid conversion in RT-QuIC is influenced by cofactors and inhibitors present in the test sample milieu. Previous reports (personal and multiple investigators' observations) have consistently demonstrated high concentrations of brain homogenate are unable to seed RT-QuIC reaction due to presumed inhibitors of the amyloid formation reaction (12-14). To analyze brain homogenates for PrP^{RES} seeding activity, samples must be diluted to 10^{-3} or 10^{-4} for initial RT-QuIC detection and display a linear dilution range from 10^{-4} to 10^{-7} which is consistent with removal of reaction inhibitors. The identification of these endogenous amyloid formation inhibitors present in certain sample types may not only enhance PrP^{RES} detection by RT-QuIC but also illuminate biologic features of prion conversion.

Our methodology developed to analyze fixed paraffin-embedded tissues using RT-QuIC (FPE RT-QuIC) revealed the ability to detect amyloid seeding activity at higher concentrations, 10^{-1} and 10^{-2} dilutions (15), than has previously been reported for brain homogenates. Here, we endeavored to identify the components of brain homogenate responsible for inhibiting the RT-QuIC amyloid formation reaction. We demonstrate endogenous lipids present in brain homogenate can inhibit RT-QuIC amyloid formation, in contrast to the prion conversion cofactor role previously reported. Our data suggests prion conversion *in vitro* is guided by a balance of pro-conversion lipids and anti-conversion lipids.

Methods

Cervid tissue samples:

Brain and lymph node samples used in experiments were harvested from white-tailed deer experimentally inoculated intranasally with chronic wasting disease (CWD) positive brain material (CWD+) or CWD negative brain material (CWD-) as a negative control (16). All CWD+ animals were allowed to progress to terminal disease prior to euthanasia and necropsy. At necropsy, all tissues were collected with individual prion-free instruments to avoid cross-contamination and divided into sections for freezing or fixing. Frozen tissue pieces were stored at -80^{o} C until use. Ten percent weight per volume tissue homogenates in 1xDPBS (Life Technologies) were created using zirconium oxide beads and a Blue Bullet Blender^{TM} (Next Advance) tissue homogenizer.

Recombinant Syrian hamster PrP^{C} protein substrate purification:

Purification of recombinant truncated Syrian hamster PrP^{C} (residues 90-231) (SHrPrP) used as substrate in RT-QuIC was performed as previously described (15,17). BL21 Rosetta (Novagen) *Escherichia coli* containing the truncated protein construct were cultured from a

glycerol stock at 37°C in lysogeny broth (LB) media with the selection antibiotics kanamycin and chloramphenicol to express SHrPrP until the culture optical density at 600 nm (OD_{600}) reached at least 2.5. *E.coli* cell lysis was carried out using Bugbuster™ reagent supplemented with Lysonase™ (EMD Biosciences) according to the manufacturer recommended protocol. Inclusion bodies were harvested by centrifugation at 15,000 x g and dissolved in solubilization buffer (8M guanidine hydrochloride, 100 mM Na_2HPO_4) prior to application to NiNTA flow resin (Qiagen) that had been previously equilibrated with denaturation buffer (6M guanidine hydrochloride, 100 mM Na_2HPO_4, 10mM Tris, pH 8.0). The NiNTA resin-SHrPrP was loaded onto a XK16-60 column (GE Healthcare) and purified using a Bio-Rad Duoflow™ FPLC. To induce protein refolding, a gradient from denaturation buffer to refolding buffer (100 mM Na_2HPO_4, 10mM Tris pH 5.5) was applied. Refolding was followed by a gradient from refolding to elution buffer (100mM Na_2HPO_4, 10 mM Tris, 0.5 M imidazole) and fractions from the elution peak were pooled and dialyzed against two 4L changes of buffer (20mM NaH_2PO_4, pH 5.5) overnight. Final protein concentration was calculated by measuring the A280 and using a coefficient of extinction of 25,900 in Beer's Law. Purified SHrPrP was stored at 4°C until use.

Real-time quaking induced conversion (RT-QuIC):

RT-QuIC was performed as previously described (17,18). Tissue homogenates and precipitated proteins with lipids were diluted in 0.1% sodium dodecyl sulfate (SDS)/1xPBS to the desired concentration. The RT-QuIC reaction was performed by adding 2 μL of diluted sample to a buffer containing 20mM NaH_2PO_4, 320mM NaCl, 1.0 mM EDTA, 1mM Thioflavin T (ThT) and 0.1 mg/mL SHrPrP in one well of a black, optical-bottom 96-well plate (Nunc). RT-QuIC experiments were carried out in a BMG Labtech Polarstar™ fluorometer with cycles of 1 minute shaking (700 rpm, double orbital) followed by 1 minute rest, repeated for 15

minutes. ThT fluorescence was read (excitation 450 nm, emission 480 nm, gain of 1700) at the conclusion of each 15 minute shake/rest cycle and each well was measured with 20 flashes per well with an orbital average of 4. Each RT-QuIC experiment was performed for a minimum of 100 cycles. RT-QuIC amyloid formation was determined to be positive if the fluorescence exceeded a threshold determined to be 5 standard deviations above the average baseline fluorescence. RT-QuIC amyloid formation rates in RT-QuIC were analyzed by calculating the inverse of the time to threshold.

Lipid extraction from brain homogenates:

Lipids were extracted from 10% brain homogenates using a modification of the Folch method (19). Briefly, 100 μL of a 10% brain homogenate was incubated with 900 μL of 100% ethanol at room temperature for 5 minutes. Following incubation, brain homogenate-alcohol solutions were centrifuged at 15,000 x g for 5 minutes to precipitate proteins. The ethanol supernatant was saved and the alcohol extraction process was repeated. Pooled ethanol supernatants were dried under a stream of nitrogen gas prior to resuspension in 100 μL a chloroform/methanol solution (2:1) to maintain original concentration (Figure 4.1A). Extracted lipids in the chloroform/methanol solvent were added to precipitated proteins from tissue samples. Commercially purchased total brain lipid extract and polar brain lipid extracts (Avanti Polar Lipids) were dissolved in chloroform/methanol solvent (2:1) immediately prior to use to create the desired weight/volume concentration and added to precipitated proteins from tissue samples.

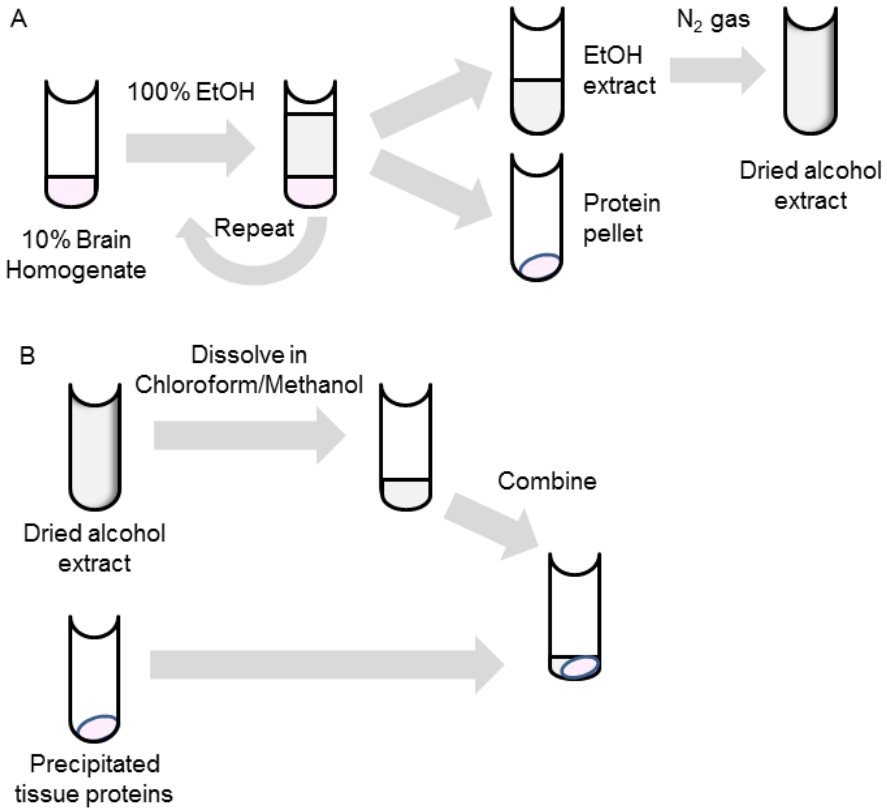

Figure 4.1 Overview of methods.
A. Lipid extraction from 10% brain homogenate. Brain homogenate was treated with 100% ethanol (EtOH) and proteins pelleted by centrifugation. The ethanol supernatant and its dissolved contents were removed and dried under a stream of nitrogen gas. B. Sample preparation for RT-QuIC. Dried alcohol extracts were resuspended in chloroform/methanol solvent. Resuspended extracts were combined with alcohol precipitated proteins (in A) for use in the RT-QuIC assay.

Isolation of polar lipids

Total brain lipid extracts were separated into polar and neutral/non-polar fractions with acetone precipitation. Approximately 20-30x volume of acetone was added to dried total lipid extracts and incubated on ice for 1 hour. The acetone-lipid mixture was centrifuged at 15,000 x rpm for 5 minutes to pellet polar lipids. The entire procedure was repeated and acetone supernatants combined. Lipid pellets and acetone supernatants were dried under a stream of nitrogen gas prior to resuspension in chloroform/methanol solvent (2:1) in volumes equivalent to

the starting material to maintain physiologic concentrations. Acetone fractionated lipids were added to alcohol-precipitated proteins to seed the RT-QuIC reaction as previously described.

Fixed paraffin-embedded (FPE) RT-QuIC

FPE tissue blocks were processed and proteins extracted as previously described (15). Briefly, a microtome (Leica) was used to cut 8-10 μm thick paraffin-embedded tissue-wax curls from paraffin blocks. Tissue-wax curls were treated sequentially with xylene to remove paraffin, a series of graded alcohol washes (100%, 95%, and 70%) to rehydrate the tissue sections, and a final 1xPBS wash to remove any remaining solvents with a five minute centrifugation at 15,000 rpm to pellet tissue pieces between each wash step. Rehydrated FPE tissue samples were homogenized in 1xPBS to create a standard 10% weight per volume using a bead homogenizer as described above. FPE homogenates were diluted in RT-QuIC dilution buffer (0.1% SDS/1xPBS) to the desired concentration prior to RT-QuIC analysis.

Western blotting of RT-QuIC products

Protease resistant amyloid products of the RT-QuIC reaction were detected by western blotting. RT-QuIC products were collected at the completion of the assay by washing each well with the RT-QuIC reaction buffer and combining replicates seeded by the same sample. Nine μL of collected RT-QuIC products were digested with proteinase K (PK) at a final concentration of 1 μg/mL and incubated at 37°C for 30 minutes with shaking followed by 45°C for 10 minutes with shaking. Samples were mixed with reducing agent (10x)/LDS sample buffer (4x) (Invitrogen) at a final concentration of 1x, heated at 95°C for 5 minutes then electrophoresed through a NuPAGE 10% Bis-Tris gel (Invitrogen) at 135 V for 1.5 hours. Proteins were transferred to a polyvinylidene fluoride (PVDF) membrane using the Transblot Turbo™ system (Bio-Rad) following manufacturer instructions. The membrane was loaded into a pre-wetted

SNAP i.d. blot holder (Millipore) then sequentially blocked with blocking buffer (Blocker Casein in TBS [Thermo-Scientific] and 0.1% Tween-20 [Sigma]) for 3 minutes and probed with antibody BAR224 (Cayman Chemical) conjugated to horseradish-peroxidase (HRP) diluted to 0.2µg/mL in blocking buffer for 10 minutes. Antibody was removed by vacuuming through the membrane using the SNAP i.d. system (Millipore) and the membrane was washed three times with 30 mL wash buffer (50% Blocker Casein in TBS, 50% 1X TBS, 0.1% Tween-20) with continuous vacuum. The membrane was developed with ECL-Plus Western Blotting Detection Reagents (GE) and viewed on a Luminescent Image Analyzer LAS-3000 (GE).

Results

Identification of lipids as inhibitors of prion amyloid formation

Studies performed when developing the FPE RT-QuIC method demonstrated RT-QuIC amyloid seeding at higher concentrations of FPE samples than had been previously possible (15). Amyloid seeding in FPE brain derived samples had a linear detection range extending from 10^{-1} to 10^{-7} whereas non-FPE frozen brain homogenate samples displayed a linear range extending from 10^{-4} to 10^{-8} due to inhibitors at high concentrations consistent with published literature (Figure 4.2A) (12,13). In contrast, retropharyngeal lymph node homogenates did not contain inhibitors at high tissue concentrations and successfully seeded RT-QuIC amyloid formation (Figure 4.2B). These observations indicated a component of brain homogenates not present in lymph node homogenates could inhibit prion enciphered amyloid formation and the FPE sample preparation protocol was capable of removing this inhibitor.

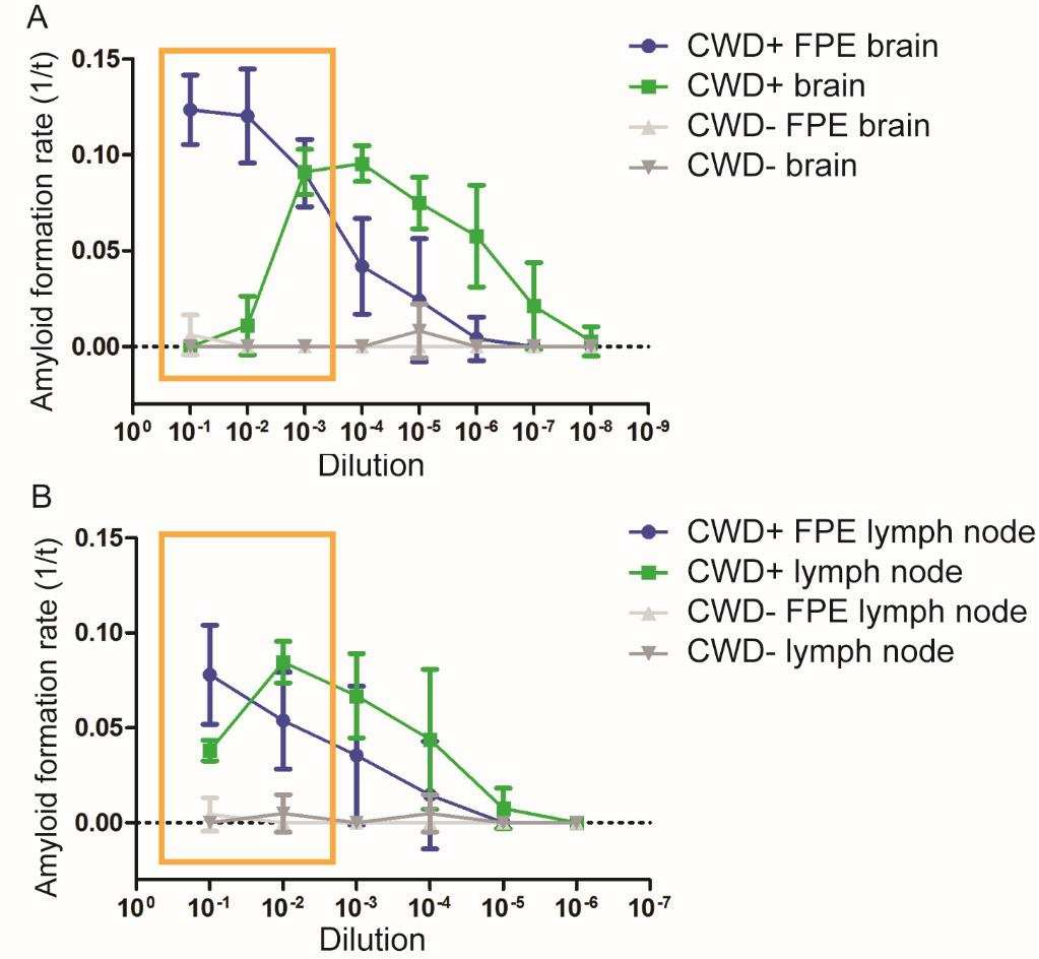

Figure 4.2 RT-QuIC dilutional series of FPE and frozen tissue homogenates
A. RT-QuIC dilutional series of FPE and frozen brain homogenate samples. The FPE protocol allowed prion-enciphered RT-QuIC amyloid formation with higher sample seed concentrations, extending the linear range of detection from 10^{-1} to 10^{-7} while inhibitors in higher concentration of brain homogenates prevented amyloid formation (highlighted by yellow box).
B. RT-QuIC dilutional series of FPE and frozen lymph node homogenate samples. In contrast to brain (A), higher concentrations of frozen lymph node homogenates are able to seed the RT-QuIC reaction similar to FPE lymph node homogenates (yellow box) allowing detection at all dilutions examined and displays a linear range from 10^{-2} to 10^{-6}.

To determine which component of our FPE RT-QuIC protocol was responsible for removal of RT-QuIC reaction inhibitors in brain samples, we isolated and tested each step of the FPE sample preparation protocol. To analyze the effects of tissue fixation on RT-QuIC amyloid seeding ability, a frozen section of CWD+ obex was fixed in paraformaldehyde-lysine-periodate fixative (PLP) for 48 hours prior to homogenization. The PLP CWD+ brain homogenate and

standard frozen brain homogenates were further treated with either a combination of xylene/alcohol or alcohol alone prior to seeding RT-QuIC (Figure 4.3). CWD+ frozen brain homogenate contained the greatest amount of reaction inhibitors, demonstrated by no amyloid formation at 10^{-1} dilution and a slower rate at 10^{-2} dilution. CWD+ PLP-fixed brain homogenate (Figure 4.3, green line) had amyloid formation kinetics similar to frozen brain homogenate, with no amyloid formation at a 10^{-1} and a slower rate of formation at a 10^{-2} dilution. These results indicated PLP fixation alone was not responsible for removal of amyloid formation inhibitors. Treatment of both the PLP-fixed and frozen brain homogenates with both xylene/alcohol steps demonstrated similar kinetic curves with amyloid seeding detection at 10^{-1} and 10^{-2} dilutions (Figure 4.3, black and red lines). Both samples had rates of amyloid formation that were indistinguishable from CWD+ FPE brain homogenate (Figure 4.3, blue line). To determine which of the xylene and alcohol solvents removed inhibitors, CWD+ frozen brain homogenate was treated with a series of alcohol dilutions. This sample preparation produced the highest rate of amyloid formation and displayed a linear dilution range from 10^{-1} to 10^{-3} (Figure 4.3, orange line). A dilutional series of frozen CWD+ brain homogenate treated with alcohol (Figure 4.3B) confirmed this solvent removed RT-QuIC inhibitors and did not alter amyloid formation kinetics.

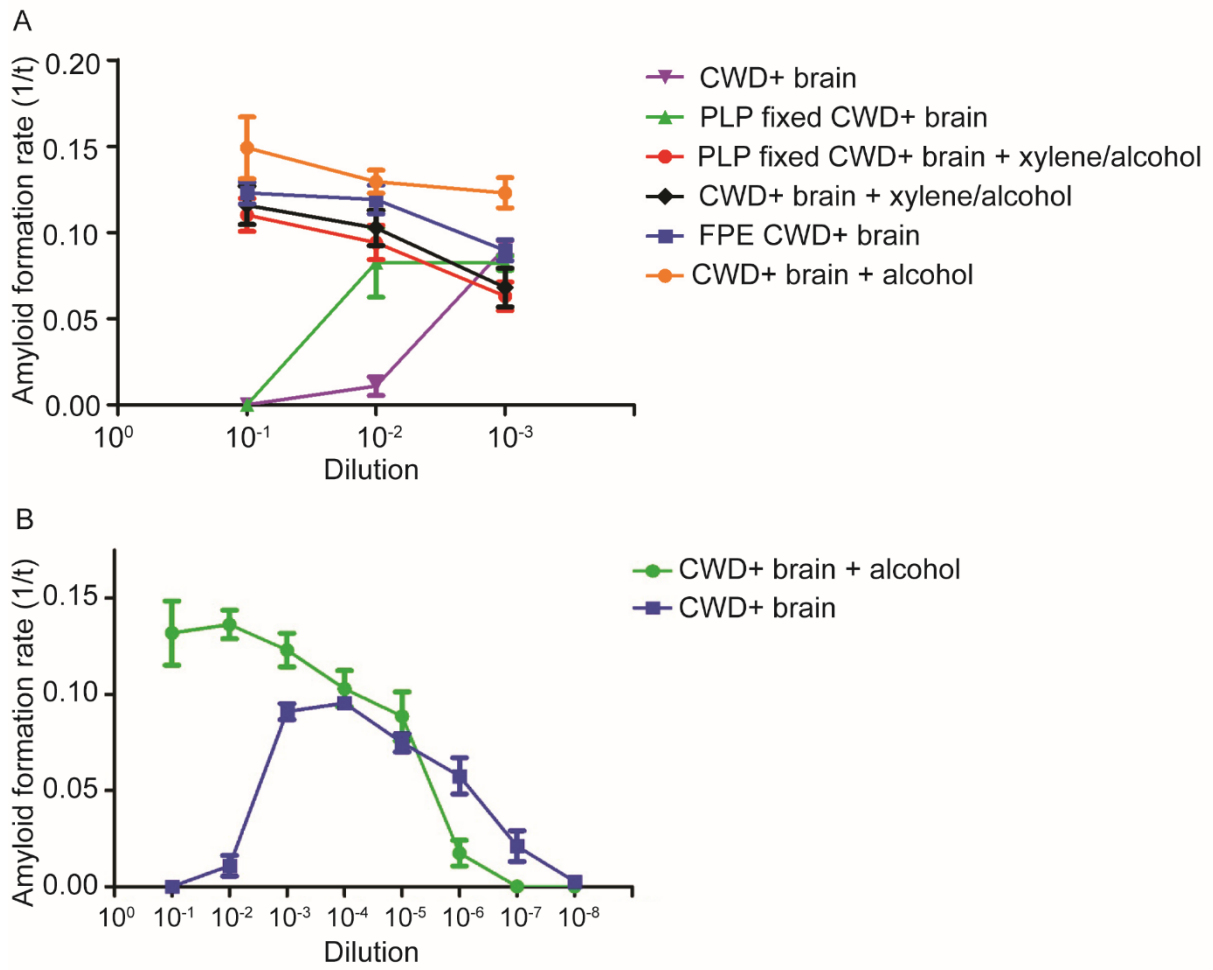

Figure 4.3 RT-QuIC detection of prion amyloid seeds following different solvent treatments.
A. RT-QuIC prion detection following FPE protocol solvent treatments. CWD+ brain homogenate (purple) prion seeding showed inhibition at 10^{-1} and 10^{-2} dilutions. PLP fixation (green) of CWD+ sample showed inhibition at 10-1 dilution. Treatment of CWD+ brain homogenate (black) and PLP-fixed CWD+ brain homogenate (red) with xylene and alcohol solvents allowed amyloid seeding at all dilutions comparable to FPE CWD+ sample (black). CWD+ brain homogenates treated only with alcohol (orange) allowed prion-seeded detection at all dilutions and had the highest rates of amyloid formation.
B. RT-QuIC dilutional series following alcohol treatment. The alcohol treatment removed brain homogenate inhibitors at high concentrations and allowed prion-seeded amyloid formation from 10^{-1} to 10^{-7}.

Alcohols are known solvents of lipids (20). Thus, we hypothesized brain-derived lipids were inhibiting the RT-QuIC amyloid formation reaction. To test this hypothesis, a commercial preparation of total brain lipid extract was applied to CWD+ alcohol precipitated samples at

approximate physiological concentrations (21). The addition of commercial lipids inhibited amyloid formation in a dose dependent manner with 6% commercial lipids in chloroform/methanol solvent completely inhibiting all sample dilutions tested and 3% commercial lipids only inhibiting amyloid formation at the 10^{-1} dilution (Figure 4.4A). The negative control of chloroform/methanol solvent displayed minor inhibition at the 10^{-1} dilution but did not abolish amyloid formation. These results confirmed brain derived lipids can inhibit the RT-QuIC amyloid formation reaction.

Since the detection of amyloid formation in RT-QuIC relies on thioflavin T binding amyloid structures and subsequent fluorescence we wanted to ensure the lack of RT-QuIC fluorescence signal in our experiments was due to lack of seeded amyloid formation and not thioflavin T binding. To test this, RT-QuIC reaction products from Figure 4.4A were examined by western blot for prion-enciphered PK resistant amyloid material. Replicates from the 10^{-1} dilution seeded reactions were pooled and treated with 10 μg/mL PK solution prior to western blotting. PK resistant material was only observed in the CWD+ chloroform/methanol solvent seeded reaction (Figure 4.4B) which corresponded to the positive fluorescence signal detected by RT-QuIC. These results confirmed total brain lipids were inhibiting prion-seeded amyloid formation and not the detection of amyloid structures.

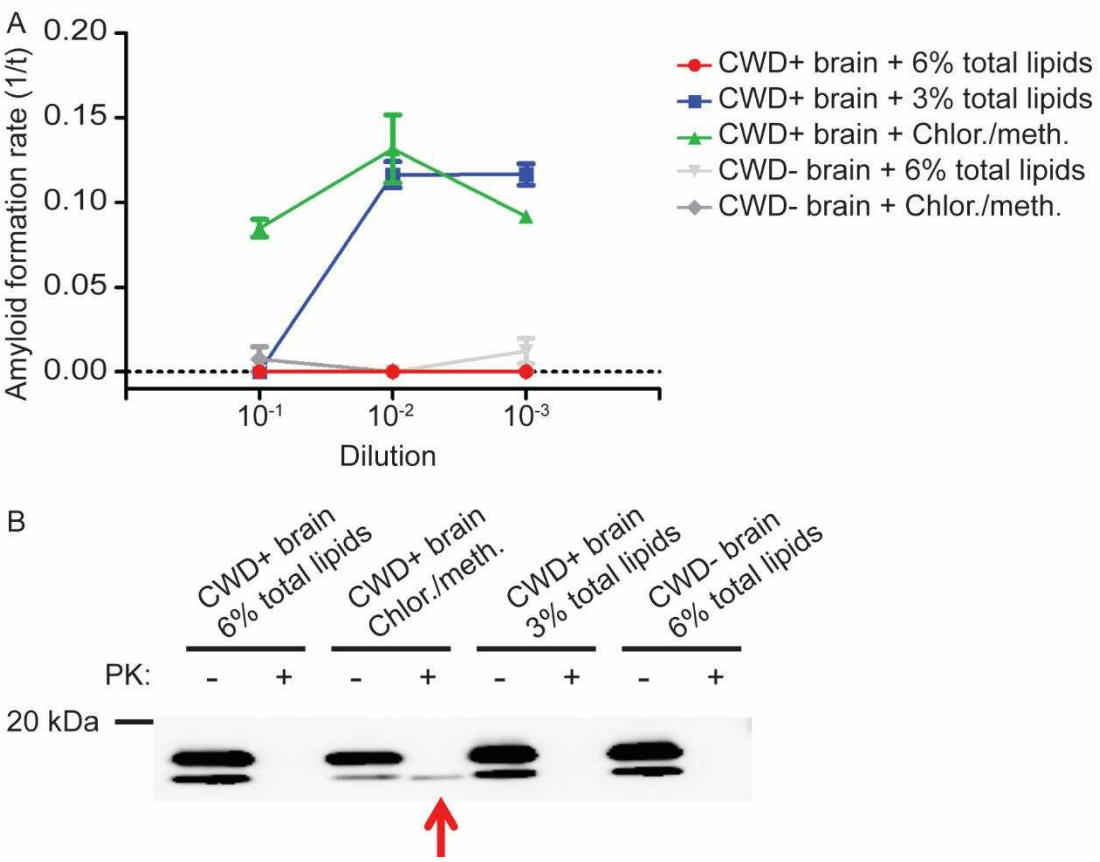

Figure 4.4 Total brain lipid extracts inhibit prion-enciphered amyloid formation
A. RT-QuIC of CWD+ seeds with commercial total brain lipid extracts. The addition of total brain lipids inhibited RT-QuIC in a dose dependent manner. The lipid delivery solvent, chloroform/methanol, had a minimal effect on the RT-QuIC reaction.
B. Western blot of RT-QuIC reaction products from 10^{-1} seed concentration. The western blot of RT-QuIC products from the experiment in A only detected PK-resistant prion-enciphered amyloid material from samples seeded with CWD+ brain-3% total lipids (red arrow). This result corresponded with the fluorescence observed at this seed dilution (green).

Next, we sought to assess the ability of brain extracted lipids to inhibit prion-seeded RT-QuIC amyloid formation in lymph node homogenates that naturally do not contain the same inhibitors. First, we extracted brain lipids from CWD-negative white-tailed deer brain homogenate and added these deer origin brain lipids to alcohol precipitated CWD+ brain protein. We observed similar amyloid formation kinetics as frozen CWD+ brain homogenates (Figure 4.5A). This ensured our alcohol extraction technique could isolate brain lipids and transfer them to other samples. We then added deer origin brain lipids to alcohol-precipitated CWD+

retropharyngeal lymph node samples. Prion seeded amyloid formation in the lymph node treated with deer-origin brain lipids was inhibited at 10^{-1} dilution whereas the alcohol-precipitated and frozen homogenate of the same origin lymph node displayed amyloid seeding at the same dilution (Figure 4.5B). This further demonstrated brain-derived lipids alter prion-seeded amyloid formation kinetics in RT-QuIC.

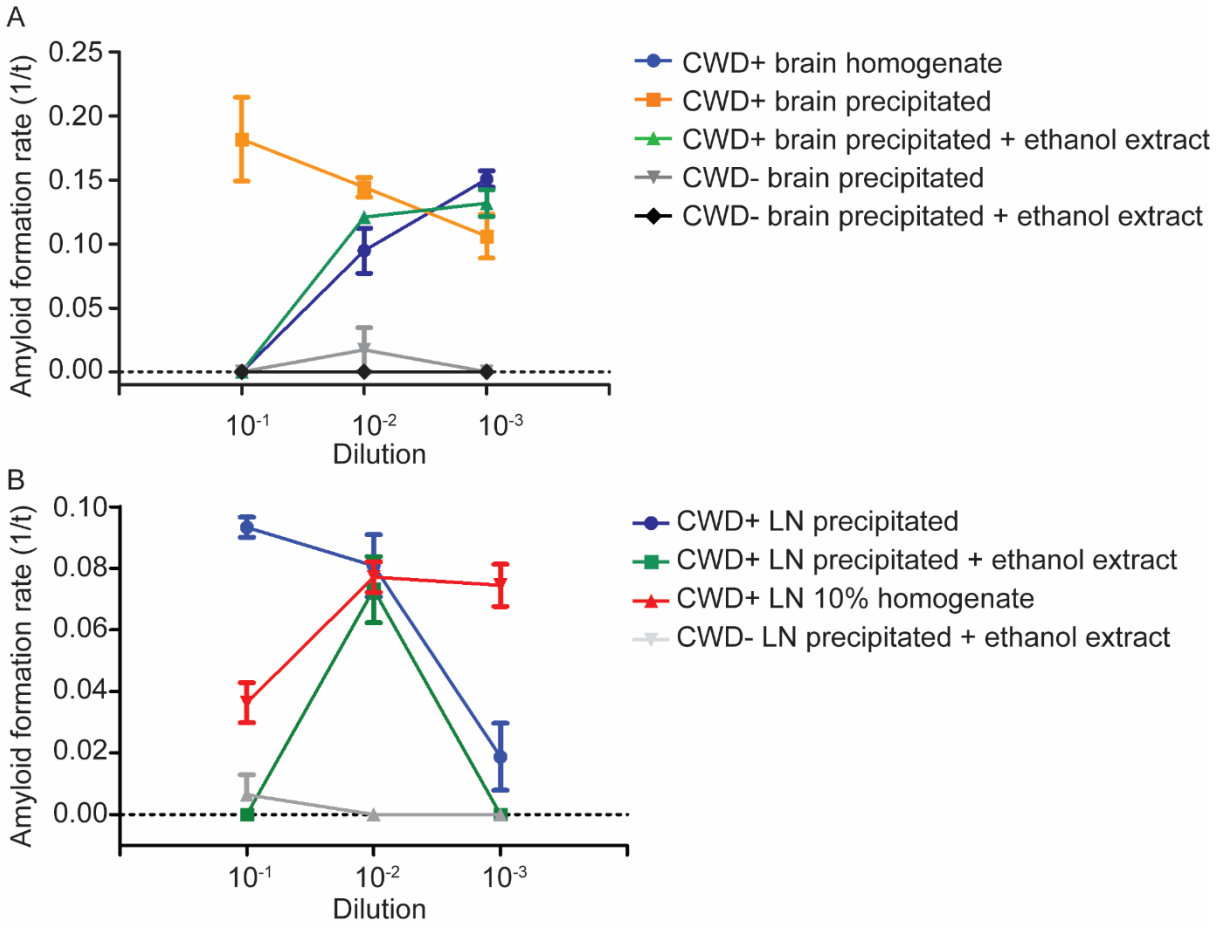

Figures 4.5 Extracted deer brain lipids can inhibit RT-QuIC
A. Alcohol-extraction can remove white-tailed deer brain lipids. The alcohol extraction protocol was used to remove lipids from CWD- brain homogenate. The removed lipids were added to alcohol precipitated CWD+ brain homogenate (green) and caused inhibition at 10^{-1} and 10^{-2} dilutions with amyloid formation kinetics comparable with 10% brain homogenate (blue).
B. Total brain lipids inhibit lymph node seeded RT-QuIC. Brain lipids extracted from CWD- brain homogenate were added to alcohol-precipitated lymph node prion seeds (green). The addition of lipids inhibited RT-QuIC prion-seeded amyloid formation at 10^{-1} dilution where inhibition was not present in the initial lymph node homogenate (blue).

Polar lipids inhibit prion-seeded amyloid formation

Lipids can be divided into classes based on their polarity. We used acetone precipitation to separate endogenous brain lipids into polar and neutral/nonpolar fractions and tested these groups for RT-QuIC inhibitor activity. Alcohol precipitated CWD+ brain seeds treated with the acetone lipid pellet containing polar lipids were inhibited at the 10^{-1} concentration (Figure 4.6A) but displayed amyloid formation at greater dilutions. In contrast, when the same CWD+ brain seeds were treated with the acetone supernatant containing neutral and nonpolar lipids amyloid formation occurred at all dilutions, albeit with a slower formation rate at the 10^{-1} dilution. To confirm these results, CWD+ brain seeds were treated with commercially prepared polar lipids at physiologic concentrations. The addition of polar lipids inhibited prion-seeded amyloid formation in a dose dependent manner with 5% polar lipids showing complete inhibition at all dilutions, with 0.5% inhibiting only the 10^{-1} concentration of prion seeds (Figure 4.6B). These results indicated polar lipids contain the majority of lipid amyloid forming inhibitory properties in brain lipid extracts.

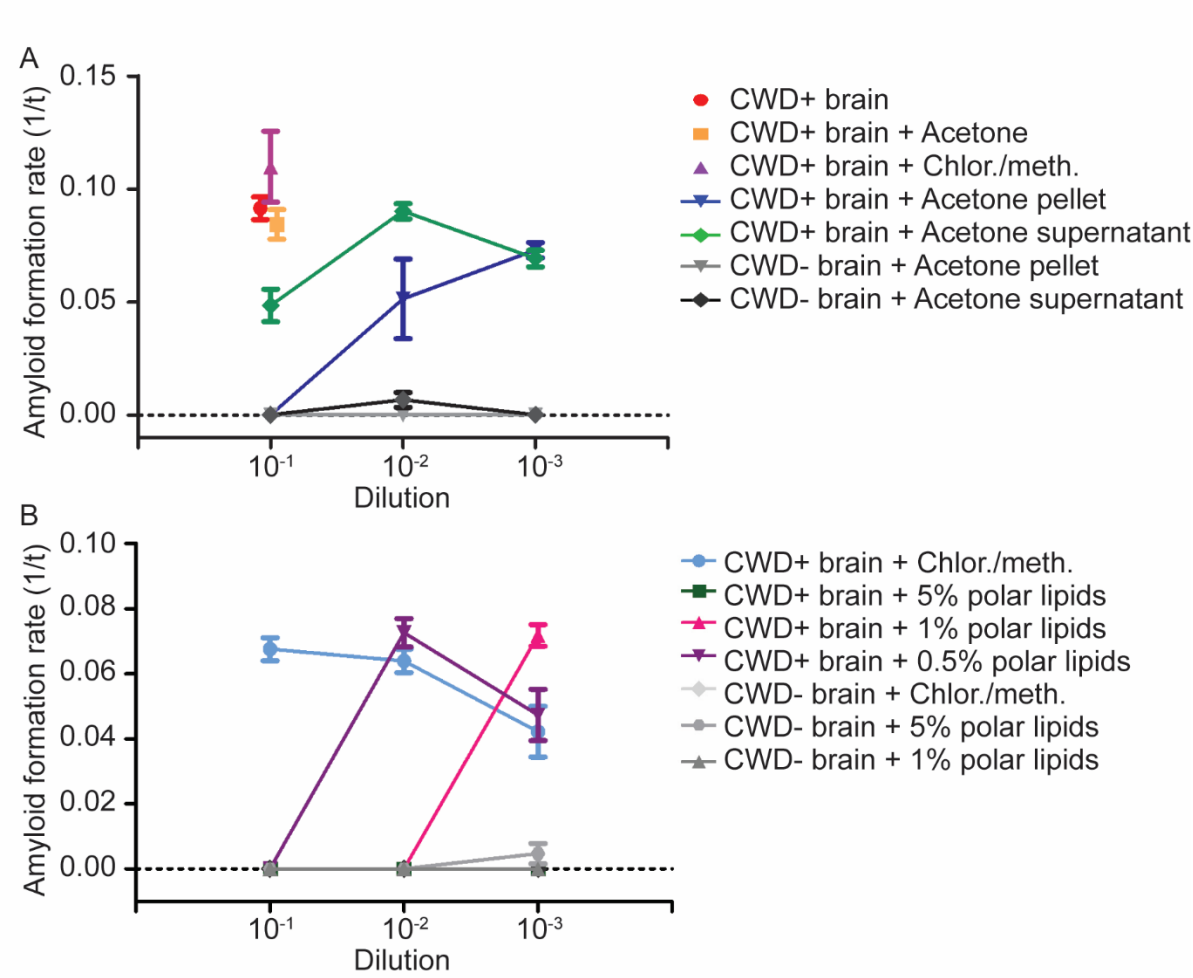

Figure 4.6 Polar lipids inhibit prion seeded amyloid formation

A. Acetone fractionation of total brain lipid extracts. Acetone was used to fraction total brain lipids into polar lipids, contained in the pellet, and non-polar lipids, contained in the supernatant. The addition of the pelleted lipid fraction to CWD+ seeds inhibited RT-QuIC at 10^{-1} dilution whereas addition of the acetone supernatant caused minor inhibition of RT-QuIC at the same dilution.

B. Commercial polar lipids inhibit RT-QuIC. Adding commercially prepared polar lipids to CWD+ seeds caused inhibition of amyloid formation in a dose-dependent manner with complete absence of amyloid formation at 5% lipid concentration and no inhibition at a 0.5% lipid concentration.

Discussion

PrP^{C}, like other GPI-anchored surface proteins, resides in lipid rafts within the outer leaflet of the cell membrane, a location that has been shown to be essential for the prion conversion process (2,22,23). Lipid raft microdomains are enriched in sphingolipids and cholesterol to maintain structural integrity and coalesce signaling molecules (24) and alterations in these components, such as disrupting cellular cholesterol homeostasis (25) or treatment with the enzyme filipin (26), decreased surface PrP^{C} and resulted in decreased formation of PrP^{RES}. In contrast to cholesterol, sphingomyelin depletion in N2a cell membranes caused an increase in PrP^{RES} through an unknown mechanism (27). The membrane lipid environment has been shown to directly promote prion propagation by destabilizing the C-terminal domain, facilitating PrP^{RES} conversion and fibril formation (28,29). These studies highlight the important role lipids play in prion propagation at a cellular level. Prion diseases also alter lipid homeostasis at the whole-organism level. A transgenic mouse model of scrapie has shown alterations in lipid compositions in the brain at terminal disease (30).

Many of the lipid-protein interactions implicated in prion diseases mirror those described in the pathogenesis of amyloid-β (Aβ) aggregation in Alzheimer's disease. Like PrP^{C}, amyloid-β precursor protein (APP) is an integral plasma membrane protein, although it is characterized by a transmembrane domain instead of a GPI anchor (31,32). The lipid environment surrounding APP and the secretase enzymes that perform the post-translational processing can impact the form of Aβ produced at membranes; when APP has been isolated from lipid rafts it was more likely to be associated with γ-secretase cleavage and amyloidogenic forms (33-36). The influence of lipid raft location on Aβ formation is also determined by cholesterol and an increase in membrane cholesterol shifts toward Aβ aggregations (37,38). Similar to the effect on the

prion conversion process, membrane lipids can also destabilize the Aβ conformational structure and induce the protein to acquire an additional β-sheet which increases fibrillization and aggregation (39,40). With the similarities in pro-amyloid protein-lipid interactions in prion and Alzheimer's disease, it would be interesting to investigate whether the inhibitory lipid function we identified can cross protein species.

Not only does the lipid bilayer influence protein misfolding but may also contribute to prion pathology as toxic nonfibrillar prion oligomers have been shown to directly interact with membrane lipids (41,42). Proposed mechanisms of toxicity include prion oligomer membrane insertion as pores or channels similar to Aβ in Alzheimer's disease pathology (43,44); detergent-like activity similar to islet amyloid precursor protein in diabetes pathology (45); or prion fibrillization on the surface of lipid rafts leading to a functional loss of membrane domain organization (41). These toxic interactions appear to depend on the composition of the lipid bilayer. The ability of amyloid-β to form pores and fragment lipid bilayers depended on the presence of gangliosides (44). Studies altering the content of anionic cellular membrane lipids induced a switch in prion oligomer membrane interactions from micelle formation to increased formation of fibrils on lipid microdomains (41). Membrane lipids, specifically phosphatidylethanolamine, have been shown to be a cofactor in prion protein conversion *in vitro* (10) by facilitating protein structural changes (46). Taken together, these studies and the presented data illustrate a variety of roles for lipids in the prion conversion process and suggest the composition of the lipid environment may be a crucial component of prion pathology.

Our western blot data suggests that polar lipids interfere with the prion conversion process; however, the mechanism of how this is accomplished needs further investigation. Other molecules identified as potential prion disease therapeutics that also limit prion conversion can

provide insight into potential mechanisms of action. Glycosaminoglycans and the azo dye Congo red mechanistically decrease PrP^{RES} formation by competitive inhibition. Both have been shown to bind PrP^{C} and decrease its availability for PrP^{RES} interaction and prion conversion (47,48). Congo red dye has also been shown to hyperstabilize prion amyloid fibrils which prevents fragmentation and seeded amyloidogenesis (49,50).

Our experiments highlight a potential exciting use of RT-QuIC for investigating molecules that can alter prion formation kinetics. Currently, investigations into potential therapeutics are limited to cell culture assays and costly animal bioassays (51). A modified PMCA technique using recombinant protein (10) as well as other amyloid seeding assays have previously been used in a limited number of prion conversion cofactor investigations. We show that the different alcohol based solvents used to deliver lipids did not themselves alter RT-QuIC amyloid formation kinetics. Additional study is needed to establish the robustness of RT-QuIC when used with a variety of delivery solvents or compounds. However, the ease and high throughput nature of RT-QuIC can facilitate widespread screening for molecules that inhibit prion amyloid formation (52).

In summary, we have demonstrated endogenous brain polar lipids can inhibit prion amyloid conversion *in vitro*. This is the first identification of an inhibitory function of lipids and suggests prion conversion is a balance of pro-conversion and inhibitory lipid molecules. Future avenues of investigation include examining the role the lipid environment plays on the generation of prion strains and determining which cells are permissive to prion infection.

Future Directions

Future experiments aim to parse out which class of endogenous lipids and/or individual lipids are responsible for inhibiting amyloid formation. We plan to use adsorption chromatography to separate polar lipids into neutral lipids, glycolipids/ceramides, and phospholipids based on their respective solvency and evaluate each lipid class's influence on amyloid formation kinetics. Once the class type with inhibitory features has been identified, we aim to perform mass spectrometry to characterize the lipids present in that fraction. Following this identification, we will purchase individual lipids and test each for the ability to inhibit RT-QuIC amyloid formation.

CHAPTER 4 REFERENCES

1. Vey, M., Pilkuhn, S., Wille, H., Nixon, R., DeArmond, S. J., Smart, E. J., Anderson, R. G., Taraboulos, A., and Prusiner, S. B. (1996) Subcellular colocalization of the cellular and scrapie prion proteins in caveolae-like membranous domains. *Proc Natl Acad Sci U S A* **93**, 14945-14949
2. Naslavsky, N., Stein, R., Yanai, A., Friedlander, G., and Taraboulos, A. (1997) Characterization of detergent-insoluble complexes containing the cellular prion protein and its scrapie isoform. *The Journal of biological chemistry* **272**, 6324-6331
3. Gorodinsky, A., and Harris, D. A. (1995) Glycolipid-anchored proteins in neuroblastoma cells form detergent-resistant complexes without caveolin. *J Cell Biol* **129**, 619-627
4. Mange, A., Nishida, N., Milhavet, O., McMahon, H. E., Casanova, D., and Lehmann, S. (2000) Amphotericin B inhibits the generation of the scrapie isoform of the prion protein in infected cultures. *Journal of virology* **74**, 3135-3140
5. Kaneko, K., Vey, M., Scott, M., Pilkuhn, S., Cohen, F. E., and Prusiner, S. B. (1997) COOH-terminal sequence of the cellular prion protein directs subcellular trafficking and controls conversion into the scrapie isoform. *Proc Natl Acad Sci U S A* **94**, 2333-2338
6. Gilch, S., Kehler, C., and Schatzl, H. M. (2006) The prion protein requires cholesterol for cell surface localization. *Molecular and cellular neurosciences* **31**, 346-353
7. Baron, G. S., Wehrly, K., Dorward, D. W., Chesebro, B., and Caughey, B. (2002) Conversion of raft associated prion protein to the protease-resistant state requires insertion of PrP-res (PrP(Sc)) into contiguous membranes. *The EMBO journal* **21**, 1031-1040
8. Goold, R., Rabbanian, S., Sutton, L., Andre, R., Arora, P., Moonga, J., Clarke, A. R., Schiavo, G., Jat, P., Collinge, J., and Tabrizi, S. J. (2011) Rapid cell-surface prion protein conversion revealed using a novel cell system. *Nat Commun* **2**, 281
9. Deleault, N. R., Kascsak, R., Geoghegan, J. C., and Supattapone, S. (2010) Species-dependent differences in cofactor utilization for formation of the protease-resistant prion protein in vitro. *Biochemistry* **49**, 3928-3934
10. Deleault, N. R., Piro, J. R., Walsh, D. J., Wang, F., Ma, J., Geoghegan, J. C., and Supattapone, S. (2012) Isolation of phosphatidylethanolamine as a solitary cofactor for prion formation in the absence of nucleic acids. *Proc Natl Acad Sci U S A* **109**, 8546-8551
11. Atarashi, R., Wilham, J. M., Christensen, L., Hughson, A. G., Moore, R. A., Johnson, L. M., Onwubiko, H. A., Priola, S. A., and Caughey, B. (2008) Simplified ultrasensitive prion detection by recombinant PrP conversion with shaking. *Nature methods* **5**, 211-212
12. Wilham, J. M., Orru, C. D., Bessen, R. A., Atarashi, R., Sano, K., Race, B., Meade-White, K. D., Taubner, L. M., Timmes, A., and Caughey, B. (2010) Rapid end-point quantitation of prion seeding activity with sensitivity comparable to bioassays. *PLoS pathogens* **6**, e1001217
13. Takatsuki, H., Satoh, K., Sano, K., Fuse, T., Nakagaki, T., Mori, T., Ishibashi, D., Mihara, B., Takao, M., Iwasaki, Y., Yoshida, M., Atarashi, R., and Nishida, N. (2015) Rapid and Quantitative Assay of Amyloid-Seeding Activity in Human Brains Affected with Prion Diseases. *PloS one* **10**, e0126930

14. Mori, T., Atarashi, R., Furukawa, K., Takatsuki, H., Satoh, K., Sano, K., Nakagaki, T., Ishibashi, D., Ichimiya, K., Hamada, M., Nakayama, T., and Nishida, N. (2016) A direct assessment of human prion adhered to steel wire using real-time quaking-induced conversion. *Sci Rep* **6**, 24993
15. Hoover, C. E., Davenport, K. A., Henderson, D. M., Pulscher, L. A., Mathiason, C. K., Zabel, M. D., and Hoover, E. A. (2016) Detection and Quantification of CWD Prions in Fixed Paraffin Embedded Tissues by Real-Time Quaking-Induced Conversion. *Sci Rep* **6**, 25098
16. Denkers, N. D., Hayes-Klug, J., Anderson, K. R., Seelig, D. M., Haley, N. J., Dahmes, S. J., Osborn, D. A., Miller, K. V., Warren, R. J., Mathiason, C. K., and Hoover, E. A. (2013) Aerosol transmission of chronic wasting disease in white-tailed deer. *Journal of virology* **87**, 1890-1892
17. Henderson, D. M., Davenport, K. A., Haley, N. J., Denkers, N. D., Mathiason, C. K., and Hoover, E. A. (2015) Quantitative assessment of prion infectivity in tissues and body fluids by real-time quaking-induced conversion. *The Journal of general virology* **96**, 210-219
18. Henderson, D. M., Denkers, N. D., Hoover, C. E., Garbino, N., Mathiason, C. K., and Hoover, E. A. (2015) Longitudinal Detection of Prion Shedding in Saliva and Urine by Chronic Wasting Disease-Infected Deer by Real-Time Quaking-Induced Conversion. *Journal of virology* **89**, 9338-9347
19. Folch, J., Lees, M., and Sloane Stanley, G. H. (1957) A simple method for the isolation and purification of total lipides from animal tissues. *The Journal of biological chemistry* **226**, 497-509
20. Reis, A., Rudnitskaya, A., Blackburn, G. J., Mohd Fauzi, N., Pitt, A. R., and Spickett, C. M. (2013) A comparison of five lipid extraction solvent systems for lipidomic studies of human LDL. *J Lipid Res* **54**, 1812-1824
21. Brady, S. T., Siegel, G. J., Albers, R. W., Price, D. L., and Benjamins, J. (2012) *Basic neurochemistry : principles of molecular, cellular, and medical neurobiology*, 8th ed., Elsevier/Academic Press, Amsterdam ; Boston
22. Caughey, B., and Raymond, G. J. (1991) The scrapie-associated form of PrP is made from a cell surface precursor that is both protease- and phospholipase-sensitive. *The Journal of biological chemistry* **266**, 18217-18223
23. Stahl, N., Borchelt, D. R., and Prusiner, S. B. (1990) Differential release of cellular and scrapie prion proteins from cellular membranes by phosphatidylinositol-specific phospholipase C. *Biochemistry* **29**, 5405-5412
24. Simons, K., and Toomre, D. (2000) Lipid rafts and signal transduction. *Nat Rev Mol Cell Biol* **1**, 31-39
25. Gilch, S., Bach, C., Lutzny, G., Vorberg, I., and Schatzl, H. M. (2009) Inhibition of cholesterol recycling impairs cellular PrP(Sc) propagation. *Cell Mol Life Sci* **66**, 3979-3991
26. Marella, M., Lehmann, S., Grassi, J., and Chabry, J. (2002) Filipin prevents pathological prion protein accumulation by reducing endocytosis and inducing cellular PrP release. *The Journal of biological chemistry* **277**, 25457-25464
27. Naslavsky, N., Shmeeda, H., Friedlander, G., Yanai, A., Futerman, A. H., Barenholz, Y., and Taraboulos, A. (1999) Sphingolipid depletion increases formation of the scrapie

prion protein in neuroblastoma cells infected with prions. *The Journal of biological chemistry* **274**, 20763-20771
28. Morillas, M., Swietnicki, W., Gambetti, P., and Surewicz, W. K. (1999) Membrane environment alters the conformational structure of the recombinant human prion protein. *The Journal of biological chemistry* **274**, 36859-36865
29. Critchley, P., Kazlauskaite, J., Eason, R., and Pinheiro, T. J. (2004) Binding of prion proteins to lipid membranes. *Biochemical and biophysical research communications* **313**, 559-567
30. Guan, Z., Soderberg, M., Sindelar, P., Prusiner, S. B., Kristensson, K., and Dallner, G. (1996) Lipid composition in scrapie-infected mouse brain: prion infection increases the levels of dolichyl phosphate and ubiquinone. *Journal of neurochemistry* **66**, 277-285
31. Zheng, H., and Koo, E. H. (2006) The amyloid precursor protein: beyond amyloid. *Mol Neurodegener* **1**, 5
32. Selkoe, D. J. (2001) Alzheimer's disease: genes, proteins, and therapy. *Physiol Rev* **81**, 741-766
33. Zha, Q., Ruan, Y., Hartmann, T., Beyreuther, K., and Zhang, D. (2004) GM1 ganglioside regulates the proteolysis of amyloid precursor protein. *Mol Psychiatry* **9**, 946-952
34. Lee, S. J., Liyanage, U., Bickel, P. E., Xia, W., Lansbury, P. T., Jr., and Kosik, K. S. (1998) A detergent-insoluble membrane compartment contains A beta in vivo. *Nature medicine* **4**, 730-734
35. Morishima-Kawashima, M., and Ihara, Y. (1998) The presence of amyloid beta-protein in the detergent-insoluble membrane compartment of human neuroblastoma cells. *Biochemistry* **37**, 15247-15253
36. Parkin, E. T., Hussain, I., Karran, E. H., Turner, A. J., and Hooper, N. M. (1999) Characterization of detergent-insoluble complexes containing the familial Alzheimer's disease-associated presenilins. *Journal of neurochemistry* **72**, 1534-1543
37. Simons, M., Keller, P., De Strooper, B., Beyreuther, K., Dotti, C. G., and Simons, K. (1998) Cholesterol depletion inhibits the generation of beta-amyloid in hippocampal neurons. *Proc Natl Acad Sci U S A* **95**, 6460-6464
38. Refolo, L. M., Malester, B., LaFrancois, J., Bryant-Thomas, T., Wang, R., Tint, G. S., Sambamurti, K., Duff, K., and Pappolla, M. A. (2000) Hypercholesterolemia accelerates the Alzheimer's amyloid pathology in a transgenic mouse model. *Neurobiol Dis* **7**, 321-331
39. Fezoui, Y., and Teplow, D. B. (2002) Kinetic studies of amyloid beta-protein fibril assembly. Differential effects of alpha-helix stabilization. *The Journal of biological chemistry* **277**, 36948-36954
40. McLaurin, J., Franklin, T., Chakrabartty, A., and Fraser, P. E. (1998) Phosphatidylinositol and inositol involvement in Alzheimer amyloid-beta fibril growth and arrest. *Journal of molecular biology* **278**, 183-194
41. Walsh, P., Vanderlee, G., Yau, J., Campeau, J., Sim, V. L., Yip, C. M., and Sharpe, S. (2014) The mechanism of membrane disruption by cytotoxic amyloid oligomers formed by prion protein(106-126) is dependent on bilayer composition. *The Journal of biological chemistry* **289**, 10419-10430
42. Caughey, B., Baron, G. S., Chesebro, B., and Jeffrey, M. (2009) Getting a grip on prions: oligomers, amyloids, and pathological membrane interactions. *Annual review of biochemistry* **78**, 177-204

43. Kayed, R., Sokolov, Y., Edmonds, B., McIntire, T. M., Milton, S. C., Hall, J. E., and Glabe, C. G. (2004) Permeabilization of lipid bilayers is a common conformation-dependent activity of soluble amyloid oligomers in protein misfolding diseases. *The Journal of biological chemistry* **279**, 46363-46366
44. Sciacca, M. F., Kotler, S. A., Brender, J. R., Chen, J., Lee, D. K., and Ramamoorthy, A. (2012) Two-step mechanism of membrane disruption by Abeta through membrane fragmentation and pore formation. *Biophysical journal* **103**, 702-710
45. Brender, J. R., Salamekh, S., and Ramamoorthy, A. (2012) Membrane disruption and early events in the aggregation of the diabetes related peptide IAPP from a molecular perspective. *Accounts of chemical research* **45**, 454-462
46. Miller, M. B., Wang, D. W., Wang, F., Noble, G. P., Ma, J., Woods, V. L., Jr., Li, S., and Supattapone, S. (2013) Cofactor molecules induce structural transformation during infectious prion formation. *Structure* **21**, 2061-2068
47. Caughey, B., Brown, K., Raymond, G. J., Katzenstein, G. E., and Thresher, W. (1994) Binding of the protease-sensitive form of PrP (prion protein) to sulfated glycosaminoglycan and congo red [corrected]. *Journal of virology* **68**, 2135-2141
48. Shyng, S. L., Lehmann, S., Moulder, K. L., and Harris, D. A. (1995) Sulfated glycans stimulate endocytosis of the cellular isoform of the prion protein, PrPC, in cultured cells. *The Journal of biological chemistry* **270**, 30221-30229
49. Caughey, B., and Race, R. E. (1992) Potent inhibition of scrapie-associated PrP accumulation by congo red. *Journal of neurochemistry* **59**, 768-771
50. Caughey, B., Ernst, D., and Race, R. E. (1993) Congo red inhibition of scrapie agent replication. *Journal of virology* **67**, 6270-6272
51. Trevitt, C. R., and Collinge, J. (2006) A systematic review of prion therapeutics in experimental models. *Brain : a journal of neurology* **129**, 2241-2265
52. Ferreira, N. C., Marques, I. A., Conceicao, W. A., Macedo, B., Machado, C. S., Mascarello, A., Chiaradia-Delatorre, L. D., Yunes, R. A., Nunes, R. J., Hughson, A. G., Raymond, L. D., Pascutti, P. G., Caughey, B., and Cordeiro, Y. (2014) Anti-prion activity of a panel of aromatic chemical compounds: in vitro and in silico approaches. *PloS one* **9**, e84531

CONCLUSIONS AND FUTURE DIRECTIONS

Through the work presented in this dissertation, I have investigated various aspects of prion pathogenesis. First, I demonstrated the expression of heat shock protein 72 does not alter the pathogenesis of prion propagation in murine neuroblastoma cells or C57Bl/6 mice. Second, I mapped the distribution of PrP^{CWD} in the early pre-clinical phase of chronic wasting disease, illustrating the progression from oropharyngeal lymphoid tissues to systemic lymphoid tissues prior to neuroinvasion. Third, in the process of investigating early PrP^{CWD} distribution, I developed a new technique to detect PrP^{CWD} amyloid seeding activity in fixed paraffin-embedded tissues using RT-QuIC. Analysis of RT-QuIC amyloid formation kinetics in these samples yielded a semi-quantitative estimate of the prion burden without the need for animal bioassay. Finally, in the process of developing FPE RT-QuIC, I was able to demonstrate that endogenous brain lipids can inhibit prion-seeded amyloid formation in RT-QuIC, the first identification of such activity in these molecules.

Although our investigations of HSP72 function in prion protection yielded negative results it still contributes to the prion field by being the first *in vivo* study of this chaperone-mediated function. Several possible reasons were identified as to why prion-chaperone interactions are different than other protein-misfolding diseases, including: (1) is there a cellular spatial separation between HSP72 expression and prion protein misfolding, (2) do PrP^{C} and PrP^{RES} have a binding domain for HSP72, and (3) is the HSP72 expression level too low to be therapeutic by limiting HSP72 expression levels to neurons? Future investigations to further understand these negative results might involve, analysis of the binding affinity of HSP72 to PrP^{C} and various aggregation forms of PrP^{RES} by specific plasmon resonance (Biacore) technology, *in vitro* co-culture of prion-susceptible cells with HSP72-expressing astrocytes or

microglia, and *in vivo* prion infection with mice expressing HSP72 in all cell types under control of the β-actin promotor or limited to specific cell types.

In the study of PrP^{CWD} distribution during early CWD disease, I focused on lymphoid tissues draining the gastrointestinal tract. Future investigations will evaluate the remaining 50+ tissues collected at necropsy from the same animals to get a whole-animal picture of prion distribution during early infection. To rapidly evaluate this large number of samples, we plan to adapt RT-QuIC to an end-point fluorescence read. In addition to the numerous tissues collected at necropsy, excreta samples including saliva and urine, were also collected from the same animals. A more complete picture of prion distribution and shedding potential at these early stages of disease are useful in enhancing our understanding of prion pathogenesis and to develop therapeutic intervention strategies.

The identification of PrP^{CWD} in lymphoid tissues during early CWD infection in deer revealed two separate patterns: (1) an initial prion replication phase in oropharyngeal lymphoid tissues and (2) a later systemic prion replication phase. Although we demonstrated all lymphoid tissues appear to have the same prion replication kinetics by RT-QuIC analysis, it is unknown if the same cell types are involved and if any, which cells are involved in systemic prion spread. Potential future studies will type prion-positive cells using double-label immunohistochemistry in tissue sections, or, if possible to collect through thoracic duct ligation, analyze lymph over the course of early disease for prion-associated cells or lipoprotein molecules.

The accurate diagnosis of prion diseases during preclinical disease stages is crucial to the management of CWD populations and design of interventional strategies. The small number of samples evaluated as part of our development of FPE RT-QuIC suggested our new methodology has greater detection sensitivity than IHC in fixed paraffin-embedded tissues; however, a larger

sample analysis is necessary to establish sensitivities and specificities as a diagnostic test. Additionally, a large scale assessment of current assays, such as RT-QuIC, TSA-IHC, and End-point QuIC, would be beneficial in determining their diagnostic application to the preclinical disease phase and guide the selection of tests for experimental needs. Furthermore, the identification of PrP^{CWD} seeding activity in FPE samples by RT-QuIC lays the groundwork for the development of an *in situ* amyloid seeding assay using RT-QuIC technology.

Finally, the discovery of endogenous brain lipids, specifically polar lipids, as inhibitors of prion amyloid formation *in vitro* is the first identification of RT-QuIC reaction inhibitors and the first identification of such an inhibitory function of these molecules. Future studies aim to specify which lipids or class of lipids are responsible for this function by adsorption chromatography separation of lipid classes and mass spectrometry to categorize the lipids present in our extractions. Many questions follow from our RT-QuIC lipid observations including: (1) does the polar lipid inhibitory property in RT-QuIC apply to other prion species besides CWD, (2) can polar lipids inhibit amyloid seeding in general, or is the action specific to prions, (3) what are the lipid requirements for prion conversion *in vivo*? The first question could be addressed with RT-QuIC experiments and brain samples available. The second question requires development of amyloid seeding assays, similar to RT-QuIC, that are specific to the other protein misfolding diseases. Development of these assays could also have a greater application beyond the evaluation of lipid-protein interactions. Lastly, the third question could be evaluated through lipid membrane models and cell culture.

In conclusion, the studies presented in this dissertation have contributed to furthering the knowledge of prion propagation and pathogenesis. Moreover, these studies have provided tools and established a basis for future investigations into prion and protein misfolding pathogenesis.